UNIVERSITÀ DEGLI STUDI DI PALERMO

PHD COURSE IN PHYSICS AND CHEMISTRY

Cycle XXXV

General approaches of processes involved in neurodegeneration using protein and printed phospholipids models

PhD Candidate:

Daniele Gulli

Tutor Universitario:

Bruno Giuseppe Pignataro

Tutor Aziendale

Caterina Alfano

Outline of the work

Neurodegenerative disorders belong to a class of diseases characterized by the progressive loss of neurons which leads to cognitive and motor dysfunction. Protein aggregation is a hallmark of many neurodegenerative disorders in which misfolded proteins aggregate to form insoluble deposits in the brain. In this context the interaction between aggregates or aggregating proteins with cellular membranes is crucial in the toxicity mechanisms in cellular environment.

Despite the extensive amount of research, many questions regarding the mechanisms involved in protein aggregation and membrane protein interactions in neurodegeneration are still unanswered. Specifically, the general laws and the interactions that regulate protein misfolding and supramolecular assemblies are not clarified yet. Currently, many studies are also focused on the identification of chemical compounds, like small molecules, that can inhibit or modify protein aggregation at early stages or reduce the ability of oligomers to disrupt membrane organisation thus reducing lowering of toxicity due to protein aggregates. Understanding these complex processes is critical in order to develop effective therapies for neurodegenerative disorders. This will pave the way to the development of targeted therapeutics to treat these diseases.

The present PhD project is funded by an Industrial PhD fellowship (PON R&I 2014-2020, Axis I) based on a collaboration between University of Palermo and Ri.Med Foundation.

This work is divided into 6 chapters, the first two (Chapter 1 and 2) are an introduction to the scientific problems and the 3rd describes the processes that were carried out to obtain the results. Results are discussed in the 4th and 5th chapter where all the results concern protein aggregation and the fundamental involvement of electrostatic forces in the aggregation process are presented. Furthermore, I will show the results involving protein interaction and printed models of the cell membrane varying the electrostatics of the process. Finally, in the last chapter the results and future perspectives are analysed and summarized.

Chapter 1 introduces protein aggregation and its connection to neurodegeneration, as well as the use of model proteins that are very useful for basic science studies, with a focus on Bovine Serum Albumin (BSA), a protein used in my work. The advantages and drawbacks of the chosen model protein are described, as well as its current state-of-the-art in terms of protein aggregation with a focus on BSA-EGCG interactions.

Chapter 2 introduces the protein-membrane interaction and its involvement in neurodegenerative diseases, it is followed by the introduction of membrane models and techniques, in particular a focus on Dip Pen Nanolithography and microcantilever spotting is discussed. Finally, I've discussed the state-of-the-art regarding protein-membrane models' interaction.

Chapter 3 is dedicated to the used techniques and materials. A Specific reference is addressed to spectroscopy, Fluorescence and Atomic Force Microscopy techniques which help to characterize the interaction process. On the other hand, Isothermal titration calorimetry helps us to define the type of binding and the thermodynamics behind the process. All the processes leading to the formation of membrane models are described in detail. Finally, the last part of the chapter is dedicated to materials and sample preparations.

Chapter 4 presents the results obtained from the interaction process between the BSA model protein used in my study and a promising anti-aggregating molecule called EGCG. The results show that the electrostatic forces greatly affect the interaction and the possible binding between the two molecules. In Chapter 5, I will present the results on the printed model membrane system setup and first attempts of studying their interactions with proteins. The interaction processes between the membrane models and the selected model proteins (Lysozyme and Concanavalin A) are then described, as a function of changes in electrostatic forces. Finally, a summary of the results together with suggestions to further develop specific problems raised in this Thesis constitute the Conclusions and Perspectives paragraph.

Aim and Hypothesis of the work

On the hypothesis that general law regulates protein aggregation and association with membranes and referring to the literature, I carried on my studies aimed at developing an experimental platform by using model proteins, small drug molecules and printed phospholipids models in order to highlight characteristic features of these phenomena. As regards this work I've choosen a model protein named Bovine Serum Albumin (BSA) as a model system. BSA was chosen because it is a well-known protein that is extremely stable, inexpensive and furthermore it is a highly scientifically studied protein, that makes BSA an ideal model protein. The BSA has been used to characterize the anti-aggregation properties of a promising molecule, a polyphenol called Epigallocatechin gallate (EGCG) depending on the electrostatic field. By using this well-known protein model, it is possible to extrapolate results from our study to more complex proteins, such as those involved in neurodegeneration. This simplification allows us to obtain results that can help us better understand the laws governing these complex processes. To produce model membranes, it was used an innovative printing biology technique, named micro contact spotting (μCS), in order to develop a system micronsized membrane layer with defined geometry that may mimic cellular membranes by using a fluorescent bio ink. The aim of this part of the work is instead to obtain a system that mimics the cell membrane and allows the generation of thousands of testable systems, which can be modified in terms of geometry, size, and phospholipid content. This system differs from conventional methodologies and can be easily analysed using fluorescence microscopy techniques and enabling the study of the role of the surface in promoting neurodegenerative processes.

INDEX

1 Protein Aggregation and Neurodegeneration: BSA as a Model Protein

1.1 Introduction

The neurodegeneration processes have been affecting millions of people worldwide for over a hundred years. The increasing life expectancy of individuals will almost certainly lead to a dizzying increase in these strongly impactful diseases in the world. Understanding the basic mechanisms of those processes is critical. Among the processes underlying neurodegenerative diseases, one of the most important, is that which leads to the formation of insoluble ordered aggregates inside the neuronal membranes [1]. These aggregates, called amyloid fibrils, are the final product of a very complex protein unfolding process that is still debated today. The formation of these insoluble aggregates ultimately leads to the death of neurons present in the brain, probably due to oxidative stress. In the last years the idea that general laws regulate these types of interactions has widely widespread so that many feature of these phenomena can also be highlighted thanks to the use of model proteins. BSA has been chosen in this study as a model protein.

1.2 Protein Aggregation and Misfolding processes

Living systems are composed of four key macromolecules: proteins, carbohydrates, nucleic acids, and lipids. Proteins are one of the most abundant molecules in biology which stimulate or control virtually every chemical process on which our lives depend. Different proteins are distinguished by a different order of amino acids in the polymeric sequence. Following their biosynthesis, the most part of proteins must be converted into tightly folded compact structures to function [2]. Protein folding is a process by which a protein chain acquires its native 3-dimensional structure, a conformation that is usually biologically functional, in an expeditious and reproducible manner[2]. Folding is usually extremely efficient and a remarkable testament to the power of evolutionary biology, and it is considered a particular aspect of self-assembly in cell-biology[2].

It is now known that within the cells of living organisms there are large numbers of auxiliary factors that assist in the folding process, including molecular chaperones. These factors serve to enable polypeptide chains to fold efficiently into the native conformation. These represent a clear example of biological complexity [3]

A protein is misfolded if it cannot achieve the correct native state[2], a model description of this process was reported in Figure 1.1. If a certain polypeptide chain is unable to fold properly, or loses its tightly packed natural state, there arises an increase in the population of unfolded or improperly folded states[4]. These novel states exhibit a loosely packed structure, which facilitates interaction and assembly of the protein molecules into oligomeric forms. This can be due to mutations in the amino acid sequence or to the disruption of the conditions for normal folding by external factors (e.g. oxidative stress, overexpression, mutation, etc.).

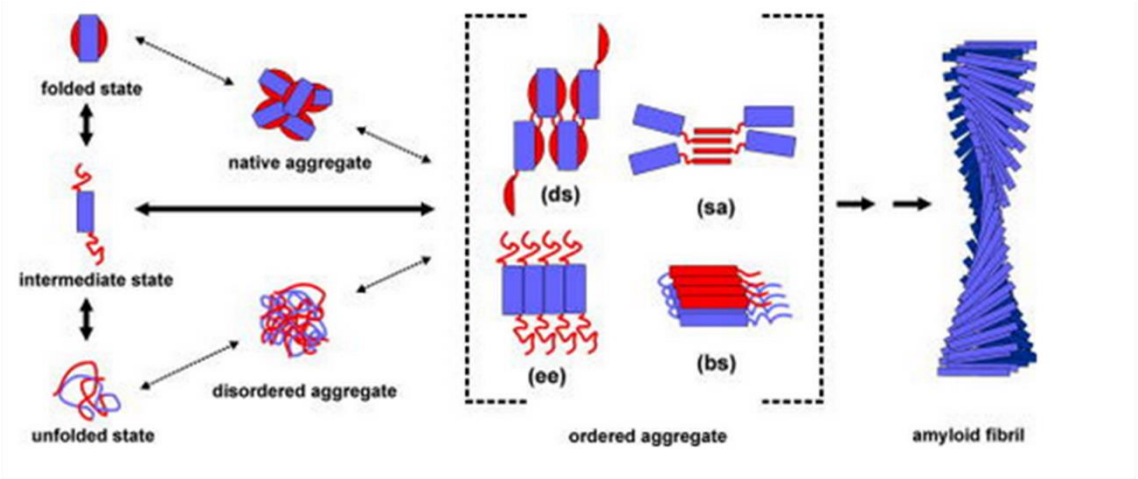

Figure 1.1 Mechanism of protein aggregation in neurodegeneration. The suggested ways of how protein aggregation occurs involve the development of amyloid fibril from partially folded intermediary states, which arises due to either the partial unravelling of the native formation or partial structuring of unfolded polypeptides. The structured entities combine in an orderly manner using techniques like domain swapping (ds), edge-edge association (ee), β-strand stacking (bs), or strand association (sa). Figure was modified from[4].

These stresses can lead the protein to conformational changes that in turn lead to toxic conditions. At specific conditions, destabilised protein often undergoes specific supramolecular associations which are though associated to the aetiology of several human pathologies such as Alzheimer and Parkinson diseases[5]. The accumulation of these insoluble fibrous protein aggregates termed as amyloid in various organs/tissues cause their degeneration and loss of function. The aggregating proteins are different in many neurodegenerative disorders[6]. Further, the occurrence of these diseases can be sporadic or hereditary and the aggregates can localize in the intracellular or extracellular space.

The Presence of amyloid plaque in many patients affected from different neurodegenerative disease (Alzheimer, Parkinson, etc.) supported the close link of protein aggregation with neurodegeneration[1]. Initial studies postulated amyloid fibrils to be the primary cause of cell death and disease pathogenesis. In cultured neurons, fibrils increased frequency of action potentials and membrane depolarization reduced the cell viability. During the formation of amyloid structures many aggregate species are formed, depending on the external conditions, different intermediate states with different structure and specificity are created, which in turn regulates the kinetics and the appearance of the final aggregates. The genesis of amyloids is a result of intricate aggregation methods involving

multiple microscopic occurrences such as primary nucleation, elongation, secondary nucleation, and fragmentation[5]. These combine to form various intermediates as monomers interact in solution while initial small soluble aggregates form. Additionally, existing fibrils increase in length by incorporating monomers, surface of present aggregates catalyse the formation of new small soluble aggregates, and existing fibrils break apart resulting in an increase in the total number of fibrils. The intermediate and oligomer states, which may be soluble or insoluble, are recognized as key effectors of toxicity. Accumulating evidence suggests that amyloid-related toxicity is not directly associated with the presence of mature fibrils, but rather by the presence of a heterogeneous ensemble of aggregated structures generated during fibril assembly, which may modulate and potentially permeate cell membranes, thereby initiating a common group of downstream pathologic processes[7]. Numerous studies investigate interactions of amyloidogenic species with cell membranes, yet the molecular processes underlying cytotoxicity remains unclear.

The mechanisms of protein aggregation mentioned above do not solely occur at the cellular level. In fact, native protein solutions can be induced to form aggregates *in vitro* under certain chemical and physical conditions, providing an opportunity to thoroughly study the underlying interactions. Factors such as pH, temperature, ionic strength, and denaturant agents can trigger the formation of aggregate deposits[8]. The formation of protein aggregates can be attributed to a combination of protein-solvent and protein-protein interactions. Altering the solvent's physical properties, such as extreme temperatures or a pH level outside of the physiological range, can disrupt the equilibrium of forces responsible for proper protein arrangement, leading to the introduction of new intermolecular interactions. Through *in vitro* studies of proteins and the use of proteins models as well, it is possible to characterize and track the process of protein aggregationin order to better understand all the macromolecular details that lead to the onset of diseases. A better comprehension of these processes will also make possible to intervene earlier and to slow down or even prevent the progression of the disease.

1.3 Therapeutic strategies: polyphenols compound

Since the origins of the amyloid field, several different compounds were developed for research purpose in order to characterize the amyloid structure. Currently, many structural analyses rely on the use of molecular probes that change their spectroscopic properties upon binding to amyloid fibrils. Thioflavin-T (ThT), a fluorescent molecule, which, in a certain approximation emits only in the presence of amyloid structure and is commonly employed for monitoring the time evolution of amyloid aggregates in vitro[9]. Other compounds like 1-anilinonaphthalene-8-sulfonic acid (ANS),

are commonly used to detect protein-folding intermediates [10]. These compounds recognise solvent-exposed hydrophobic patches of proteins and are useful in characterising early-stage oligomerization and initial structural rearrangements of amyloidogenic proteins. As previously mentioned, the process of protein aggregation goes through a series of small oligomeric aggregates that have been found to be highly toxic to the organism. Reducing or even avoiding the formation of these aggregates is the new challenge of science. Compounds such as steroids, Tetracyclines, Antibodies, and antibody fragments have demonstrated anti-aggregating properties. Different natural compounds have recently been studied as anti-aggregating molecules. Among the small molecules currently under study, the most interesting are certainly polyphenols like Epigallocatechin-gallate (EGCG) and its derivatives.

Figure 1.2 shows the possible different interactions from polyphenols and different types of protein aggregates. As the Figure shows, the polyphenols can interact with different stages of formation of fibrils from the more toxic oligomers to the final fibrils.

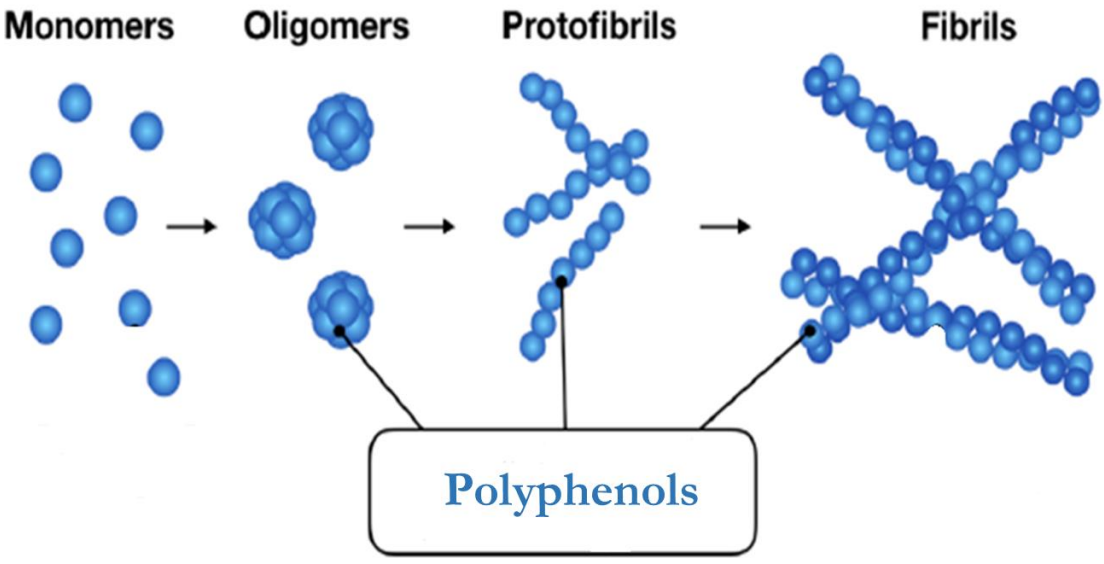

Figure 1.2. Interaction of polyphenols and possible target aggregates. Images was modified from [9]

Polyphenols are chemical compounds that occur in nature, but there are also synthetic and semi-synthetic versions that contain phenolic structures. These compounds can be found in a variety of food sources, such as fruits, vegetables, cereals, and beverages. Flavonoids are categorized into

different classes, such as anthocyanins and anthoxanthins, it'is based on their molecular arrangement (a classification was showed in Figure 1.3). The group of anthoxanthins is further divided into flavonols, flavans, flavanols, flavones, and isoflavones. Among these ones, flavanols like catechins have been studied the most[11], [12]. Polyphenols are classified into different groups based on the number of phenol rings and the type of connections linking the rings. The structural composition and complexity, such as degree of polymerization, conjugation with other phenolics, glycosylation, acylation, hydroxylation, and molecular size, largely determine the bioavailability and absorption of dietary polyphenols.

Polyphenols possess potent antioxidant properties by either donating an electron or a hydrogen atom that neutralizes free radicals. The effectiveness of polyphenols in combating oxidative stress is linked to their specialized functionalities, such as the conjugated system and hydroxylation patterns, particularly the 3-hydroxy group present in flavanols. Polyphenols mitigate the generation of free radicals by impairing the formation or deactivating the active species as well as the precursors of free radicals. Furthermore, polyphenols perform the crucial function of directly scavenging radicals, thereby breaking the lipid peroxidation chain reactions. Aside from their antioxidant properties, polyphenols possess various other health advantages. Various research supports the notion that polyphenol-rich diets can potentially guard against the emergence of specific cancers, cardiovascular conditions, and diabetes[12].

1.4 Epigallocathechin-3-gallate (EGCG)

One of the most studied polyphenols is certainly EGCG (A representative scheme of chemical structure of polyphenols was reported in Figure1.3), this polyphenol extracted from green tea has demonstrated more antioxidant, anticancer and antiaggregogenic properties than many other similar molecules[7], [13], [14]. Observations have shown that EGCG binds directly with unfolded proteins and prevents the early formation of β-sheet structures in the amyloid formation cascade[15], [16].

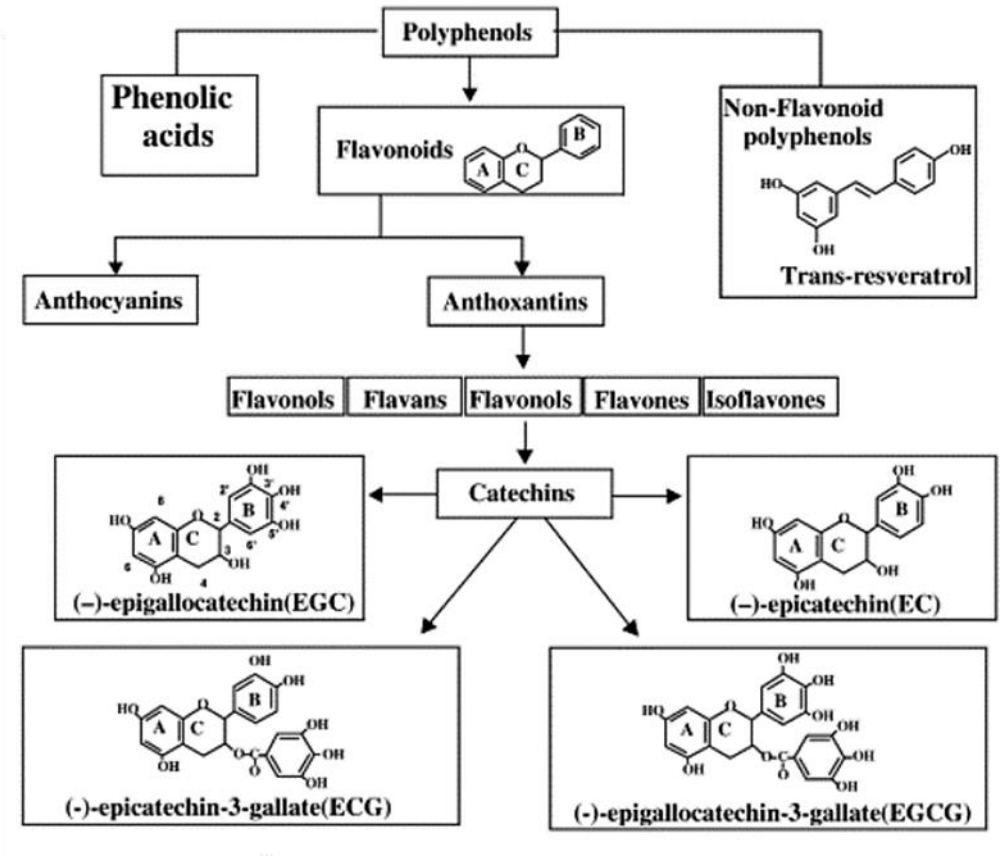

Figure 1.3. Classification and chemical structure of natural poliphenols. Figure was modified from[12].

This occurs through the reaction of EGCG with free primary amine groups of proteins, resulting in the formation of a Schiff base and inducing fibril remodelling. Unfortunately, due to poor chemical stability, restricted bioavailability and decreased anti-amyloidogenic performance, utilizing this unique property of EGCG is challenging in the presence of a cell membrane. According to recent literature, EGCG has been found to have the ability to inhibit the aggregation of various proteins or peptides that could potentially lead to the development of amyloidosis, such as Aβ and α-syn [7], [15]. The way for EGCG exerts its effects may vary depending on the specific target proteins involved, but the most observed characteristic is its ability to shift the aggregation process towards non-toxic β-sheet-poor aggregates that do not follow the intended pathway, or alternatively, modify the aggregates after they have formed. Regarding the anti-amyloid effect of EGCG and its counterparts, the non-covalent interactions involved are known to be intricate. Various studies have shown the presence of hydrogen bonding with the protein backbone and hydrophilic side chains, as well as hydrophobic interactions, particularly with aromatic residues. One notable finding is that EGCG could form a Schiff base with lysines in target proteins, which could contribute to the

irreversible transformation of proteins into non-toxic aggregates[17]. Recent reports suggest that quinone or quinonoid substances, which are oxidation products, may be even more effective at preventing amyloid aggregation by covalently binding to the target protein[18].

Different works report results on EGCG indicating it as a molecule with great potential, but the mechanisms of interaction between the small molecule and proteins are not yet very clear.

1.5 Bovine Serum Albumin: A model protein

BSA is a globular protein derived from cow blood, composed with 583 residues and a molecular weight of 66,4 kDa[19] which under a variety of conditions displays tendency to self-assembly in large macromolecular aggregates. BSA, like all serum albumins, is a transport protein that specifically transports fatty acids, bilirubin, and minerals within the body. Being a transport protein, it can easily interact with multiple compounds. Studies have shown different interactions between BSA and metal complexes, ionic surfactants, small molecules, imaging agents, and others. This characteristic makes it a promising protein for the local transport of drugs. As previously stated, BSA is a highly studied and well-known protein, with known behaviours in terms of aggregations and interactions. It is highly stable, easily available, and low-cost, all these qualities make it undoubtedly one of the currently known model proteins par excellences.

The structure of BSA reported in Figure 1.4 is composed of a single polypeptide chain, organized into three domains (I, II and III), each one formed by six helices[19]–[21]. At room temperature, its secondary structure is predominantly α-helical. BSA has two tryptophans, whose position is indicated by the blue arrows in Figure 1.4, embedded in two different domains: Trp134, located in domain I, in a hydrophobic pocket near the surface of the protein molecule; Trp213 located in an internal part of domain II[20]. BSA have an Isoelectric point of 4.5-4.7[19]. This causes the protein to become

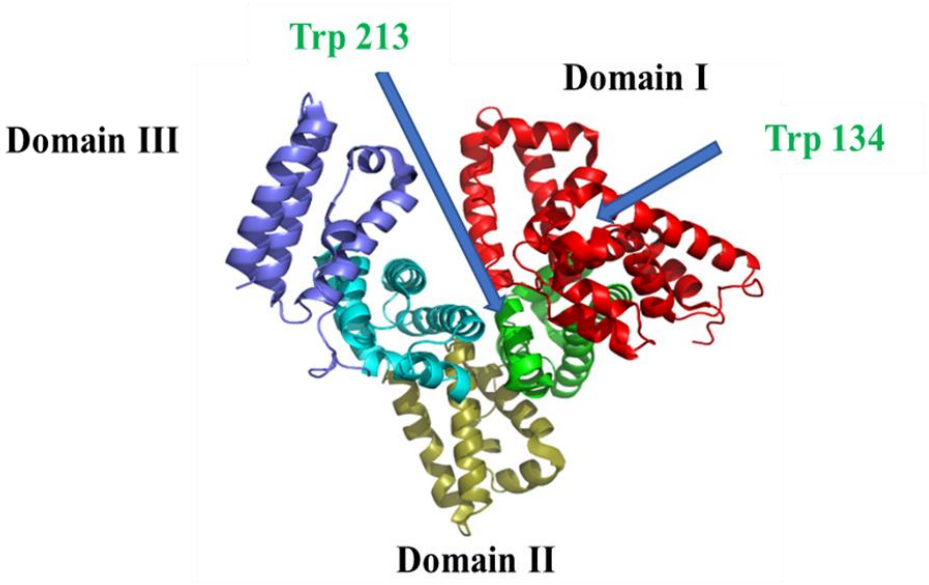

Figure 1.4. Crystallographic structure of Bovine serum Albumin. Modified from Protein Data Bank (PDB 4F5S).

negatively charged at alkaline pH and positively charged at acid pH. The electrostatics of the protein play an essential role during the protein aggregation process. The 17 disulphide bridges ensure some rigidity within each subdomain but at the same time allow significant modifications in the shape and size of serum albumin in response to changes in pH and other influences[21].

Several studies were carried out to characterize the BSA aggregation at different solution condition, pH, and temperature[19], [21], [22]. Results indicate that net charge of the protein, and so electrostatics interaction play a fundamental role in protein aggregation. When the temperature rises, the native structure of a protein can partially unfold and expose reactive areas that lead to aggregation. The pH of the solution can be adjusted to steer the aggregation process towards the formation of amorphous aggregates or fibrils. Amorphous aggregates form mainly through hydrophobic interactions at pH values near the isoelectric point, where electrostatic repulsion is lacking. At pH values far from the isoelectric point, larger repulsion between molecules slows down aggregation and promotes the structural reorganization of the protein. This can result in the growth of fibrillar structures characterised by β-structures at molecular level [21]. The dependence of the final structure's morphology as a function of pH in the low concentration regime for BSA aggregation in aqueous solution is sketched in Figure 1.5.

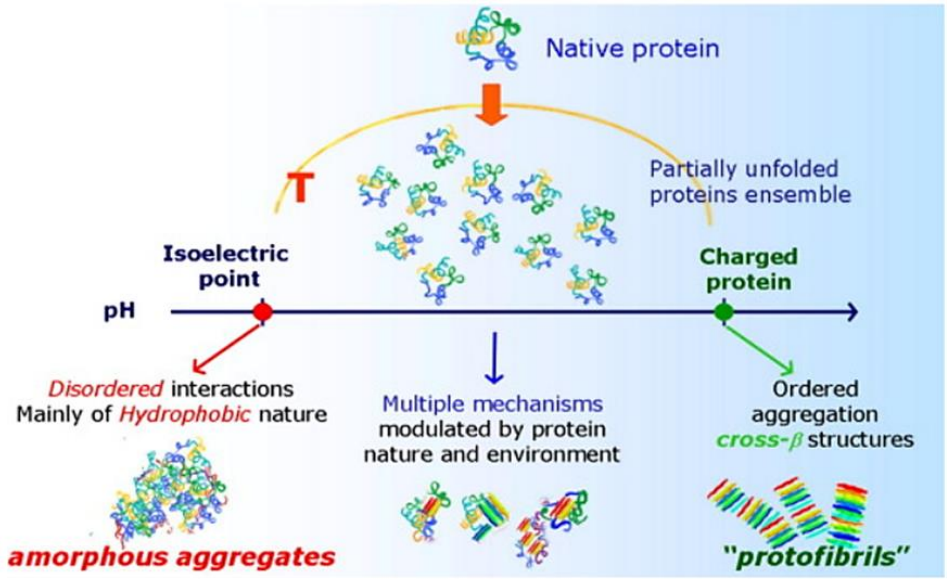

Figure 1.5. Proposed mechanism in the BSA protein aggregation as a function of different pH. Images was modified from [21].

1.6 BSA and EGCG interactions

Several studies on the interaction between BSA and EGCG under different solution conditions were conducted, they highlight the large variety of factors which may modify it, nevertheless, a unified description doesn't exist yet, and the results reported in the literature are often antithetical.

The interaction between EGCG and BSA has been widely studied by using mainly spectroscopic methods such as fluorescence and Circular Dichroism. Scientific results highlight the fact that intrinsic fluorescence of BSA was strongly influenced by the presence of EGCG. A big quenching of intrinsic fluorescence intensity of BSA is reported. BSA has two tryptophans residues, Trp213 and Trp134, which show intrinsic fluorescence[21]. This quenching was explained by a possible interaction of EGCG near one of the two tryptophans of BSA. This interaction was evaluated in some studies as strong (covalent)[23] or in other cases of weaker (electrostatic) magnitude[24]. The interaction seems to occur near the Tryptophan 213, buried in the hydrophobic task in the domain II. Circular Dichroism analyses reveal that BSA changes its secondary structure in presence of EGCG, but only at very high concentrations[23].Other researchers do not find the same results[24].

The interaction between the polyphenol and the protein has been studied by varying different physical and chemical parameters. One parameter that strongly affects the interaction between the two

compounds is the pH. The modification of pH strongly affects the electrostatic interactions, which certainly influences the behaviour of the two compounds. There are different studies that have investigated this interaction by varying the pH with a spectroscopic approach. Skrt et al. [24] in 2012 had made a study where different polyphenols and EGCG were tested at pH 7.5 in the presence of BSA. They founded that EGCG had a remarkable quenching effect on the intrinsic fluorescence of the protein. They propose that the quenching effect it is related to a binding event of EGCG near Trp213. Skrt also found a red shift of the intrinsic fluorescence peak of BSA in presence of EGCG, so a change in tertiary structure of BSA. Soares et al.[25] found similar fluoresce results at pH 4 and 5, individuating no differences in term of BSA quenching in both pH. They founded an equal interaction with both BSA tryptophans. A recent study[23] has reported a BSA-EGCG interaction at different pH 7.4, 5 and 3. Results indicate a different Tryptophan quenching from 3 to 7.4. Different fluorescence quenchings are related to different interactions from BSA and EGCG. They found that the big interaction from BSA and EGCG occur at neutral pH, with negatively protein charge. They also confirm a change in the tertiary structure of the protein during the EGCG interaction at neutral pH. By supposing a binding near the Trp213 like Skrt, they propose a covalent binding of EGCG in BSA hydrophobic task.

Different scientific studies have provided about varying responses regarding the interaction between BSA and EGCG. The results are highly conflicting and unclear and this makes the topic currently debated. In Chapter 4, a study will be presented, it's aim is to characterize this interaction process. By using both spectroscopic and microscopic approaches, it will be demonstrated the results obtained from examining the interaction between EGCG and BSA while altering the electrostatic of the process.

2 Membrane-Protein interactions: from neurodegeneration to model membranes

2.1 Introduction

The neuronal membranes are crucial for numerous processes that maintain cell integrity; dysregulation or dysfunction of the membrane is observed in many neurodegenerative pathologies. The recent evidence highlights the importance of the plasma membrane in regulating the main mechanisms leading to neurodegeneration in illnesses like Alzheimer's, Parkinson's, and synucleopathies[26], [27]. Abnormal processing of protein markers such as amyloid precursor protein, prion protein, and alpha-synuclein, which interact with the plasma membrane, is predicted to cause changes in their function and binding properties. These markers can accumulate in an abnormal state, leading to neuronal impairment and adverse effects such as oxidative stress, lipid metabolism defects and impaired neuronal trafficking[28]. To date, the mechanism of interaction between proteins involved in neurodegeneration and cellular membranes is not very clear yet. It seems that the interaction may lead to processes that thin out or even break the cell membrane with a superficial type of interaction[29]. Studying these very complex processes by using systems that mimic and simplify the problem, can help us to understand the entire process. After an introduction to the protein-membrane interaction problem, the most used printing biology techniques will be presented together with a focus Dip pen nanolithography and Microcantilever spotting. Finally, a state-of-the-art of membrane-protein interactions will be presented.

2.2 Protein-membrane interactions in neurodegeneration

Direct interactions of misfolded protein assemblies with the outer lipid leaflet of the plasma membrane contribute to their binding to cells. The cellular phospholipid membrane, also known as the plasma membrane, is a thin, flexible layer that surrounds and encloses the contents of a cell. It is composed primarily of phospholipid molecules, which form a bilayer that acts as a barrier between the inside and outside of the cell[30]. Other components of the membrane include proteins, cholesterol, and other lipids that help to maintain the structure and function of the membrane. The phospholipid membrane is selectively permeable, it means that it allows certain molecules to pass through while preventing others from doing so. This is essential for maintaining the proper balance of nutrients and waste products within the cell, and for regulating the exchange of signals and other important molecules between the cell and its environment. Various mechanisms have been suggested for the cytotoxic impact, including membrane disturbance, permeabilization of pore-like membranes[27], as well as more subtle actions like destabilization or thinning of the membrane. Protein assemblies that are pathogenic could bind to multiple molecules on the surface of cells. Despite not possessing any specific receptors, these protein assemblies interact with a variety of membrane-associated molecules and protein assemblies[31].
They display distinct surface properties which lead to vary affinities towards molecules at the cell surface. These protein assemblies attach themselves to the plasma membrane of both neuronal and non-neuronal cells, resulting in harmful effects that alter lipid bilayer fluidity, membrane structure, and the regular distribution of membranous proteins. One of the factors that seem to underlie the interaction mechanism is electrostatics which is the basis of the protein-membrane interaction[32]. Negatively charged membranes appear to be more susceptible to this type of interaction[33]. The composition of the membranes is another factor that determines the interaction, in particular the presence of cholesterol[34] or sphingomyelin[33] increases the probability of protein-membrane interaction. Some studies have instead shown that some proteins involved in neurodegeneration do not have a specific phospholipid binding related to the involved membranes.

An example of proteins involved in these interactions is α-synuclein (α-Syn), a protein that is responsible for Parkinson's disease. The protein's monomeric structure is predominantly found within the presynaptic terminals of the brain, while smaller amounts can be found in other organs such as the heart, muscle, and other tissues. Monomeric α-Syn consists of 140 amino acid residues and has a molecular weight of 14.4 kDa[35]. Typically, it is soluble and characterized by intrinsic disorder. Various morphologies such as chain-like, pore-like (annular), and tubular have been observed in the oligomeric α-Syn that emerges from the aggregation of multiple monomeric units. Both oligomeric

and polymeric (fibrillar) configurations of α-Syn have been associated with cytotoxicity. The full length α-Syn molecule comprises three distinct areas: the N-terminal, the non-Aβ component (NAC), and the C-terminal regions[36]. The N-terminal region, which spans 60 amino acids, includes seven imperfect hexameric repeats that are highly conserved, each consisting of the same 11 residues without gaps, with a motif of KTK(E/Q)GV[37]. These amino acids could self-assemble into an amphipathic alpha-helix, which can bind to membranes with different lipid compositions. The localization of α-Syn in the presynaptic synapse could result in its interaction with synaptic vesicles, which may have a crucial impact on the modulation of synaptic plasticity and the release of neurotransmitters[38]. α-Syn is present in intrinsically disordered states, when it interacts with membrane it adopts α -helical structure[37], [39].

The simple mechanism of interaction between membranes and α-Syn it is summarized as an example in Figure 2.1. In the initial phase in 2.1A, the unfolded native protein approaches the membrane, and in the following stages sketched Figure 2.1B, it attaches to the lipid membrane undergoing changes in the secondary structure.

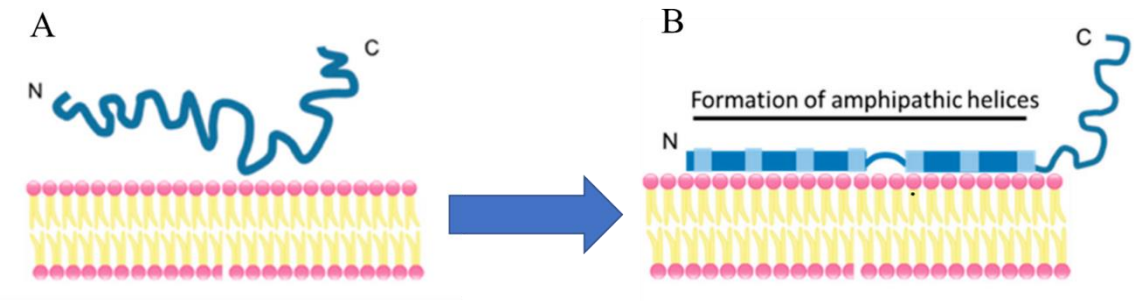

Figure 2.1. Model of binding process from phospholipids membrane and α-synuclein. A) an unfolded α-synuclein near a phospholipid membrane before the interaction. B) After the structural change of the protein, α-synuclein bind to membrane. Figure was modified from [39].

All forms of α-Syn, (monomer, oligomer, and fibril), are responsible for membrane binding and remodeling, (e.g.induced membrane curvature)[40]. To date, many questions are still unresolved, such as the mechanisms of protein unfolding, why only a part of the protein interacts with the membrane, and the function of alpha-syn, among others. These disordered proteins present numerous difficulties in the study of aggregation and interaction processes, the explanation of phenomena and

their interaction is often not easy to follow and interpret. This because they are not easily available, we need stable protocols to obtain them, furthermore they are very expensive and intrinsically unstable.

Since the interaction processes between proteins and membranes are regulated by fundamental laws, it is possible to use model proteins for their study in order to overcome to these issues, it will help to better understand the general mechanisms of interactions. An example is provided by the work of Trusova[41], where the lysozyme is used as a model protein, specifically lysozyme monomers and fibrils that interact with lipid vesicles. The study shows that both lysozyme monomers and fibrils interact with the vesicles. The interaction of the fibrillar aggregates is stronger and induces a destruction of the vesicle membrane. The forces within the interaction are made of electrostatic and hydrophobic type. Another example is Vetri's work [42], in this case Concanavalin A is used as a protein model. They have shown that oligomeric Concanavalin A is toxic to neuroblastoma cells and attaches to the cell membrane inducing apoptosis via an extrinsic pathway. These examples demonstrate how model proteins help us understand complex phenomena by simplifying the system.

The analysis of protein membrane interaction may be exploited by coupling bulk methods within situ imaging experiments in order to study the mechanisms involved in the initiation and growth of amyloid species, since the very early events. Bulk experiments give the possibility to systematically investigate the effects of environmental factors on the various phases of aggregation in the presence and in the absence of and the effects of small molecules. Energy barriers of the occurring reactions can be quantified and averaged information about the behaviour of an ensemble of molecules can be readily obtained.

Fluorescence microscopy methods may be used for non-invasive, real-time analysis of amyloid growth dynamics, eliciting specific features with non-ergodic behaviour, this method may give better performances on mincronsized lipid membranes built over a suitable coverglass, this will provide fully controllable models in terms of composition, size, and geometry. The ability of selecting simultaneously membrane composition and environmental properties (pH, salt concentration, presence of specific molecules in membrane or in solution) may lead to the definition of suitable models for the molecular mechanisms involved in amyloid related pathology. A new experimental approach inspired from “synthetic printing biology” will be employed to do that.

2.3 Synthetic Printing Biology

The fabrication of bioanalytical platforms from material-saving approaches is of paramount importance to reduce the cost of analytical devices[43]. Indeed, analytical assays in small droplets (especially at sub-picoliter scale) are the workhorse for multiplex biological analysis coupling minimal samples volumes with maximized chemical/biological information. Indeed, the miniaturization of devices is also beneficial in making them portable and lightweight. Molecular printing employs both 2D and 3D printing methods, which can be executed using contact and non-contact techniques[44]. Contact methods involve the use of a dispensing tool that physically interacts with the substrate, such as Pin Printing, Microcontact spotting, and Dip Pen Nanopatterning[45]. This contrasts with non-contact methods, such as Inkjet Printing. Besides materials science, the development of printing approaches has also advanced various bio related fields, including genomics[46], proteomics[47], and biochips manufacturing[48]. Recently, it has also emerged as a valuable tool in Synthetic Biology, which originated in the 20th century with the creation of simple protocells in the laboratory to study artificial life assemblies. Synthetic Biology employs two different approaches, i.e., the so called top-down and bottom-up[49].

The first approach pertains to practical techniques that originate from metabolic and genetic engineering, which introduce external biomolecular components or modules into living cells, often in the form of DNA fragments or complete genes. On the other hand, the bottom-up approach involves combining molecular or biomolecular building blocks outside of living systems to create structured and effective biosystems. Synthetic Biology, with a bottom-up approach, creates synthetic compartments with nanoscopic membranes that become increasingly complex. These compartments include lipidic or polymeric membrane-bound assemblies such as liposomes[50] and polymersomes[51] respectively, as well as oil-in-water and water-in-oil[52] emulsions stabilized by amphiphilic membranes.

2.4 Printed Phospholipid: Useful models for studying proteins and membrane interactions

Dip pen nanolithography is a technique of nanofabrication in which a small-scale pen is dipped into a solution containing nano-sized particles, such as molecules, metal ions, or quantum dots. The pen is then maneuvered over a surface to deposit the particles, creating a pattern or design[43]. DPN-based Printing Biology places a high emphasis on phospholipids as they are crucial biomolecules found in cell and organelle membranes. This has led to the development of the L-DPN acronym for lipid patterning using DPN. Interestingly, phospholipid inks possess unique properties compared to

diffusive and liquid inks. Phospholipid molecules on the DPN tip undergo hydration, which depends on humidity, then they are released onto the substrate[43]. Once hydrated, these molecules diffuse towards the support via the water meniscus like a diffusive ink environment. The using of phospholipid inks, displays a unique combination of properties from both diffusive and liquid inks. This offers exciting possibilities for molecular printing with alternative rheology. Additionally, the chemical structure of phospholipid molecules, specifically the hydrophobic chains, plays a crucial role in maintaining ink fluidity during printing. Therefore, it is important to maintain a suitable printing temperature above the transition temperature. It is also worth noting that L-DPN can be carried out in aqueous environments using these inks. To ensure suitable ink fluidity and achieve a successful direct-writing process, it is essential to maintain the temperature above the transition temperature[44]. Interestingly, the use of aqueous solutions is also possible for L-DPN by leveraging the insolubility and stability of lipid patterns in water. When deposited by DPN, these patterns can form multiple stacks of hydrated bilayers. Solid lipid bilayers are printed membrane models which allow a very interesting and promising mimicking of cellular membranes. These SLBs can be obtained with various printing biology techniques, but one of the best suited for the printing and production of these models is DPN. Hence, by using DPN, we can obtain multiple membrane models using very small quantities of ink. By varying parameters such as dwell time, substrate hydrophilicity, and glycerol content, for example, it will be possible to change the geometry and final dimensions of the lipid spots. These systems deposit on surfaces such as glass or mica mimic cellular compartments. Numerous studies report the protein-membrane interaction with SLBs. An example of interaction is reported in Figure 3.2, where the interaction between fluorescent membrane models and Sar1 is shown. As depicted in Figure 3.2B, after just over eight minutes, we have a remodelling of the bilayer into semisphere[53]. Vikulina et al. [54] proposed a study to explore the feasibility of using a soft bio polyelectrolyte-based multilayer substrate as a cellular interface to support a lipid bilayer. Milhiet [55] proposed the spontaneous insertion of phosphatase into model lipids. A crucial factor to consider would be the fluidity of the bilayer, which is linked to the lateral mobility of the lipids. This factor could be affected not only by the type and composition of the lipids, but also by the labelling of the lipids, the surface on which they are placed, and the way in which the surface is cleaned[56]. Another parameter that can be monitored and measured through these systems is the curvature of the membranes. Curvature is a parameter that affects the formation of lipid domains. Cheney[57] created a model that reproduces the curvature of a double layer phospholipid by using a surface modelled with nanoparticles. Sekula [58] developed a new platform of HEMA polymer for binding studies using microcontact spotting approach.

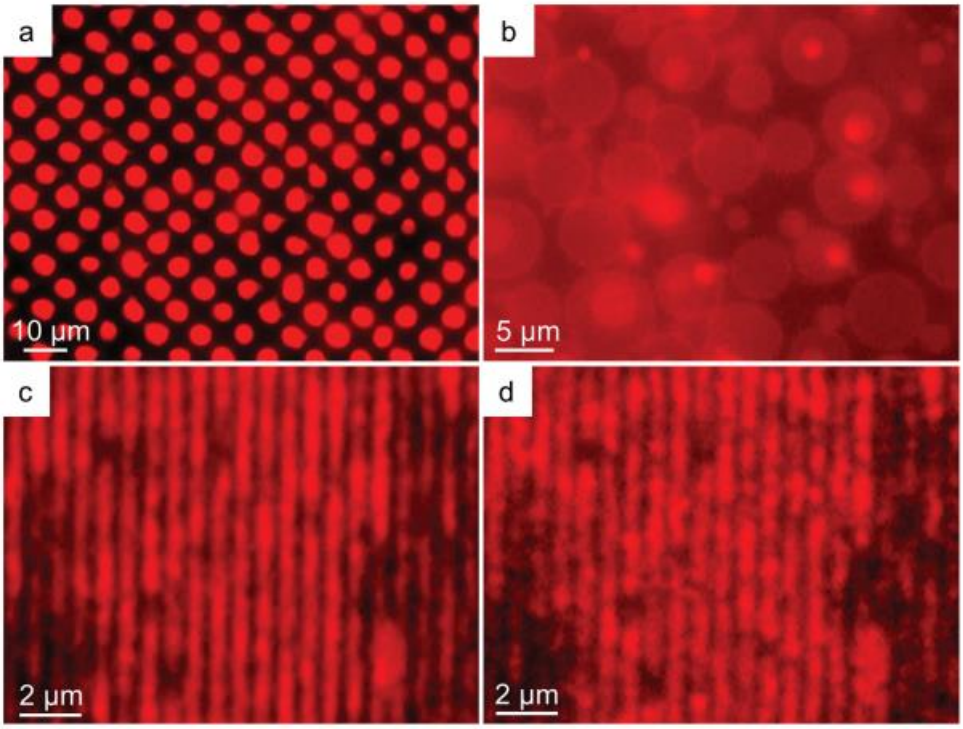

Figure 3.2. Fluoresce microscopy of fluorescent lipid multilayer exposed to protein Sar1. a) initial step of florescent SLBs. b) after 7.5 min of incubation with Sar1. c) grating before addiction of Sar1. d) Grating after incubation of 25 minute at Sar1. Figure was modified from [53].

The versatility of these instruments makes them an excellent model for the cell membrane in basic science studies. [23],[24]. Undoubtedly, this technique boasts an exceptional level of precision, even though its major drawback is its incessant ink refill, particularly when producing numerous spots. Hirtz[58] has tackled this predicament with the "surface patterning tool" (Spt), which employs a microfluidic channel linking an ink reservoir to a miniature tip positioned at the end of a cantilever. Termed "microchannel cantilever spotting", "microcantilever spotting" or “microcontact spotting” (µCS), this innovation provides a feasible solution to this issue[59]. This technique leverages the same benefits and peculiarities of DPN, but additionally, it is possible to print thousands of spots without the ink refill issue.

In this work, µCS was used to study the interaction processes between fluorescent anionic membranes and model proteins through the variation of the involved electrostatic forces (Chapter 5).

3 Materials and Methods

3.1 Aim of the Chapter

This chapter will shortly describe the fundamentals of the experimental techniques used in this thesis together with a recap of the methods used in the performed experiments.

The chapter presents two different approaches for investigating the interaction between a model protein and an anti-aggregating molecule. The first approach utilizes spectroscopic and fluorescence microscopy methods to provide detailed characterization of the sample morphology and describe possible interactions. The second approach uses fluorescence microscopy techniques to track the interaction between printed molecules by using an innovative technique of printing biology and model proteins.

Bulk experiments such as steady state fluorescence or circular dichroism (CD) in cuvette are used to systematically investigate the reactions and provide averaged information about the behaviors of an ensemble of molecules. However, the chapter emphasizes the use of quantitative fluorescence microscopy methods in order to follow dynamic events in real time and provide information immediately.

The final part of the chapter will highlight the importance of accurate samples preparation and treatment procedures in obtaining reliable experimental results on fibril formation. An overview of the materials, samples preparation, and treatment procedures will be provided for the reader's convenience.

3.2 Model Protein and Anti-aggregogenic molecule methods

3.2.1 UV-vis absorbance

The absorbance of ultraviolet-visible (UV-vis) radiations by intrinsic chromophores is a commonly used method for measuring samples concentration. Absorption measurements were carried out on a Jasco V-570 Spectrophotometer before each kinetic experiment, the protein concentration was obtained from the BSA molar extinction coefficient 43.824 $cm^{-1}M^{-1}$[19], [21]. The EGCG concentration was obtained from EGCG molar extinction coefficient 11.500 $cm^{-1}M^{-1}$ [60].

3.2.2 Circular Dichroism

Circular dichroism (CD) spectroscopy is an analytical method employed for the examination of optically active substances, which are characterized by their chiral properties. It measures the discrepancy in the absorption of light that is polarized in left and right circular directions. Particularly, in the far ultraviolet region, the technique exhibits an exceptional ability to detect changes in the proteins structure at the molecular level. It is noteworthy that the signal arises from the peptide bond chromophore, which is in a structured and organized environment[61].

Figure 3.1 reports that the alpha helix motif exhibits significant CD bands with negative ellipticity at 222 and 208 nm, and positive ellipticity at 193 nm[62]. A broad negative band near 218 nm and a large positive band near 195 nm characterize beta-sheets, while disordered extended chains display a weak broad positive CD band near 217 nm and a large negative band near 200 nm. The protein's overall spectrum is the sum of its conformational elements' spectra. As a result, CD spectroscopy is a valuable tool in structural biology that can be used to analyse proteins, polypeptides, and peptide structures and to monitor any structural changes that may occur because of changes in environmental conditions such as pH, temperature, ionic strength, and/or interaction with other molecules.

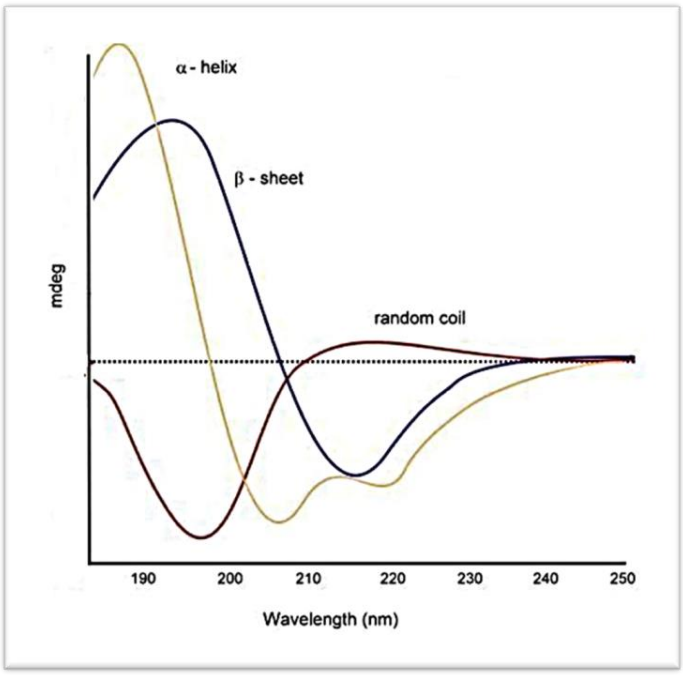

figure 3.1. Different "pure" protein secondary structure by CD measurements. Figure was modified from[62].

In our work the CD measurement was used to evaluate the change in BSA secondary structure as a function of changing in pH, interaction with EGCG or changing due to an aggregogenic process.

Experimental settings: Measurements were performed using a Jasco J-1500 spectrophotometer equipped with a Jasco PCT 348WI temperature controller. Complete CD spectra, as well as single wavelength CD data during kinetics experiments were taken in the far UV region. Sample cell paths were 0.2 and 0.5 mm for complete spectra and single wavelength measurements, respectively. Spectra were sequentially recorded, using a scan speed of 50 nm/min, 1 nm bandwidth and a data pitch of 0.1 nm with 3 accumulations. For measurements at RT, ten spectra were averaged to improve signal to noise ratio. Variations in the absorption spectra and significant changes in the HT value during these measurements were not observed.

3.2.3 Rayleigh Scattering

Rayleigh scattering is a physical phenomenon which describes light scattering from small particles whose size is smaller than the wavelength of the light. In this hypothesis, the scattering intensity is related to the size of the particles. It is possible to conceptually divide particles into smaller regions known as scatterers. In practical applications, individual atoms or molecules can be chosen as scatterers, by using their known scattering and absorption cross-sections[63]. In case of small particles (x<<<1), where each particle is made up of multiple scatterers, the scenario is simplified because all the individual scatterers emit waves that are in phase, leading to constructive interference between the scattered waves. For particle composed of *n* identical scattering cross section [63] (1):

$$\sigma_{sca} = \left(\sum_{i=1}^{n} \sqrt{\sigma_{sca}\_i}\right)\text{^}2 = n^2 \sigma_{sca}\_i \quad (1)$$

Were n^2 is equal to the product of number density N and particle volume V. For spherical particle, the cross action can be written as (2):

$$n = NV = N\frac{4}{3}\pi r^3 \quad (2)$$

where r is the radius. Scattering cross-action becomes (3):

$$\sigma_{sca} = (NV)\text{^}2\sigma_{sca}\_i = \left(\frac{4}{3}\pi\right)\text{^}2 r^6\, \sigma_{sca}\_\text{i} \quad (3)$$

This equation relates the cross section of an individual scattererσ_{sca}_i to the cross section σ_{sca} a small particle in the Rayleigh regime, neglecting effects due to the interaction between scatterers [63].

The Rayleigh scattering was used during the kinetic aggregation of BSA in order to monitor the increasing of dimensions of the BSA aggregates in presence or in absence of EGCG at both pH.

3.2.4 Dynamic Light Scattering (DLS)

Dynamic light scattering (DLS) utilizes the Brownian motion of particles dispersed in a liquid to measure their hydrodynamic diameter. The principle of Brownian motion involves particles colliding with solvent molecules, which transfer energy and induce particle movement.

The Stokes-Einstein equation (8) describes the relationship between particle size and speed, with the speed determined by the translational diffusion coefficient D (4):

$$D = \frac{k_B T}{6\pi\eta R_H} \quad (4)$$

were k_B is the Boltzmann constant, T is temperature in K, η is viscosity.

Experimental settings: DLS measurements were performed on the aggregate solutions with a Zetasizer nano-s (Malvern instruments). The samples were inserted in a Uv-cuvette semi-micro 1,5 ml and the analyses were run 3 times for every sample. The parameters of measurements are temperature 25 °C, material RI 1.45, dispersant RI=1.330, viscosity 0,8872.

3.2.5 Isothermal Titration Calorimetry (ITC)

ITC is a titration-based method for binding interaction analysis, performed in solution at constant temperature where only the thermal effects are measured. Practically, every change in absorbed or released heat were captured from the instrument. One of the best advantages of ITC is its capability to offer a complete thermodynamic overview of an interacting system through a single experiment. This includes the determination of enthalpy, entropy and association or dissociation constant, and in addition the identification of the stoichiometry of interaction. Thanks to this technique it was evaluated the possible binding interactions between BSA and EGCG at pH 5 and 7.

Experimental settings: Binding of EGCG to BSA was analysed by calorimetry using a MicroCal PEAQ-ITC instrument (Malvern Panalytical). Prior to ITC analysis recombinant BSA and EGCG were dissolved in potassium phosphate buffer 0.1M pH 7 or pH 5. EGCG binding to BSA was evaluated in buffer pH 7 or pH 5 by titrating 2 µl of 250 µM or 370 µM EGCG solution into the sample cell containing 18 µM protein. The reference cell of the PEAQ-ITC was filled with ultrapure water. Experiments were performed at 25°C, with 19 injections (the first injection was of 0.4 µl). The initial spacing was set at 60 s and the spacing between injections was set at 150 s. The Sample cell stirring was set at 150 r.p.m. The DP (Differential Power) between the reference and sample cell was set to 10. Calorimetric data for EGCG binding to BSA were analysed by using the "One Set of Sites" model included in the Microcal PEQ-ITC analysis software (Malvern Panalytical). Data from control titrations were subtracted prior the analysis.

Calorimetric data were fitted using the one set of binding sites model. The fitting models were used to determine the binding constant (Ka) and the enthalpy variation associated with binding (ΔH). Then, ΔH and Ka values were used to calculate the variation in free energy (ΔG) and entropy (ΔS) through the following equations (10,11):

$$\Delta G = -RT \ln K_a \quad (5)$$

$$\Delta G = \Delta H - T\Delta S \quad (6)$$

The dissociation constants were obtained from the fitted Ka using (7):

$$K_d = 1/Ka \quad (7)$$

3.2.6 Fluorescence

Fluorescence is an advantageous method for studying biological systems and the different processes that happen inside them. This phenomenon involves the absorption of light by an electron, which results in its transition to an excited state and subsequent emission of light upon its return to the ground state. Such processes are often represented through a Jablonski diagram (Figure 3.2), which showcases the different steps involved between absorption and emission of light. When excited by light, the molecules experience a rapid transition from a ground state (S_0) to higher singlet excited states in mere femtoseconds. Afterwards, non-radiative processes referred to as internal conversions, cause these electrons to undergo vibrational relaxation to the lowest vibrational level of the excited state (known as S_1). At this point, radiative or non-radiative processes allow the dye molecules to return to the ground state (S0). Being a radiative process, fluorescence witnesses the fluorophores' molecular decay from S1 to the ground state by emitting easily detectable photons within a timescale of 10^{-9} seconds[64].

When vibrational relaxation and internal conversions cause the energy loss required to reach level S1, it results in a red shift of fluorescence emission relative to absorption (Stokes shift). The effectiveness of emission is established by quantum yield (Φ), which is the number of emitted photons divided by the total number of absorbed photons[64], [65]. Additionally, Φ equals the ratio of the rate of radiative transition (kr) to the total rates of all transitions (kr + knr) that involves the excited state.

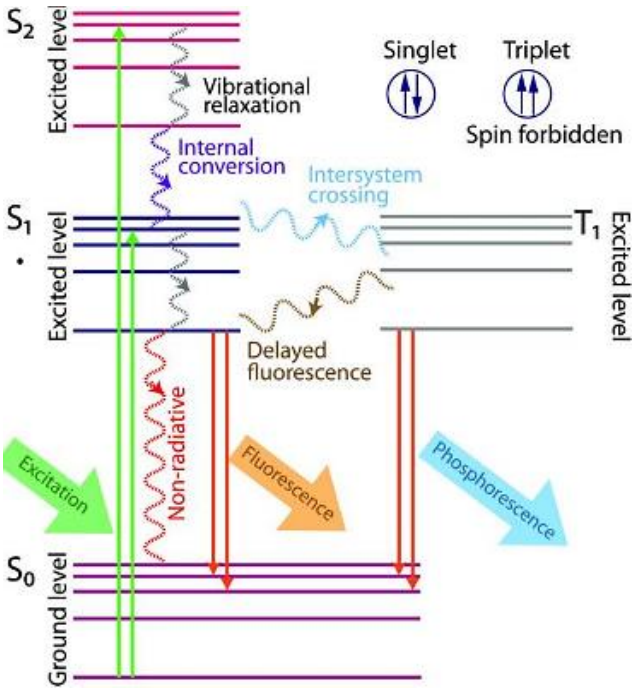

Figure 3.2. Jablonski Diagram. Image was modified from [65].

Consequently, any non-radiative depopulation of the excited state due to a molecular mechanism reduces the quantum yield (8):

$$\Phi = k_r / k_r + k_{nr} \quad (8)$$

The time response of fluorescence is a significant feature, where the excited molecule population produced at the excitation moment (t=0) steadily diminishes through radiative (k_r) and non-radiative (k_{nr}) transitions towards the ground state. This process is characterized by the fluorescence lifetime τ (9):

$$\tau = 1 / k_r + k_{nr} \quad (9)$$

3.2.7 Steady state fluorescence: intrinsic and extrinsic

Intrinsic fluorescence

Intrinsic fluorescence of proteins is sourced from aromatic amino acids, typically tryptophan's one is the higher contribution. Tryptophan fluorescence is highly responsive to polarity changes in the surrounding environment. For example, a red shift in the emission spectrum may indicate a decrease in fluorescence intensity due to Trp residues that were exposed to polar conditions, while a blue shift signals an increase in hydrophobicity around Trp residues[66]. Emission spectra changes from tryptophan can occur in response to various processes such as protein conformational transitions, aggregation, molecular binding, or denaturation, affecting the environment surrounding the indole ring, which reflects in spectra changes.

Experimental settings: Steady state fluorescence measurements were carried out on a Jasco FP-8500 equipped with a Jasco ETC-815T Peltier-thermostat in order to follow the kinetic aggregation in presence or not in presence of EGCG at pH5 and 7. Samples were positioned in a 1 cm path quartz cuvette, and after thermal equilibration, the emission spectra were recorded with 0.5 nm wavelength intervals, emission and excitation bandwidth of 3 nm, scan-speed of 100 nm/min and integration time of 1 s at λ_{exc} = 270 nm (intrinsic). The tryptophans emission spectra were obtained under excitation at λ_{exc} = 270 nm, wavelength chosen as a good compromise between spectral quality and the requirement to avoid significant tyrosine contributions to the emission. Simultaneously, Rayleigh scattering was also measured as the maximum of the elastic peaks of the excitation light at λ_{exc} = 270 nm. The experimental errors were about 5% for fluorescence and scattering data. Spectra were analysed by calculating the integrated intensity of the spectral distributions after subtracting a suitable baseline.

Extrinsic fluorescence: Nile Red, ANS

The use of different extrinsic fluorescent dyes presents supplementary opportunities for protein characterization. Extrinsic dyes can be covalently affixed to proteins through lysine's, ε-amino group, the N-terminus' α-amino group, or cysteine's thiol group, or can non-covalently interact with proteins through hydrophobic or electrostatic interactions. The interaction between dye molecules and proteins can cause fluorescence emission changes by altering the preferred relaxation pathway, which has resulted in many applications in protein sample characterization. These applications include monitoring refolding and unfolding processes, evaluating surface hydrophobicity, investigating

active sites of enzymes, characterizing aggregation and fibrillation, and tracking conformational changes induced by chemical degradation.

This work used 1-Anilinonaphthalene-8-Sulfonic Acid) or ANS to characterize the binding interaction between an antiaggregogenic molecule (Epigallocatechingallate) and a model protein BSA during the kinetic aggregation process. ANS is a hydrophobic and negatively charged dye ANS which is commonly employed to examine the surface hydrophobicity of proteins, as well as their unfolding/folding and aggregation conformation[67]. ANS interacts with proteins through hydrophobic and electrostatic interactions between the negatively charged sulfonate groups and the positively charged amino acids (such as histidine, lysine, and arginine), which can lead to alterations in the polarity and viscosity of the surrounding environment and consequently changes in the emission spectrum. Specifically, exposure to a more hydrophobic environment elicits a more intense fluorescence and a blue shift in the spectrum.

Nile Red or (9-diethylamino-5H-benzo[α]phenoxazine-5-one) was used for the characterization of BSA aggregates and for the characterization of phospholipids spot. Nile Red is an uncharged hydrophobic dye, used to localize and quantitate lipids, particularly neutral lipid droplets[68], [69]. In proteins, Nile Red attaches itself to the hydrophobic surfaces, which become exposed and accessible for binding. In a setting that is hydrophobic, Nile Red displays a high quantum yield and emits a bright fluorescence; however, when placed in an aqueous medium, Nile Red is considerably insoluble, resulting in significant quenching of its fluorescence[69]. A representation of the chemical structure of the two compound is showed in Figure 3.3.

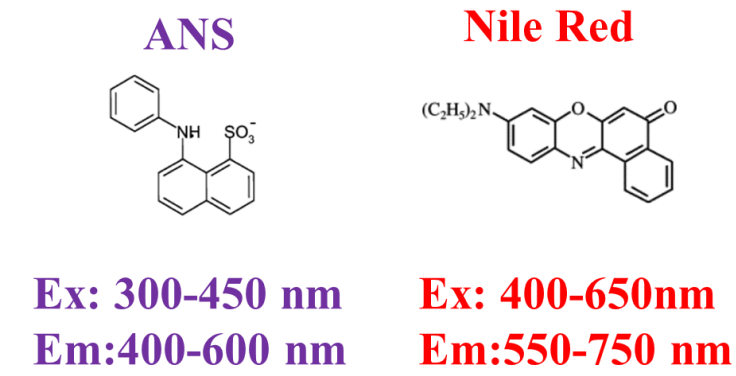

Figure 3.3. Chemical structure of fluorescent dyes. ANS, and Nile Red chemical structure with respective excitation and emission values.

3.2.8 Confocal Fluorescence Microscopy Measurements

Confocal fluorescence microscopy is a microscopic technique that provides true three-dimensional (3D) optical resolution. To achieve true 3D resolution in confocal fluorescence microscopy, it is necessary to actively eliminate any signal emanated from planes that are out of focus. This is

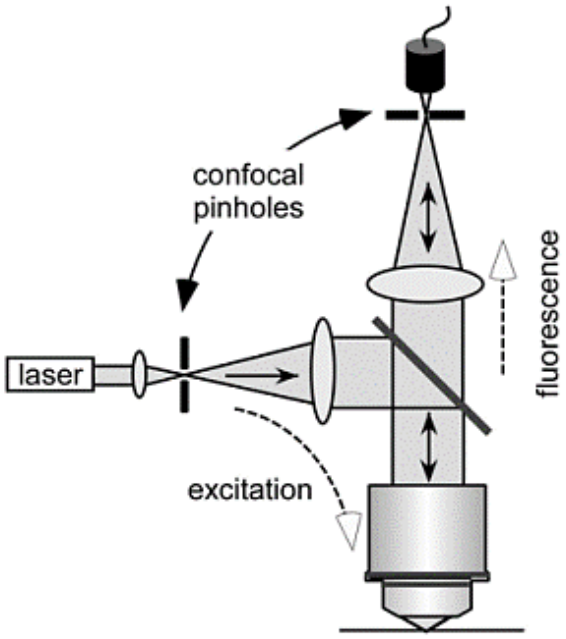

Figure 3.4. Confocal fluoresce microscopy scheme. Image was modified from [70].

accomplished by implementing a pinhole in front of the detector, as illustrated in Figure 3.4. The microscope objective captures light from the in-focus plane and allows it to pass through the pinhole, while significantly obstructing light originating from out-of-focus planes. In a confocal fluorescence microscope, a laser is commonly used to illuminate the specimen. The process of generating contrast is referred to as "excitation" rather than "illumination," as it specifically involves the absorption and subsequent fluorescence of fluorophores[70]. The laser light goes through an excitation pinhole and is bounced off a dichroic mirror before being concentrated to a tiny area in the specimen by a microscope objective. The dichroic mirror reflects shorter wavelength light (e.g. 488 nm from an Argon-ion laser) and allows longer wavelength light to pass through (e.g. fluorescence >510 nm from fluorescein). Dichroic mirrors can be customized to accommodate the specific wavelength ranges of excitation and fluorescence.

Confocal fluoresce microscopy was used to characterize the morphology of the BSA aggregates and specially to follow the interaction processes between membrane models and model proteins.

Experimental settings: Fluorescence microscopy experiments were performed to characterize the BSA in presence or not in presence of EGCG at pH5. Depositing aliquots of 300 μ of protein aggregates solutions diluted 1:2 v/v with a 40 μl of Nile Red on the microscope-chamber cover glasses (Lab-Tek II Nunc), after the aggregation of BSA with and without EGCG at pH=5 the measurements were acquired using an oil objective 60x (1.2 NA) of Olympus FluoView 1200 confocal laser scanning microscope (Olympus, Japan) with a λ_{exc} = 515 nm e λ_{em} = 600-700 nm.

BSA Diameters distributions analysis: analysis was obtained via measuring different diameters using imagej-win64, manually measuring 20 particles from 5 different images. Data were exported in .txt format and were analysed and plotted with Origin software.

Fluorescence lifetime imaging microscopy (FLIM)

FLIM is a form of fluorescence imaging that utilizes fluorescent chromophores lifetime as source of contrast in the sample. FLIM techniques offer numerous benefits in studying biological specimens that are complex and constantly changing. Their dynamism and heterogeneity make them particularly suited for FLIM measurements. FLIM offers a significant benefit compared to fluorescence intensity imaging, as fluorescence lifetimes remain unaffected by variations in fluorophore concentration and laser excitation intensity.

The phasor analysis, described by [71] was used for the analysis of FLIM data. Phasor approach is a Fourier domain technique that allows the transformation of the signal in every pixel of the image to a single point called “phasor”. The phasor plot includes s and g coordinates that are defined by the normalized Fourier sine and cosine transforms expressed through the following relations (10,11):

$$g_{i,j}(\omega) = \int_0^\infty I(t)\cos(n\omega t)dt / \int_0^\infty I(t)dt \quad (10)$$

$$s_{i,j}(\omega) = \int_0^\infty I(t)\sin(n\omega t)dt / \int_0^\infty I(t)dt \quad (11)$$

where ω is the laser repetition angular frequency, and the indexes i and j identify a pixel of the image.

In this representation, all possible single exponential decays lie on the “universal circle” defined as a semicircle, with radius 1/2, going from point (0, 0), corresponding to $\tau = \infty$, to point (1, 0), corresponding to $\tau = 0$. Instead, complex decays are represented by phasors within the universal circle. Importantly, given that the phasors follow the vector algebra, it is possible to geometrically resolve the fractions of two fluorescent species (in the simplest case) by the lever rule of vector additions. Indeed, the linear combination of two single-exponential decays components generates phasors within the universal circle (Figure 3.5), which lie on a straight line joining the phasors of the two single components[72]. The contribution/fraction from one single component to the lifetime is proportional to the distance of the phasor from it. In the phasor plot, it is also possible to select these lifetime distributions using coloured cursors and the corresponding pixels will result with the same colour of the cursors to the image pixels by which the so-called “lifetime maps” are obtained. Following previous results in the literature, it may be concluded that if the membrane-sensitive dyes exhibit single-exponential. FLIM data have been processed by the SimFCS software (Laboratory for Fluorescence Dynamics, University of California, Irvine, CA, available at www.lfd. uci.edu). FLIM calibration of the system was performed by measuring the known lifetime of the fluorescein that is a single exponential of 4.0 ns.

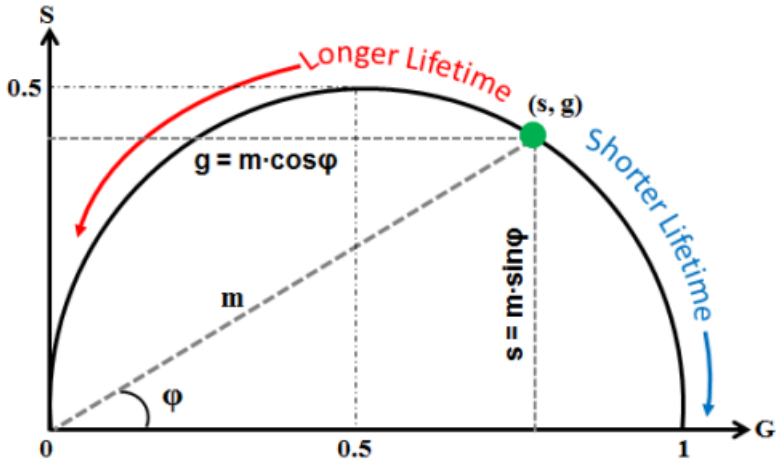

Figure 3.5. The phasor plot vector space and the universal circle. A single decay component is represented by a point (s,g) on the universal circle. Image was modified from [72].

FLIM Experimental settings: 256 × 256 pixels FLIM images were collected depositing aliquots of 300 µL of protein aggregates solutions diluted 1:2 v/v with a 40 µl of Nile Red (2M) on the microscope-chamber cover glasses (Lab-Tek II Nunc), after the aggregation of Bovine Serum Albumin with and without EGCG at pH=5, in the time domain using the Leica TCS SP5 microscope coupled with a PicoHarp 300 TCSPC Module (PicoQuant, Berlin, Germany). Nile Red fluorescence was acquired using excitation at 550 nm from the pulsed White Light Laser (Leica Microsystem) in the range 570-700 nm. Images was analysed using ImageJ 1,53t (Wayne Rasband).

3.2.9 Epigallocatechin-gallate (EGCG): a fluorescent antiaggregogenic probe

EGCG (Figure 3.6A) is the major catechin in green tea, it exhibits antioxidant[73], [74], anticancer[75] and antiaggregogenic[76]–[78] properties. The presence of many exposed hydroxyl groups, makes molecule extremely reactive. Figure 3.6B reported the absorption and emission spectra of EGCG as a function of a different solution condition.

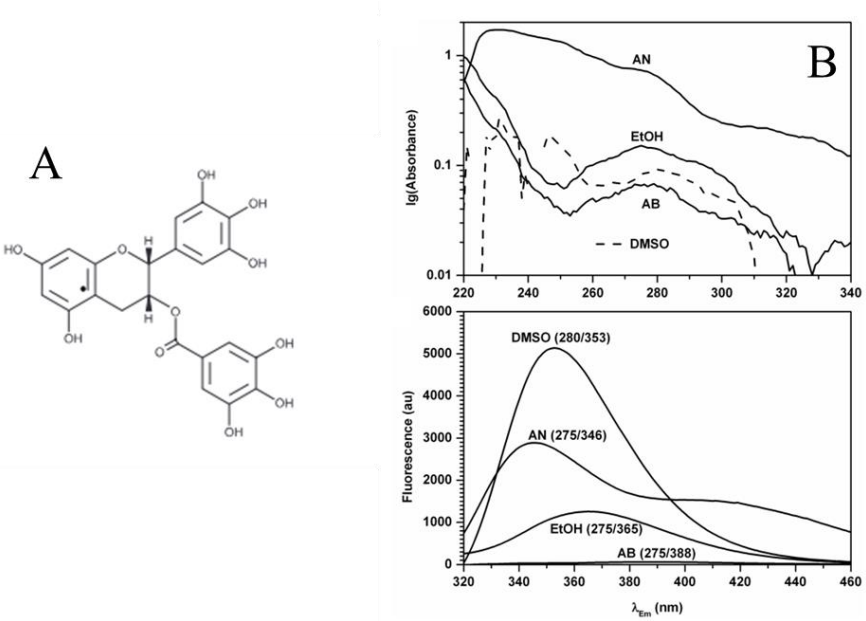

Figure 3.6. Chemical structure of EGCG and spectral properties of EGCG. A) chemical structure of EGCG. B) spectral properties of EGCG in different solvent solution dimethylsulfoxide (DMSO), acetonitrile (AN), ethanol (EtOH), and aqueous buffer (AB). Figure was modified from[79].

EGCG is a highly fluorescent molecule when excited approximately to 275 nm with emission maxima between 350 and 400nm depending on the solvent. It shows that the fluorescence intensity is particularly quenched in aqueous buffer, and 80 times higher in DMSO[79]. In general, it can be said that with this solution-dependent system which drastically changes the intensity and emission of fluorescence, it can be used to distinguish whether EGCG is in a polar environment or not. Generally, EGCG shows a big stability at acidic pH. A change in pH dramatically changes the stability of the molecule. An increase in temperature increases the degradation of the EGCG compound. In this work, EGCG solution was used as an antiaggregogenic molecules and was tested in a kinetic aggregation with BSA at two different pH[80].

3.2.10 Atomic Force Microscopy (AFM)

Scanning probe microscopes (SPM) define a broad group of instruments used to measure properties of material, chemical, and biological surfaces. SPM images are obtained by scanning a sharp probe across a surface while monitoring and compiling the tip sample interactions to provide an image.

Atomic Force Microscopy (AFM)[81] allows high-resolution imaging of surfaces by using a cantilever with a micrometric tip and laser beam, which can scan in three dimensions. The AFM can maintain a constant distance between the probe and the surface while scanning; a feedback system adjusts the voltage to the piezoelectric component to correct for any changes in distance. Various scan techniques are available, including contact and non-contact modes, tapping mode is preferred for biological specimens in order to prevent surface degradation. Image formation involves the manipulation of the tip's position while recording the measured variable, furthermore it creates a colour map that displays the intensity of the value as a hue. A scheme of AFM was reported in Figure 3.7. AFM images were fundamentals to characterize the dimensions and the geometry of the BSA aggregates after the kinetic aggregations at 60°c for both pH.

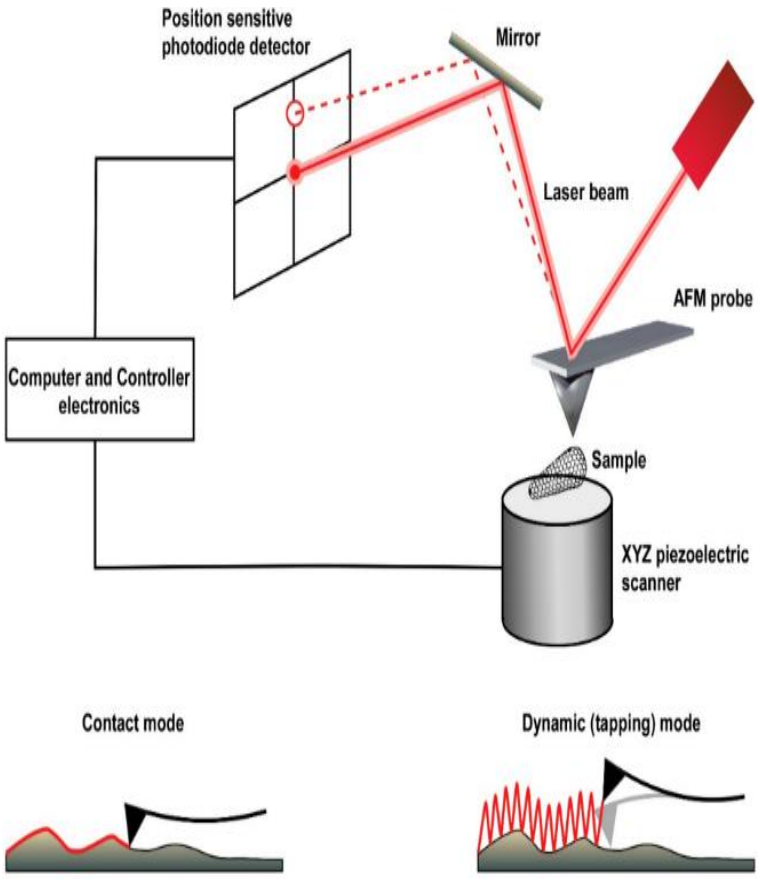

Figure 3.7. A schematic drawing of the main components of an atomic force microscope (AFM). The AFM is composed of an XYZ piezoelectric scanner, a laser source, a position-sensitive photodiode detector (PSD), and a controller. Below were reported two possible measurement modes: tapping and contact mode. Figure was modified from [81].

Experimental settings: The AFM images were acquired in air by means of a Bruker FAST-SCAN microscope equipped with a closed-loop scanner. The scans were obtained in tapping mode by using FAST-SCAN-A probes with a pixel resolution comparable to the tip size. The diameter of the nanoparticles was estimated by evaluating their height from the AFM scans. Images were analysed using Gwiddion 2.57 (2020). AFM were used for the analysis of the aggregates of BSA with and without EGCG at pH=7.

Aggregates height distribution analysis: Data were obtained from different images of BSA, from different AFM profile extracted using Gwiddion 2.57, data were analysed with the OriginPro2017 software. By using the function "peak analyser", it was analysed more than 100 peaks for every sample.

3.2.11 Samples preparation

Bovine Serum Albumin (BSA), Epigallocatechingallate (EGCG), 8-anilino-1-naphthalenesulfonic acid (ANS), DOPE was purchased from Sigma Aldrich, DHPE-FITC was purchased from Thermo Fischer and they were used without further purification. All the measurements were performed in Potassium phosphate buffer 0.1 M at pH 5 and 7. Every solution was freshly prepared and filtered just before the measurements and the protein concentration was spectrophotometrically determined. The protein concentration was approximately 7 μM.

EGCG Stock solution: A stock EGCG solution was prepared every 48-72 hours by dissolving the powder in milliQ water at a final concentration of 1 mg/ml. The solution was covered to avoid direct exposure to light. It was kept in the fridge and diluted 1 to 10 for the experiments. Every time it was used, an absorption spectrum of EGCG was made to evaluate the stability of the molecule.

EGCG oxidation: EGCG was solved in a Potassium phosphate buffer 0.2M pH=8 in a concentration of 2 mg/ml following[18], 1 ml of solution was inserted in an Eppendorf and had been heated for 24 hours at 37 °C. Changes in EGCG structure were confirmed from changes in colour solution and through Absorption measurements.

Protocol for AFM measurements: The aggregate solutions of BSA obtained from kinetic aggregation in cuvette at 60°C at pH5 and 7, were diluted with milliQ water 1:100 v/v; 36 μl of the

solution were spattered on mica samples, after 1 minute, sample were washed with fresh water twice, then the sample were dried with nitrogen flow to eliminate all the liquid phase.

3.3 Printing Methods

The fabrication of artificial biosystems is essential to comprehend the physicochemical principles that govern droplet formation processes and their compatibility with solutions containing biomolecules, also known as "molecular inks," as numerous printing methods are used in the process. Commonly, the molecular ink droplet can be expressed by using three dimensionless quantities: the Weber number We, the Ohnesorge number Oh, and the Reynolds number Re (12-14)[44]:

$$We = (\rho D V^2)/\sigma \tag{12}$$

$$Oh = \mu/(\rho\sigma D) \tag{13}$$

$$Re = We^2/Oh \tag{14}$$

The variables used in these equations include ρ, representing the density of the fluid (kg m^{-3}) , D denoting the diameter of the droplet in meters, V indicating the velocity of the droplet in (m s), μ representing the dynamic viscosity of the fluid in (mPa s), and σ indicating the surface tension of the fluid in millinewtons per meter. The We number is a measure of the ratio between inertial and surface tension forces, while the Oh number relates the viscous force to inertial and surface tension forces, and the Re number represents the ratio of inertial to viscous forces. These numbers are employed to quantify the droplets formation conditions and the droplet impact process into the substrate.

Printing technologies can be categorized into contact and non-contact methods. Among the contact printing techniques, Pin Printing, Microcontact spotting, Dip Pen Nanolithography (DPN), Polymer Pens, and Hard-Tip Soft-Spring Lithography are the most significant ones for Printing Biology[43].

3.3.1 Microcontact spotting approach

DPN is primarily concerned with the transfer of materials, with ink-coated scanning probes, also known as tips which are used to transfer materials into a substrate through a connecting meniscus. DPN enables the direct transfer of a diverse assortment of material "inks" (such as small molecules, polymers, DNA, proteins, peptides, colloidal nanoparticles, metal ions, etc.), ranging in size from micrometers to less than 50nm[43], [44], [49], [82]. An interesting upgrade of the DPN technique is provided by microcontact spotting, a technique that uses the same deposition principles as DPN with two major advantages: it is very economical and does not require continuous ink refilling. In fact, this technique uses an SPT, a surface patterning tool, which has a reservoir inside that allows printing of thousands of spots without ever stopping[43], [58]. The process of materials transport is intricate, influenced by various factors like the properties of the ink, surface tension, wettability at the interface, tip structure, ink coverage on the tip, Laplace pressure, environmental conditions like humidity, temperature, and operational parameters. The properties of the ink, in particular, are crucial and can be categorized as either diffusive or liquid. The first type refers to molecules that are physically adsorbed on the tip surface, while the latter type is made up of actual liquid solutions that contain the material that is being patterned. The inks differ in how they transport the material from the tip to the support[83]. The deposition of diffusive inks can be explained by using a numerical/analytical model based on a two-dimensional diffusion process originating from the tip [43]–[45]. This model assumes that the molecular flux creates a concentration gradient around the tip which triggers the diffusion of further molecules. The feature deposited has a lateral size that is resolved at the nanoscale. This analytical model can be used to explain the radial deposition from the tip by considering the dwell time of the tip on the surface, which is represented by a straightforward expression (15):

$$R\,(t)^2 = 4Dt * \ln\left(\frac{n}{4D\pi\rho}\right) \tag{15}$$

The variables in the equation are as follows: the dwell time contact is represented by t (s), the monolayer density in ($Å^{-2}$), the coefficient of diffusion is represented by D ($\mu m^2\ s^{-1}$), and the number of ink molecules deposited per unit time is represented by n (s^{-1}).

The mechanism behind liquid ink deposition through DPN differs from diffusive methods due to the solvent molecules present in the droplet. Specifically, the formation of droplets occurs due to the difference in Laplace pressure between the ink-tip (ΔPtip) and the ink-air (ΔPm) menisci. Laplace pressure was expressed by the followed expression (16):

$$\Delta P = \sigma\left(\frac{1}{R_1} + \frac{1}{R_2}\right) \quad (16)$$

In order to obtain a successful deposit of the droplet onto a surface, the Laplace pressure on the interface of the tip/meniscus must exceed that one on the meniscus/substrate interface, where R1 and R2 refer to the primary curvature radii and σ represents the surface tension. A representation of the diffusive and liquid ink deposition was reported in Figure 3.8.

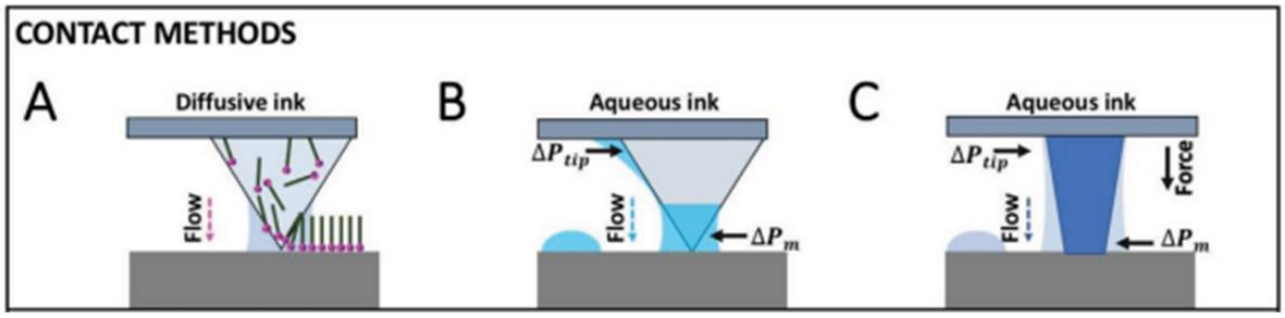

Figure 3.8. Diffusive and liquid inks. A) Diffusive ink printing made from DPN. B-C) liquid deposition made from DPN and polymer lithography respectively onto the surface. Figure was modified from [44].

The reduction in ink thickness leads to a decrease in the energy required for deposition, resulting in a slower growth rate due to the Laplace pressure gradient. As the pen with ink approaches the surface, a meniscus is formed by a mixture of ink and atmospheric water molecules. Immediately after the removal of the pen from the surface, there is a capillary force that attracts the tip. This force becomes zero when the water meniscus breaks, resulting in a micrometer-sized droplet[43], [44]. Therefore, the final size of the droplet is mainly a function of three parameters: the microchannel from which it emerges, the viscosity and the surface tension of the ink. The size can also vary depending on the surface treatment of the printing surface[44], [82]. Typically, biocompatible additives like viscous high-boiling point cosolvents are added to molecular inks to adjust their rheological characteristics. Glycerol is a popular choice due to its ability to stabilize biomolecule structures and reduce potential aggregation in aqueous solutions. Adding glycerol (usually 10-30% v/v) to protein-rich molecular inks has been shown to improve spot definition and resolution, resulting in regular shapes and dimensions. Without glycerol, spots may appear irregular[84].

3.3.2 Printing Deposition Protocol

The microcantilever spotting approach was used to pattern the phospholipids onto the glasses slice. The printing protocol is divided into several parts which are: glasses protocol, ink protocol, printing protocol and cleaning protocol of the surface patterning tool (SPTs). These ones will be discussed in detail later. All the steps that are mentioned below are crucial for the success of the experiment and must be followed diligently.

The **glasses protocol** starts with a division of the slides by a cross, that defines different areas of the sample and helps the operator in order to have some reference points. Subsequently, the slides are washed according to different protocols that define the degree of surface hydrophilicity. We can distinguish among:

- **Highly hydrophilic**: they had been sonicated with an aqueous Hellmanex^{TM}III (a liquid alkaline surfactant) 2% v/v solution for 5 minutes, then sonicated with an aqueous solution for 10 min after that sprayed with milliQ in order to completely remove any surfactant residue. They had been dried with nitrogen, and at last with ozone cleaner treatment for 20 minutes.

- **Hydrophilic**: Washed with water sonication for 10 min, sprayed with milliQ, dried with nitrogen, and at last with ozone cleaner treatment for 20 minutes.

- **Slightly hydrophilic**: they are only sprayed with milliQ water.

Once the slides are dry, they are ready for printing. Two distinct types of phospholipid inks were formulated by employing two dissimilar solvent solutions, namely an ethanolic protocol and an aqueous protocol. The two protocols were distinguished by the solvent medium employed in the solution and the time of phospholipid resuspension in solution. The details of the two ink protocols are described below:

- **Ethanolic Ink**: The methodology used to prepare the ink involved mixing DOPE stock and chloroform [20mg/ml] along with DHPE with Fitc (1:1) in a bottle in a ratio of 50 uL to 0.5 uL, respectively. The solution had been sonicated for 5 minutes before being allowed to evaporate under the hood. Then, the resulting phospholipids had been resuspended in DI water and sonicated for at least 30 minutes to ensure that the ink contained small vesicles below 50

nm, following a protocol similar to the one found in reference[58]. Glycerol was added to prepare the ink with a DI water and glycerol ratio of 8:2. This resulted in a ready-to-use ink for the study.

- **Aqueous Ink**: First, 50 uL of DOPE stock with chloroform [20mg/ml] and 0.5 uL of DHPE with Fitc (1:1) had been combined in a bottle and sonicated for 5 minutes before being evaporated under a hood. This resulted in the formation of phospholipids, which had been resuspended in DI water. Subsequently, the ink had been sonicated for at least 30 minutes to ensure proper mixing and to produce vesicles below 50 nm in size, following a protocol from a previous study[85]. Finally, glycerol was added to the ink, creating a solution with DI water and a glycerol ratio of 8:2. This resulted in a ready-to-use ink for the study.

Printing protocol

During the development of the deposition protocol, we investigated the effects of relative humidity, dwell time, and waiting time on the deposition process. To enhance the hydrophilicity of the probe, we had subjected it to an Ozone cleaner for 20 minutes. We then loaded 0.4 uL of ink into the probe and placed the SPTs slightly further back in the holder behind the T marker. We set the relative humidity to 50% and printed four arrays for one row, varying the dwell time and waiting time between each row. Then, the samples had been dried in a vacuum pump for one hour and allowed to sit for 24 hours for any residual solvent to evaporate. Our results showed that the diameter of the spotted features varied from 15-20 µm, with fluorescence intensity also dependent on dwell time.

After the deposition, it's necessary to clean up SPTs from ink residues in order to have the possibility to reuse it. The **SPTs cleaning protocol** starts with twenty minutes of ozone cleaner treatment, it is followed by a wash made with ethanol to remove any remaining contaminants. The SPTs were then carefully dried using tissue paper (kimwipe) before undergoing another 20-minute ozone cleaner treatment for thorough cleaning. These cleaning steps were crucial to ensure accurate and reliable data in µCS experiments.

3.3.3 UV-Vis Absorbance

The above-mentioned technique (described in 3.2.1) has also been used to study the interaction between protein and membrane models in order to calculate the final concentration of proteins in the

solution by using the molar coefficient extinction. As regards Lysozyme, the molar extinction coefficient was 38.940 $cm^{-1}M^{-1}$[86] and for Concanavalin A was 33.280 $cm^{-1}M^{-1}$[87].

3.3.4 Confocal fluorescence microscopy

The above-mentioned technique (described in 3.2.8) has also been used to study the interaction between protein and membrane models.

Experimental settings: Images were acquired in one or two channels with an Olympus F1200 FluorView confocal laser scanning microscope (Olympus) using a 60x (1.2 NA) objective lens to characterize the interactions between a membrane model (DOPE:DHPE-FITC (1:100)) and protein interactions. Before proceeding with the following of the protein-membranes models interaction, the glass slide had been washed 3 times with 100 µl of milliQ water to remove unbound phospholipids from the glass. Then, a gasket is placed on the monitored area which always allows to have a constant volume on the sample. Samples are hydrated with 400 ml of fresh buffer. After adding the buffer, the protein (lysozyme or concanavalin A) was added at a known concentration ranging from 0.1 to 10mg/ml. The gasket was covered with a microscope glass slide to prevent solution evaporation. During the trial, measurements are taken every 10 minutes of the kinetics without changing the focal plane. Using laser 488 nm to excite Fluorescein DHPE. Images were taken with 1024*1024 pixels resolution.

3.3.5 DHPE-FITC

A fluorescent phospholipid was used to follow the protein model membrane interactions named N-(Fluorescein-5-Thiocarbamoyl)-1,2-Dihexadecanoyl-sn-Glycero-3-Phosphoethanolamine or DHPE-FITC. The DHPE is labelled on the head group with FITC, a hydrophilic green fluorescent dye, pH-sensitive. DHPE and FITC are in a 1:1 molar ratio to each other. FITC shows a big sensitivity in term of shift in maximum emissions as a function of changing in pH. FITC presents a big quantum yield, furthermore, if it is exposed to a neutral or acid pH, it presents a double or single negative net charge[88]. A chemical representation of the dyes was reported in Figure 3.9. Experimental settings were reported previously.

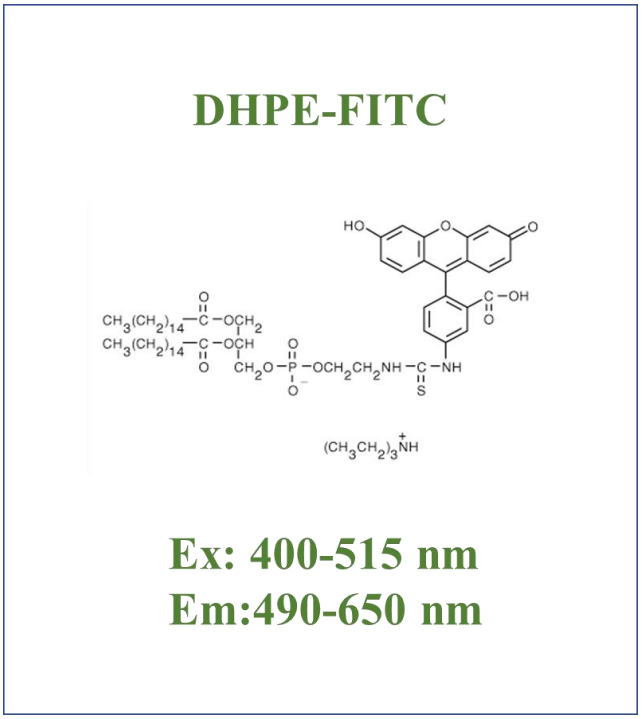

Figure 3.9. Chemical structure of DHPE-FITC. Chemical structure of DHPE-FITC with excitation and emission value.

4 A Model Protein vs Polyphenol interaction: Bovine Serum albumin and Epigallocatechin-gallate a case study

4.1 Introduction and purpose

BSA is considered as a good model protein and it is one of the most studied proteins in literature. This occurs because it is a cheap, stable, and easy to manipulate and soluble protein [19], [21], [89]–[91]. Under specific conditions, BSA (at basic pH), can form fibrillar structures[21]. As reported in the introduction, we worked on the hypothesis that general law regulates protein aggregation and associated phenomena, so, the first part of this study was focused on investigating the mechanism of interaction between EGCG with Bovine Serum Albumin, whose aggregation process have been extensively studied in different conditions by means of biophysical methods depending on the electrostatic forces[92]. This allowed the evaluation of inhibition effects, when present, and the highlighting of the dominant role of electrostatics in protein/EGCG interactions. The interactions and the effect of EGCG on the BSA kinetics aggregation were studied by using a spectroscopic approach and Isothermal titration calorimetry technique. After that, the morphological characterization of protein aggregates in presence or not presence of EGCG was performed both at nano and microscale.

4.2 Absorbance response for EGCG

In Figure 4.1 absorption spectra of BSA in the presence and absence of EGCG at pH 5 is shown in red lines, and at pH 7 in black lines. In green, it was reported the absorption of EGCG in water solution.

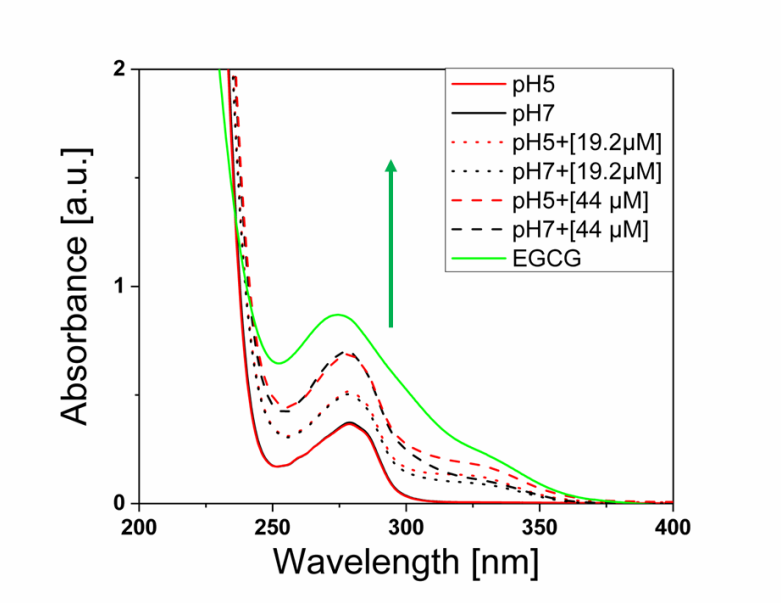

Figure 4.1. **Uv-Vis absorption spectra of BSA**. Uv-Vis Absorption spectra of a 7 μM BSA solution in phosphate buffer at pH 5 red lines and at pH 7(in black lines). Dashed lines report spectra measured at increasing concentration of EGCG dissolved in BSA solution from 19.2 and 44 μM. The EGCG spectra in water solution is reported in green line.

The analysis of BSA-EGCG interaction started from two characteristic values of pH 5 i.e. a pH value near the isoelectric point of the protein (between 4.8 and 4.5[19]), where the protein has a net charge near to zero, and pH7 away from isoelectric point, where the protein has a net negative charge. At pH5, the protein with zero net charge will have a greater tendency to protein aggregation following a disordered pattern[21]. At pH 7, instead, the protein is negatively charged. This choice was carried out in order to have the possibility to highlight the effects of the electrostatic interactions, which are one of the main acting forces during protein aggregation[92]. Furthermore, it's possible to make a comparison between the two conditions to evaluate how the interaction between EGCG and protein affects protein. The EGCG from the stock solution 1M in water was dissolved in BSA solution 7 μM after a dilution 1:10.

Figure 4.1 showed UV-vis absorption spectrum of 7 µM BSA solution in Potassium phosphate buffer at the two pH 5 (red lines) and pH7 (black lines) spectra with an increasing concentration of EGCG from 0 to 44 µM. Green line reports the absorption of EGCG in water solution. Protein spectra at the two pH present a dominant peak centred at about 280 nm, this peak was associated with aromatic residues (tryptophan, tyrosine and phenylalanine) present in BSA structure [93]. After the titration of EGCG, spectrum of BSA changes. At pH 5 and 7, the spectrum has an increasing absorption between 350 and 300nm but in a different manner as a function of solution condition. At pH 7, the increasing of absorption signal was higher than in 5. This difference in term of absorption signal can indicate different interactions between BSA and EGCG. The absorption signal is clearly modified by the presence of EGCG, while the maximum of the absorbance of EGCG corresponds right to the BSA maximum. EGCG also shows another absorbance component from 300 and 350, where the other signal increments are located. EGCG shows different absorption as a function of solvent polarity. The insertion of EGCG inside a protein was equivalent to the exposition of the protein to different polarity [79].

4.3 Fluorescence Interactions studies for EGCG-BSA Compound

In Figure 4.2 the fluoresce spectra of BSA in presence or not in presence of EGCG at pH 5 (red lines) and at pH 7 (black lines) was showed. The Dashed lines in Figure report the fluorescence spectra of BSA at both pH values with an increasing concentration of EGCG.

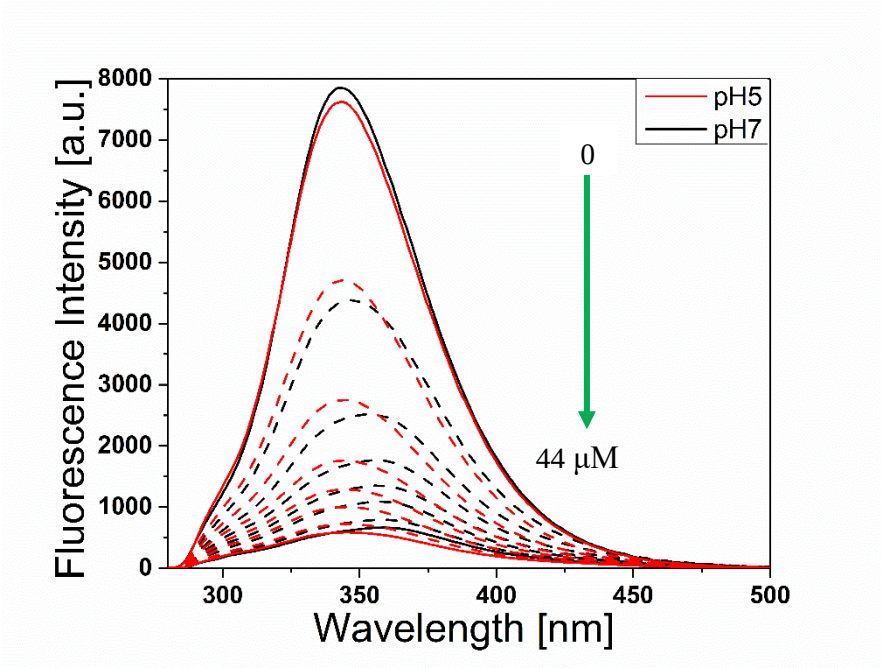

Figure 4. 2. Steady state fluorescence of BSA in presence of EGCG. Steady state fluorescence of BSA of 7 µM of BSA at two pH 5 in red and 7 in black, solved in a potassium phosphate buffer 0.1 M, measured at room temperature, λ_{exc}= 270nm in the range from 290-500nm, from 0 to 44 µM of EGCG. Dashed red and black lines report spectra of BSA with a increasing concentration of EGCG.

Were used an excitation of 270 nm, nearly the maximum peak absorption of BSA and EGCG, in order to better evaluate the signal intensity of BSA and EGCG; it was verified that significant tyrosine contributions were neglectable in the present conditions to the tryptophan emissions and it's able to avoid partial overlap between the Rayleigh scattering peak and fluorescence signal that can alter the analysis of the emission band thus maintaining good spectral quality[22]. Figure 4.2 reports the titration experiment of a 7 µM of BSA solution at pH 5 (red lines) and 7 (black lines) when it was added an increasing concentration of EGCG. At the starting point, BSA shows a big intensity in fluorescence signal with a big emission peak at 343 nm in both pH, after increasing EGCG concentration in BSA solution, the intrinsic fluorescence of BSA was quenched equally for both pH. Intrinsic fluorescence of BSA was due to the presence of the two tryptophan Trp134 and Trp213 [19], [22]. Quenching of BSA may be due to a change in the microenvironment present near the two

tryptophan [22] or a different exposure to the solvent. So, quenching is related to the interaction between EGCG and BSA and can be a binding event near the residues involved in intrinsic fluorescence. A binding event can occur near one of these amino acidic residues. The first hydrophobic pocket of BSA located near Trp134, is more accessible and exposed to the solvent, while the second near the Trp213 is buried into the protein and not easily accessible for the quenchers [22], [93], [94]. Quenching can occur by different mechanisms[64]: Collisional quenching occurs when the excited-state fluorophore is deactivated upon contact with some other molecule in solution, called quencher. In this case, the fluorophore is returned to the ground state during a diffusive encounter with the quencher. The molecules are not chemically altered in the process. During the titration studies, Rayleigh scattering does not change in intensity. If the scattering does not change, it means that even if EGCG interacts with the protein, this interaction does not lead to protein aggregation. BSA fluorescence can be quenched from both static and dynamic quenching indicating Trp134 and 213, these ones can be quenched[94] but there can unequally quench, due to their accessibility in the protein. Trp134, is responsible for 85% of the intrinsic fluorescence of the BSA, it is found on the surface of the protein and it is generally more accessible than Trp213. Our results indicate a quenching similar for both of pH, indicating that at the two pH there is an interaction between polyphenol and BSA. More than 90% of BSA intrinsic fluorescence were quenched in both conditions revealing EGCG as a big quencher for BSA. At high quencher concentrations, only the inaccessible residues will be fluorescent [64]. Maybe both EGCG and Tryptophan residues were interested in quenching; similar affinities suggest two simultaneous modes of interactions: 1) the flavonoid molecules bind within the hydrophobic pockets of BSA and 2) they surround the protein molecule[95]. EGCG has two aromatic rings with four exposed hydroxyl groups. The presence of galloyl moiety in EGCG is maybe related to the quenching capacity near to Tryptophan residues [25].

Several fluorescence studies of BSA-EGCG interactions, under different pH and ions conditions have been conducted, but in some cases, results are different. In 2012 Skrt et al.[24] conducted a study where different polyphenols and EGCG were tested at pH 7.5 in the presence of BSA. They proposed that the interaction between EGCG and BSA occurs near Trp213. Soares et al.[25] found similar trends for BSA-EGCG interaction at pH 4 and pH 5, they individuated no differences between pH and supposed an equal quenching in Tryptophan. A recent study[23] has reported BSA-EGCG interactions at pH 7.4, 5 and 3. They found a big possible binding related to the increasing pH from acid to neutral values. They propose a binding in the hydrophobic pocket of BSA near Trp213. Soares[25] has also conducted an interaction between EGCG and Human Serum Albumin (HSA). HSA presents only one Tryptophan the Trp214, located near the hydrophobic task of the protein,

papers suggest that EGCG binds to the hydrophobic pocket of the HSA. These studies can be compared because HSA and the BSA have the same protein structure. Zhang[96] makes an interaction with EGCG and BSA with and without copper, he found a big interaction at pH 7.4 and this is increased by the copper presence. Binding event from EGCG to BSA can also be confirmed by an experimental observation, indeed in a neutral buffer solution. Usually, EGCG goes into an autoxidation process, we can notice that through the change in the colour of the solution. In presence of BSA, it does not happen, and the solution is clear. That happens probably because EGCG binds in the buried hydrophobic pocket of BSA, which is not exposed to the solvent. Presence of EGCG doesn't change the pH value of the protein solution in both cases (data do not show it). Different results from the papers, suggest that the mechanism of quenching interactions between EGCG and BSA is still not clear. Our results support the thesis according to which binding interaction happens in Trp213, but at high concentration of EGCG, the first one interacts with other surrounding molecules too. In this work we pay attention to the protein charge and binding interactions. At 5 and 7, proteins keep their "heart shape" thus maintaining the two hydrophobic sites[97]. The charge of the protein varies depending on its environment and the interactions with other molecules, particularly, in the proximity of Tryptophan. Usually, quenching interaction was treated with the use of Stern-Volmer models. Quenching models can define if the quencher interacts with the environment near the residues involved in intrinsic fluorescence, furthermore, it defines if there is a static or dynamic quenching due to quencher. The models cannot define better if the quenching interactions lead to the formation of binding sites or not. We prefer to evaluate the binding event through a specifical technique named Isothermal Titration Calorimetry, which will be discussed more in details successively.

It should be noted that the maximum peak of BSA in the case of pH 7 shows a red shift. To make it more visible, we report the points of maximum intrinsic fluorescence intensity of BSA as a function

of EGCG concentration in Figure 4.3. The Figure reported the maximum of fluorescence peak emission as a function of increasing concentration of EGCG, as the Figure shows there is a big red shift of the intrinsic fluorescence of BSA from 343 nm to 359 nm at 7. While at pH 5 no shift was revealed. This red shift at pH 7 can suggest a change in the tertiary structure of the protein or a change in the surrounding environment of Tryptophan, like different polarity, due to the presence of EGCG [64]. The data certainly indicate that something in the system is changing and the environment near one of the two tryptophan of the BSA is affected and probably became more polar [24]. Fluorescence shift and different absorption spectra are consistent with the possible binding of the EGCG compound

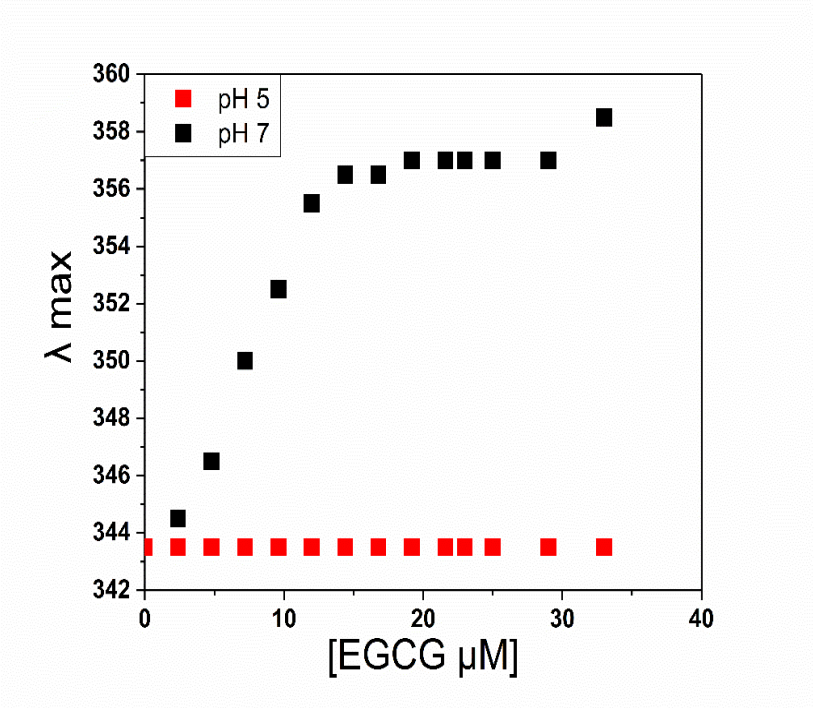

Figure 4.3. Maximum peak of BSA fluorescence as a function of EGCG concentration. Maximum fluorescence intensity at 343nm of 7µM BSA solved in a Potassium phosphate buffer 0.1 M, measured at room temperature, function of increasing concentration of EGCG from 0 to 44 µM at pH 5 (red square) and 7(black square).

near the Trp residues of BSA. A similar result was found from Li[23]. It was found a red shift of the fluoresce signal at pH 7.4, while no shift at acid pH was found. They propose a change in BSA conformation. No shift was found at pH5 and 3. Our data confirm these suggestions. Different absorption spectra are consistent with the possible binding of the EGCG compound near the Trp residues of BSA.[23]

4.4 Circular Dichroism: EGCG changes BSA secondary structure

To evaluate if the secondary structure of BSA was interested in a conformational change due to the interaction with EGCG, a Circular Dichroism (CD) studies were conducted. CD studies were made at controlled temperature 25 °C in both pH at the same concentration of EGCG 8.8 µM, these concentrations were chosen to have ratio near of 1/1 for protein/polyphenol. Figure 4.4 showed the Circular Dichroism spectra of BSA solution in presence or in absence of EGCG from 190 to 260nm.

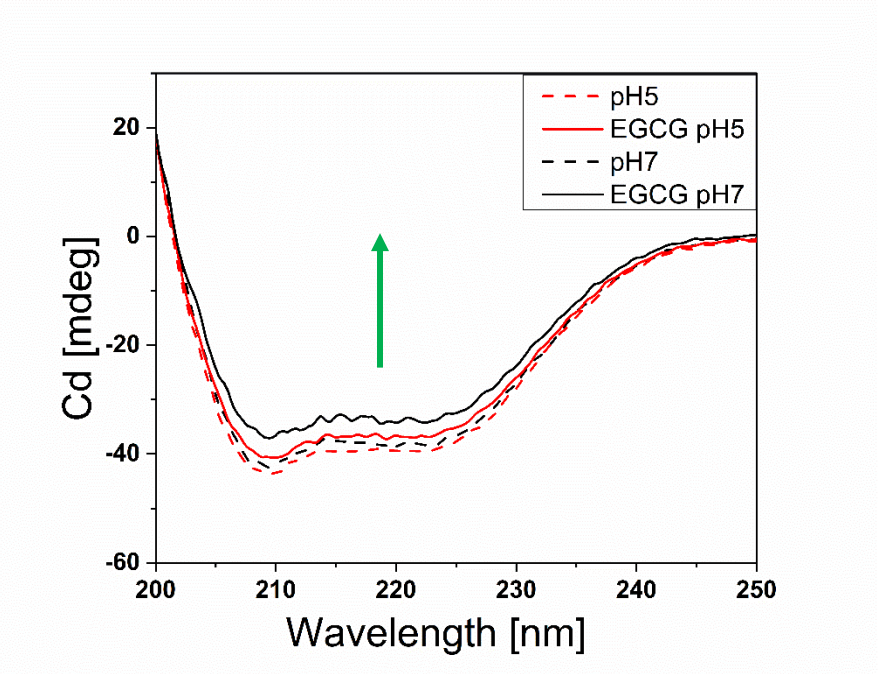

Figure 4.4. Circular Dichroism spectra of BSA with and without EGCG. Circular Dichroism of BSA solution 7µM solved in Potassium phosphate buffer 0.1M at pH5 (red lines) and 7 (black lines) in the presence or not of EGCG 8.8 µM.

Continuous and dashes lines in red are related to the pH 5 while the black lines are related to pH7. The CD spectra of BSA is in the UV region from 190 to 260 nm provided with an information on the secondary structure of BSA.

It has been reported that the native BSA contains 66% α -helix, 3% β-structure, and 31% random coil in its secondary structure[21]. Figure 4.4 reported CD data of BSA solution in the presence or not of EGCG 8.8 µM for both pH. This value of EGCG concentration was chosen to obtain a protein/polyphenol ratio near to one. Data shows two negative bands present at pH 5 and 7, in 208nm and 222nm, those π* typical in protein that has an α-helix structure, which are ascribed to n→ π*, transition, of the carbonyl group of the peptide. BSA is α-helical dominant in the secondary structure of the protein, so a losing of α-helical content, can correspond to an unfolding of BSA [98]. Curves show similar trends in ellipticity from 5 and 7 without EGCG, indicating that the secondary

structure of BSA for both pH is quietly the same. Proteins are more stable near the isoelectric point. PH influences the deprotonation equilibria of polar residues Lysine (Lys), Glutamine (Gln), and Aspartic Acid (Asp) and determines an electrostatic repulsion between ionizable groups. BSA spectra showed dominant [99]99][99][100]. In the presence of the same concentration of EGCG data show a different behaviour at pH 5 small reduction in term of ellipticity were found, which can also be attributed to the absorption of EGCG and no changes in term of spectra were found. While at pH 7, in the presence of EGCG a major decreasing in ellipticity were found. Both Circular Dichroism peak at 208nm and 220nm decreasing, go from 3.4 to 3.3 mdeg for pH 5 to 4.4 from 6.6 mdeg in 208nm at pH 7. A decreasing in ellipticity is associated with a losing of α-helix content and related to unfolding of secondary structure of BSA with related increasing in β-sheets. Reducing in ellipticity was probably involved as the different interactions at the different pH. At other concentrations of EGCG similar results were found (data do not shown). The hypothesis was that the EGCG binding on BSA can affect the secondary and/or tertiary structure of the protein at pH 7. While at pH 5 no changes in term of secondary and tertiary structure were [23] found changes in tertiary structure of EGCG at pH 7 for big concentration of EGCG (200 μM) in CD studies, while with other polyphenols no significant interactions was founded. Skrt et al. pH 7.5 [24] [99]founded at pH 7.4 a little decreasing of ellipticity, indicating a partially unfolding of the protein.

Our CD results are in accordance with [99]; different interactions between EGCG and BSA were found. No changes in term of secondary structure at pH 5 were found. While at pH 7 EGCG affect the secondary structure of BSA, with a possible modification of the secondary structure of the protein. Or the difference in term of Circular Dichroism, was due to the absorbance of EGCG.

4.5 Competitive Binding with ANS

To elucidate the location of the interactions between BSA and EGCG, were performed a competitive binding with 1-aniline-8-naphthalene sulfonate (ANS). ANS was used to investigate changes in the hydrophobic surface of proteins[101] and it is useful to characterize the binding sites of the protein. In Figure 4.5 it is reported an ANS titration study in BSA solution in absence (empty squares) and in the presence (full squares) of EGCG (24 µM). This EGCG concentration was used because, as the hypothesis that EGCG binds near one of the hydrophobic pockets of the protein, it assures that at least one of the two hydrophobic pockets was occupied. Increasing fluorescence intensity was correlated

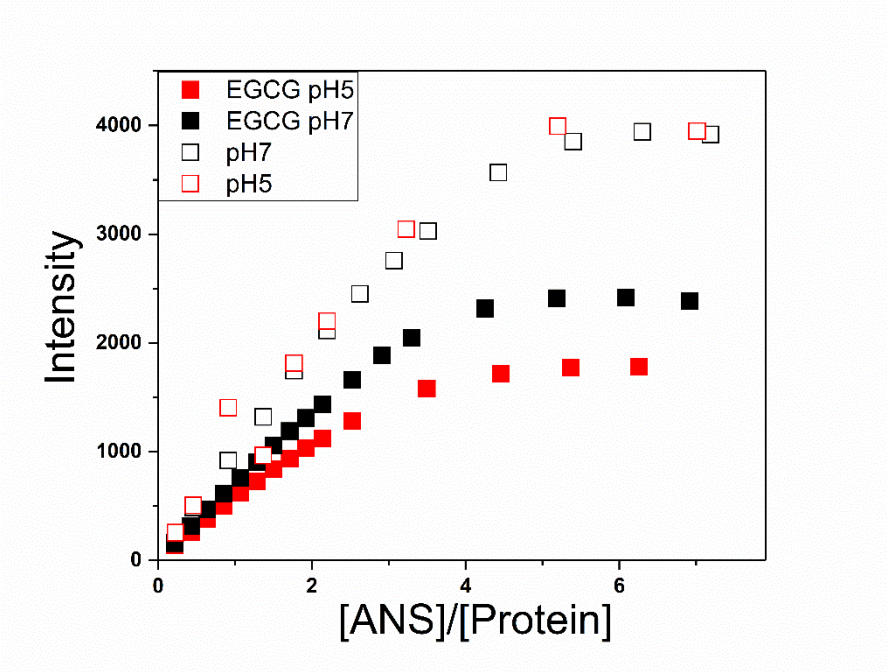

Figure 4.5. ANS binding characterization. Fluorescence Intensity of ANS emission as a function of increasing ANS/BSA ratio from 0 to 7 measured at room temperature in Potassium phosphate buffer 0.1M. Red and black empty squares for ANS titration study respectively for BSA without EGCG pH5 and pH7. Red and black full squares for ANS titration study respectively for pH5 and pH., both pH acquired with λ_{exc}=380nm.

to an insertion of ANS inside the hydrophobic pocket of the protein[101], [102]. The Figure shows an increasing trend in all curves and then a plateau. In absence of EGCG, the trend was identical for both pH levels. However, in the presence of EGCG, the ANS curve is strongly influenced. ANS is a dye that has a low fluorescence intensity in polar environments and showed a big fluoresce intensity, when bind near hydrophobic environments. ANS can show a shift of the fluorescence peak and intensity as a function of the surrounding environment[67]. In our data, no shift of the peaks during the titration studies were observed (data do not shown). Curves without EGCG showed the same increase in fluorescence intensity as a function of increasing concentration of ANS. Curves showed an initial monotonous growth of the fluorescence signal and then a plateau. In BSA, two different

binding sites for ANS are present, located in: the Domain IIIA and IIA, which is the one with least affinity, located near the hydrophobic site of the protein. ANS fluorescence intensity in BSA pure solution shows the same affinity for both pH, this probably means that the ANS affinity for both domains was the same. Intensity was also correlated to the number of possible binding sites of the ANS and binding were the same without EGCG. While, in the presence of EGCG both curves show a decrease in term of fluorescence intensity. ANS/BSA affinity in presence of EGCG was lower. This could indicate that one or more than one binding site of the protein was occupied from EGCG, or hydrophobic regions of the protein are more exposed to the solvent [20]. The affinity of ANS was reduced in the domain II of BSA. After a monotonic increase of the intensity, curves go to a plateau after the molar ratio ANS/protein goes from 1:5 for pH 7 to 1:4 to pH 5. These difference maybe can be due from a different accessibility of the hydrophobic sites of the protein in the presence of EGCG, due to a possible change in the tertiary structure of the protein as shown in the Figure 4.3. The binding nature of ANS to BSA was accepted to be hydrophobic, while other non-covalent forces (electrostatics and hydrogen) can compete with hydrophobic interactions in the binding process. In general, the alterations of hydrophobic surface, are closely associated with changes of protein secondary structures[61]. Therefore, data revealed that EGCG could effectively bind to BSA, enter inside of the hydrophobic region of the protein, and induce further exposure of hydrophobic surface of the protein in solution[103]. Different studies were conducted to characterize the BSA and ANS interactions. Denisio et al.[104] make a titration study with BSA and ANS at pH 7.4 using mathematical approaches, the results concluded that the most suitable binding site for ANS were found near the Trp213 of BSA and a lower affinity to Trp134 was reported. But in general, they have established that ANS affinity is close to one of the two Tryptophan. Tang et al.[90] performed a competitive binding study with BSA and ANS with different flavonoid including EGCG, they found a decrease in term of fluorescence intensity in presence of EGCG, they declared it according to their results in which EGCG binds near the Trp213; it's because EGCG doesn't allow ANS to enter inside the hydrophobic pocket of the protein. Our results are in accordance with Tang results [90]. The presence of EGCG inside the hydrophobic pocket was confirmed by the reduced fluorescence intensity in presence of EGCG. Our data confirm the possibility of binding within the protein's hydrophobic pocket, and they are consistent with previous results. No shift in term of peak on titration study was detected [67], no change in term of surrounding environment was found. The main interaction between the ANS and BSA (bovine serum albumin) is of hydrophobic nature [101]. The interaction between EGCG and BSA is also of hydrophobic nature.

4.6 Detection of binding interactions between BSA and EGCG

To elucidate the number of binding sites of BSA-EGCG interactions and the nature of this possible binding site, we performed an Isothermal titration calorimetry (ITC), that is a useful technique to evaluate the number of binding sites from protein-ligand interactions and for the definition of thermodynamic constants of the binding process. Figure 4.6 reported the ITC for both BSA solutions in presence of EGCG, in particular red squares for pH5 and black squares related to pH7.

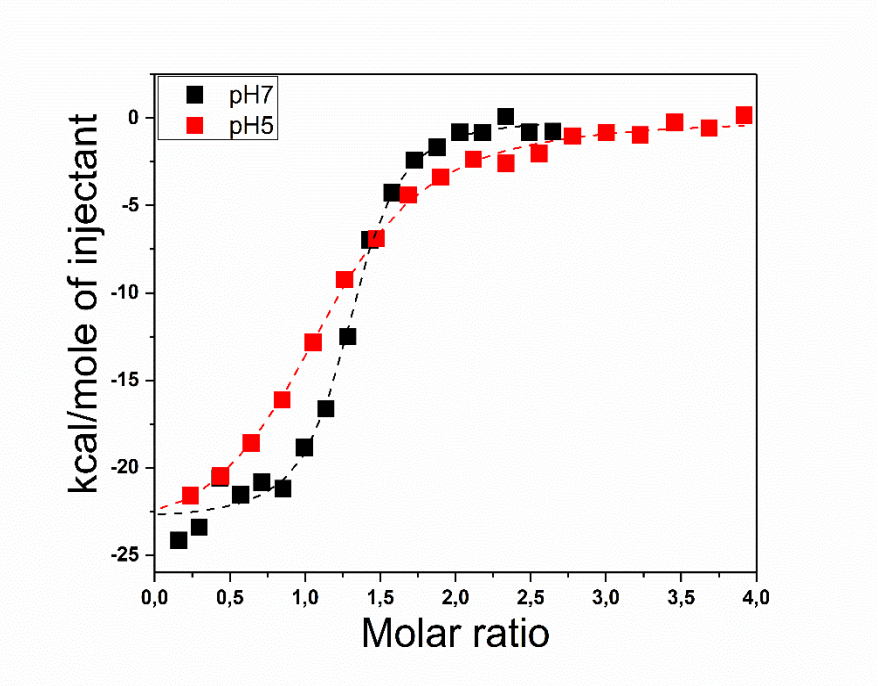

Figure 4.6. Isothermal titration calorimetry of BSA-EGCG. ITC of 18 µM BSA solution in presence of 370 µM(pH5) and 250 µM (pH7) solution of EGCG in a Potassium phosphate buffer 0.1M at two different pH 5 (red square) and 7 (black square). Red and Black dash lines are the fitting data for both pH founded from ITC.

Measurement was made with a BSA solution 18 µM of and 370 µM(pH5) and 250 µM (pH7) solution of EGCG, in the same Potassium phosphate buffer.

ITC is a titration-based method for binding interaction analysis, performed in solution at constant temperature where only the thermal effects are measured. Figure 4.6 shows the plot of the amount of heat liberated per injection as a function of the molar ratio of the EGCG to BSA. A standard nonlinear least squares regression binding model involving one binding site fitted well to the data. The thermodynamic data accompanying the binding of EGCG with the BSA are summarized in Table 1. The observed enthalpy does not have significant contributions from the buffer ionization because phosphate has a small value for enthalpy of ionization[105]. Negative enthalpy was observed, indicating an enthalpy driven exothermic interaction. However, the free energy (ΔG) was similar at

each concentration and was negative, which is a requirement for a spontaneous biomolecular interaction [106]. ΔG value confirms a non-covalent binding for both pH. In each case, the entropy term (ΔS) was negative, indicating that the interaction was driven by enthalpy as opposed to entropy. Negative entropy indicates an increase in molecular order, which would occur upon aggregation and may imply a role for hydrogen bonding in the formation of the complex. The dissociation constant K_d that is the reciprocal of K_a of the two systems were similar. K_d shows a bit higher value at pH7, this suggests a more bigger affinity binding event between EGCG and BSA. At pH 7 positive charges of the BSA are probably involved in binding event, electrostatic probably were a guide for interaction near the hydrophobic pocket. ITC results are consistent with previous data, where it is supposed only one site binding of EGCG near the Trp213 in the Domain II of BSA. ITC results shows that the binding interaction can be only on "one site". Principal forces involved in the process are electrostatics, due to the charge of the protein and hydrophobic, due to the interaction with hydrophobic residues. Hydrogen bonding may be involved in binding event, and it helps to stabilize the interaction.

pH	n (sites)	K_d ($x10^{-6}M$)	ΔH (Kcal/mol)	ΔG (Kcal/mol)	-TΔS (Kcal/mol)
5	1.10 ±0.02	2.35 ±0.03	- 5.9 ± 0.08	-7.7	-1.7
7	1.26 ±0.02	0.36 ± 0.82	- 5.51 ± 0.16	-8.8	-3.2

Table 1 - Binding parameter of ITC. Binding parameters accompanying from the ITC studies: n number of binding sites, K_d dissociation constant, ΔH enthalpy, ΔG free energy, ΔS entropy.

Similar studies were made by BSA and EGCG using Isothermal Titration Calorimetry: Frazier R. et al.[107] studies the binding interaction of epicatechin (same family of EGCG) with BSA by ITC. Results, in accordance with our data, indicated non-covalent binding of epicatechin to BSA. The energetic interactions varied with the BSA concentration in the calorimeter cell, suggesting that the binding of epicatechin (a polyphenol similar to EGCG) induced BSA aggregation. The free energy (ΔG) remained constant within a range of 47 Kcal/mol and negative entropy was observed, indicating an enthalpy driven exothermic interaction. Non-covalent epicatechin-BSA complex is formed by hydrogen bonding. Eaton et al.[108], found a multi-site binding for the EGCG with HSA with a K_d value around 40 mM, it indicates a binding in the two hydrophobic pockets K_{d1} = 21 µM and K_{d2} = 30 mM in result; it's also confirmed later with Nuclear magnetic resonance (NMR) K_{d1} = 19 µM and K_{d2} = 40 mM. They suppose that the binding interactions were inside Sudlow's I and II in the hydrophobic pocket of the protein. One binding site was found in Pal and co-worker's study[97], they

make a work with the BSA and other polyphenols like EGCG, Epicatechin and Epicatechingallate (polyphenols belong to the same family as EGCG) at pH 6.7. They found a one site binding process, with negative enthalpy and positive entropy related to hydrophobic and electrostatic interactions involved in binding event. Our results supporting the one binding site model, because other spectroscopic measurements are in accordance with ITC data. Our value of K_d result like Eaton e co-worker[108]. In the binding process are involved electrostatic, hydrophobic, and probably the H-bond. The binding was not covalent, value of ΔG is not consistent with this possibility. Our results support the hypothesis of EGCG binding to the hydrophobic pocket of the protein, in an internal area, not exposed to the solvent. The ITC was consistent with the spectroscopic results previously shown. Spectroscopic studies, in the presence of ANS confirmed the binding in the hydrophobic pocket near the Trp213, confirming the presence of a hydrophobic component. ITC results were consistent with the one-site binding model for EGCG, in accordance with Frazier [107].

In the next paragraph, the study of EGCG interaction during the macromolecular aggregation process of BSA at two different pH levels will be addressed. Its antiaggregating capacity will be evaluated, as well as the capacity of oxidized EGCG. Finally, an understanding and characterization of micro or nano aggregates will be carried out in order to fully characterize the entire process.

4.7 Kinetic Aggregation of BSA with EGCG

A kinetic aggregation study between BSA and EGCG was presented in this paragraph. EGCG was described in different papers like an antiaggregogenic molecule[7], [9], [76], while the mechanism of EGCG interactions whit proteins was still not clear. Local environment, pH, temperature,

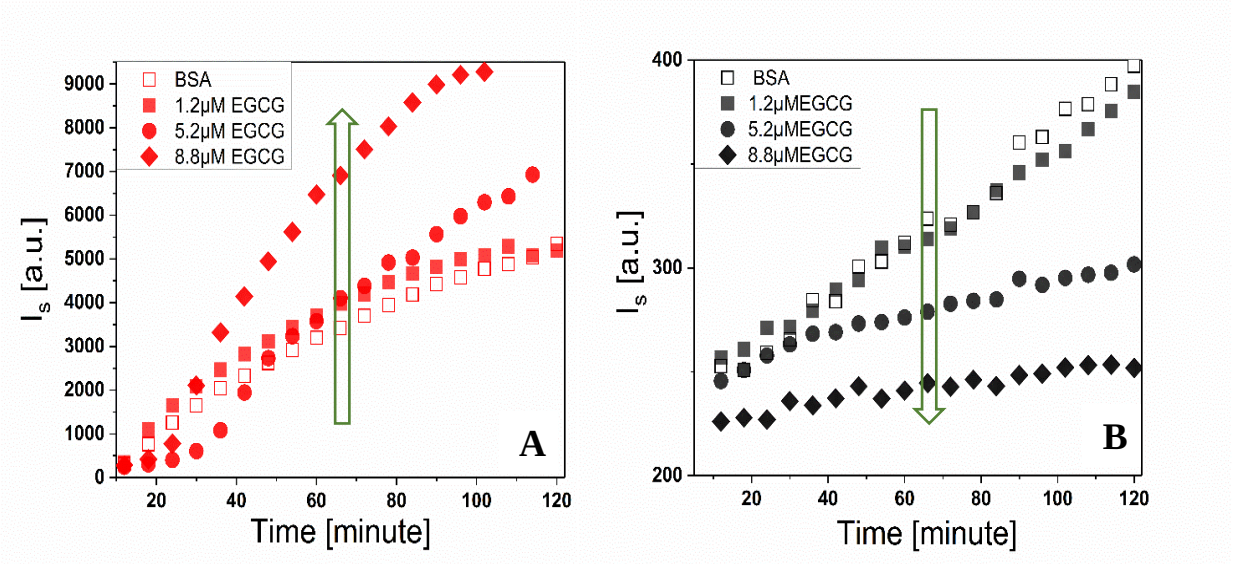

Figure 4.7. BSA Kinetic in presence or not of EGCG. A) Rayleigh scattering of BSA 7 μM in Potassium phosphate buffer 0.1M at pH 5 with (full) and without (empty) EGCG, from 0 to 8.8 μM at 60°C. B) Rayleigh scattering intensity of BSA 7 μM in Potassium phosphate buffer 0.1M at pH 7 with (full) and without EGCG (empty), from 0 to 8.8 μM at 60°C. The measurements were performed with λ_{exc}=270nm.

concentration, can modify the molecule behaviour and alter the properties of the molecule[80], [109].

Figure 4.7 shows the Rayleigh scattering intensity during the aggregation of BSA at 60°C, for pH 5 in Figure A and pH 7 in Figure B with increasing concentration of EGCG 1.2, 5.2 and 8.8 μM. Protein kinetics were performed at 60°C for both solutions. Samples were excited at λ_{exc}= 270nm, measurements were performed from 260nm to 600nm so we were able to follow Rayleigh scattering and the Fluorescence signal of protein with λ_{max} =340nm. The measurement of the Rayleigh scatterings is directly related to the size of the protein particles present in solution. For simplicity of comparison, in this case only the starting points of the BSA kinetic at pH7 were reported, however, the aggregation process was followed up to the plateau (data do not shown). The trend between the starting points and the final points has not changed, so the graph was very representative. In paragraph 4.9, a complete scattering graph at pH 7 was reported in Figure 4.10B.

Figure 4.7.A shows the kinetic trend for the BSA with and without EGCG. BSA without EGCG shows a growing monotone trend from 0 to 120 minutes. Increasing in EGCG concentration from 0 to 8.8 μM, data showed an increasing in scattering intensity signal. EGCG values were chosen to evaluate the effect in the range from 0 to 1 protein/ligand molar ratio. Concentration of 1.2 μM of EGCG don't shows a big modifying of the shape of the scattering trend, curves were superimposable. In 5.2 and 8.8 μM the effect on the trend of the curves was bigger. At the starting point scattering signal showed a lower signal than BSA without EGCG, while after thirty- or forty-minutes signal increasing a lot, and the final scattering value results bigger than native BSA. As mentioned before, the kinetic aggregation of BSA at pH5 proceeded through a disorderly process, governed by hydrophobic interactions [19], the exposure of the hydrophobic region during the initial steps of the kinetic can play an important role. In the hypothesis where EGCG bounded near Trp213, was in a partially ionized state[109], so the electrostatic interactions, combined with the exposure of the hydrophobic region of BSA, can enhance the kinetic aggregation of the protein. Charge mainly presents in the -OH group, that are involved in the stability of the polyphenol and susceptibility against pH changes, they were probably involved during kinetic aggregation[109]. In Figure 4.7B was reported the Rayleigh Scattering intensity during the aggregation of BSA at 60°C at pH 7 in presence and not in presence of EGCG. BSA without EGCG at pH 7 shows an increasing scattering intensity during the first two hour of kinetic, at this pH value BSA was negatively charged and the kinetic was more ordinated. Electrostatics mediated the kinetic interaction of BSA and lead to the formation of ordered aggregates. In presence of EGCG, scattering intensity goes down as a function of increasing concentration of EGCG. The aggregation in presence of EGCG goes via an ordinated mechanism modulated by electrostatics[21]. During aggregation, BSA residues are negatively charged, while the hydrophobic sites are exposed to the solvent. EGCG that can bind near Trp213, was also exposed to the solvent, but was not charged [109]. Probably electrostatic repulsions and the steric hindrance of EGCG, do not allow the protein to fold to an unfolded state. The kinetic aggregation at the two pH shows different behaviour, with different aggregation mechanisms. The aggregation mechanisms of BSA, seem to influence the behaviours of EGCG. In fact, near the isoelectric point of the EGCG protein it shows an aggregogenic nature, while away from the isoelectric point, EGCG shows an antiaggregogenic behaviour. Electrostatics and intra inter-molecular interactions, seem to underlie the interaction processes which then leads to the different nature of the process.

During the kinetic aggregation process, it also possible to monitor the intrinsic fluoresce signal of the protein. This is closely linked to the conformational changes of the protein and the exposure of

Tryptophan[19]. Figure 4.8 shows the intrinsic fluorescence intensity of BSA (280-500nm) at the two different pH with and without EGCG.

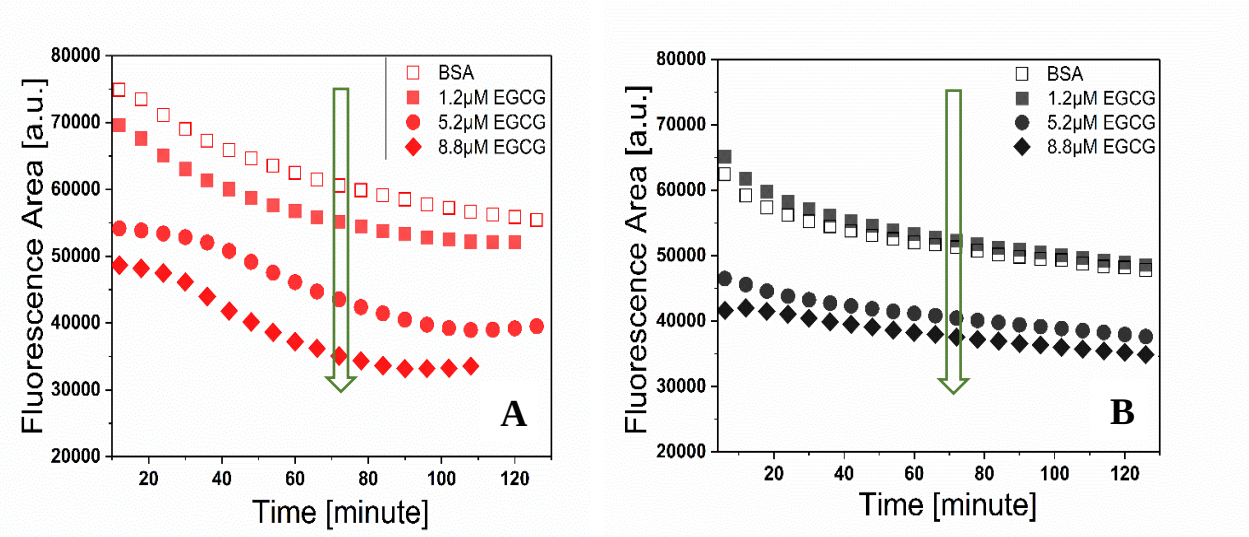

Figure 4.8. BSA fluorescence integrated intensity in presence or not of EGCG A) Fluorescence Integrated intensity of emission spectra of BSA 7 μM in Potassium phosphate buffer 0.1M at pH 5 with and without EGCG, from 0 to 8.8 μM at 60°C. B) Fluorescence Integrated intensity of emission spectra of BSA 7 μM in Potassium phosphate buffer 0.1M at pH 7 with and without EGCG, from 0 to 8.8 μM at 60°C. The measurements were performed with λ_{exc}=270nm.

Measurements are strictly correlated to the Tryptophan exposure to the solvent, so to the tertiary structure rearrangement[22]. Empty Red squares referred to BSA without EGCG at pH 5, showed a monotonal decreasing in term of intensity as a function of time. Presence of EGCG decreasing the fluorescence intensity of Tryptophan. A decrease in term of fluorescence signal, is function of major exposure of Tryptophan to the solvent. According to this, the increasing concentration of EGCG during then aggregation, enhances the rearrangement of the local Tryptophan environment. EGCG concentration also changes the trend of the curve at 8.8 μM. Initially in first 20 minute, a constant trend was observed, while after thirty-minutes curve sudden changes in slope, a sign that the environment near the Tryptophan has changed drastically. In Figure 4.8B was reported the fluoresce integrated intensity of BSA in presence or absence of EGCG at pH 7. In this case, curves with and without EGCG, showed a decrease in term of fluorescence as a function of increasing concentration of EGCG, but decrease was less pronounced than at pH 5. Curves related to native BSA and BSA with 1.2μM of EGCG are practically superimposable, while curves with 5.2 and 8.8μM of EGCG were translated down, but the trend remain linear and do not change during time. In both pH, the presence of EGCG causes an exposure of Tryptophan in the solvent. In general quenching of the two

Tryptophan at pH 5 appears more higher than at 7. The decrease of fluorescence appears more monotonic and linear at pH7. While at pH 5 with 8.8 μM of EGCG, shows two distinct steps of fluorescence intensity decrease. Changes in term of tertiary structure appear to be bigger at pH 5, near the isoelectric point of BSA[19]. In general, it was reported that BSA, at this two pH was in normal ”heartlike” structure (N-structure), so typically the mayor fluoresce signal, was attributed to Trp134[110]. At pH 7, it seems that EGCG and electrostatics, lead to a minor exposure of the Tryptophan to the solvent. These factors lead to a more orderly kinetic aggregation of BSA. Net charge favours the electrostatic repulsion between neighbours and drives towards to a more ordered aggregation pathway[19]. The variation in the decrease of Tryptophan emission can be accounted by considering that pH levels, impact the exposure rate of Tryptophan. It is conceivable that the ratio of the two Tryptophan contributions in the emission band, is also contingent on pH changes[19], [110]. EGCG, in general affect and probably change the tertiary structure as a function of increasing concentration at pH 5. While at pH 7 no big changes in term of exposure of Tryptophan were found. Results also indicate that the process is strictly dependent from the external conditions, electrostatics and hydrophobic forces change dramatically the kinetic and EGCG behaviours.

4.8 EGCG Oxidation

The same aggregation process reported before was repeated using oxidized EGCG (EGCGox). This was due to characterize the anti-aggregating properties of oxidized EGCG under the same experimental conditions, to compare them with those of EGCG. Oxidized form of EGCG [18], [78], [111] was reported as molecules enhanced their antiaggregant behaviours. The interaction mechanism of EGCG is still not clear. Changing in pH takes the EGCG molecule to change in term of stability, the presence of the galloyl moiety and of the hydroxyl groups present throughout the molecule, leads it to be very reactive[112]. Usually in acid pH near 4, EGCG was a stable molecule[80]. While at neutral pH, EGCG shows net charge equal to zero. At alkaline pH EGCG shows a double negative charge. Bioavailability and poor stability have limited its application[113], EGCG were oxidated for 24h using method proposed by An et al.[18]. In order to characterize the molecule oxidation, different absorbance spectra were used. Figure 4.9 shows normalized absorbance spectra for the two compound EGCG and EGCGox in a Phosphate buffer solution at pH 8. Inset reported the two solutions of EGCGox after 24h and EGCG native form. The absorption spectra have a different shape, therefore

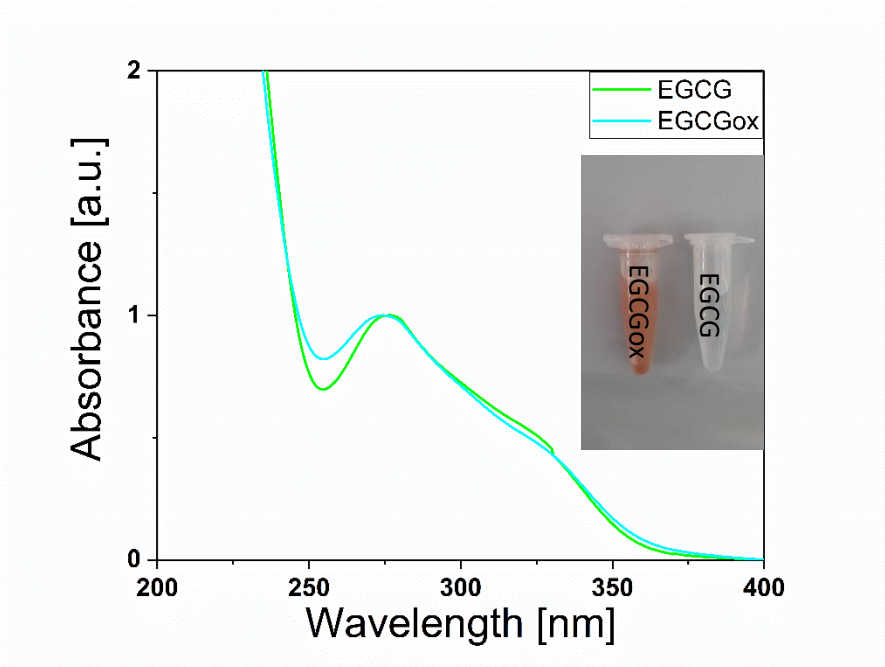

Figure 4.9. **Absorption spectra of EGCG and EGCGox.** Absorbances spectra of EGCG and EGCGox in Potassium phosphate buffer 0.1M pH8 normalized to the maximum. Inset reported the solutions in Eppendorf of EGCGox and EGCG in Potassium phosphate buffer 0.1M pH8.

it is inferred that a change within the molecule has occurred.

As showed in Figure 4.9, the two spectra in green (EGCG) and spectra in cyan (EGCGox) results different. Data were normalized at the maximum peak in 275 nm. Spectra demonstrated that EGCGox also contain a phenolic group like EGCG, because the maximum peak of absorbance remain in the same position [18]. Obtained spectra are comparable to those obtained by An et al[18]. Data suggest that EGCG degrades through an auto-oxidation pathway[112]. When the solution undergoes to the auto-oxidation, change in colour from limpid to brown. When EGCG goes to an oxidation process, oxygen obtains electron from EGCG, resulting in the formation of superoxide anions, which are eventually reduced; consequently, hydrogen peroxide was accumulated. The brown colour was probably associated to the formation of other similar species of EGCG like Gallocatechin gallate (GCG), an epimerization product of EGCG [114].

4.9 EGCGox vs EGCG anti-aggregogenic behaviour

The obtained EGCGox solution were studied with same experimental conditions, at the two different pH 5 and 7 and compared with native EGCG. Figure 4.10 showed the Rayleigh scattering measurements of BSA solution in presence or not in presence of EGCG or EGCGox at 60°C at pH 5 red figure and at pH 7 reported in black one.

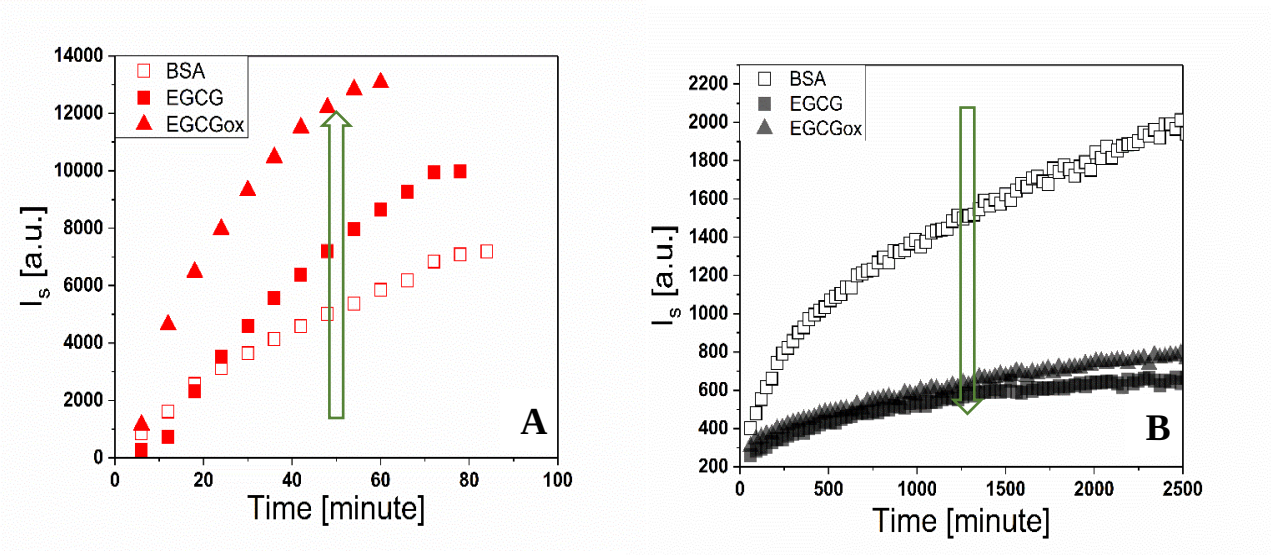

Figure 4.10. BSA Kinetic in presence or not of EGCG or EGCGox. A) Rayleigh scattering intensity at of BSA 7 µM in Potassium phosphate buffer 0.1M at pH 5 with and without EGCG and EGCGox 8.8 µM at 60°C. B) Rayleigh scattering intensity of BSA 7 µM in Potassium phosphate buffer 0.1M at pH 7 with and without EGCG and EGCGox 8.8 µM at 60°C. The measurements were performed with λ_{exc}=270nm.

Figure 4. 10 A showed the Rayleigh scattering of BSA at pH 5 in presence or not of EGCG or EGCGox at 60°C. Data indicate the same behaviour for EGCG and EGCGox during kinetic aggregation. Scattering intensity of BSA after first 20 minute goes rapidly up. Without electrostatic repulsions aggregation process was very fast and form big aggregates. In the presence of EGCGox, the scattering signal is larger than that of EGCG. The behaviours of native and oxidized form of EGCG induce at pH 5 the same results, therefore we can conclude that the behaviour is practically the same. Figure 4.10B showed the Rayleigh scattering of BSA at pH7 in presence or not in presence of EGCG or EGCGox at 60°C. In this case, as previously stated, the graph including all points is shown. The aggregation process of BSA at neutral pH was slower. Aggregation process of BSA at pH 7 was more ordered and take more time. In presence of EGCG and EGCGox scattering maintain quietly the same value from starting, this probably means that EGCG interact immediately and prevents the aggregation, at this pH. The results show a trend similar to that previously reported. The results in general indicate that EGCG and EGCGox behaviours were quietly dependent form the local environment. The EGCG compounds showed an aggregogenic behaviour at pH 5, when the protein has net charge near to zero and hydrophobics guide the process. On the other hands, when the kinetic process was more ordered and electrostatic guide the kinetics native and oxidized, EGCG showed antiaggregogenic behaviours. We can conclude that the local surrounding environment, in particular electrostatics and hydrophobic forces, had a high impact on behaviour of EGCG. Finally, EGCG oxidation, don't change the behaviour of the polyphenol, with these experimental conditions.

4.10 Aggregates characterization using AFM and Confocal fluorescence microscopy

After the kinetics, the final aggregates were characterised using microscopy techniques. Two different techniques were used: Atomic force microscopy (AFM) and Confocal fluorescence microscopy because the aggregates are very different in dimensions. At pH 5 we obtain typical big amorphous aggregates long few microns in size visible clearly with typical Confocal fluorescence microscopy. At pH 7, aggregates are more regular and the typical dimension are around nanometres, so in this case we use AFM techniques.

4.10.1 Characterization of BSA aggregates at pH 5

In order to characterize aggregates in the presence or not in the presence of EGCG at pH 5, we used Confocal fluorescence microscopy. Aggregates were visioned with the microscope using the hydrophobic probe Nile Red at 515 nm. The advantage of visualizing by Nile Red with fluorescence microscopy was evident when few aggregates were present in the solutions. The higher contrast

provided by fluorescence microscopy, allowed the detection of aggregates present in small numbers, and the relative specificity of the Nile Red staining eliminated false positives[69]. Aggregates formed during kinetics in a fluorometer of BSA and BSA with 8.8 μM EGCG were placed in Lab-Tek wells and analysed with laser intensity of 0.2%. Figure 4.11 (A-E) reported representative images taken from microscopy of the aggregates at different magnifications 3x, 5x and a single particular of the aggregates. Differences in term of fluoresce intensity are detectable from all the figures. Higher Nile Red fluorescence indicates that more or different hydrophobic pockets are available for Nile Red binding[69]. These results are consistent with those previously shown. The EGCG binding hypothesis with BSA near Trp213, leads to the occupation of at least one of the protein's hydrophobic pockets. This does not allow the Nile Red to be able to bind in the buried hydrophobic pocket of BSA. Aggregates with EGCG show minor fluoresce intensity, then those without EGCG. BSA aggregates show globular forms, rounded and more compacted aggregates. While in presence of EGCG, aggregates present are flatter and more clustered. In Figure 4.11 E and F compare BSA and BSA with EGCG, the difference in term of shape between the two types of aggregates was noted. In general, aggregation near the Isoelectric Point of the protein lead to the formation of amorphous aggregates[19], [115]. BSA at this pH is usually in N conformation, with exposure of hydrophobic internal area to the solvent[19]. The lack of electrostatic interactions means that the aggregation proceeds mainly in a disordered way and the forces involved are typically of the hydrophobic type[19], [21], [22], [115]. No change in secondary structure were found before, but only changes in tertiary structure. The presence of EGCG probably bound in Domain II near the Trp213 it can lead to a different arrangement of the tertiary structure in the solvent, which leads to a different folding process. A statistic of the diameter of the single aggregates present in the two protein samples was reported below in Figure 4.11. The BSA aggregates present an average diameter of 1.15 μm, while 1,36 μm for EGCG. Furthermore, BSA aggregates show a particle distribution that tends toward smaller diameter particles, while EGCG particles tend toward larger diameter particles. These results confirm the previous data by confirming that the size of the protein aggregates in presence of EGCG were larger than the native BSA aggregates.

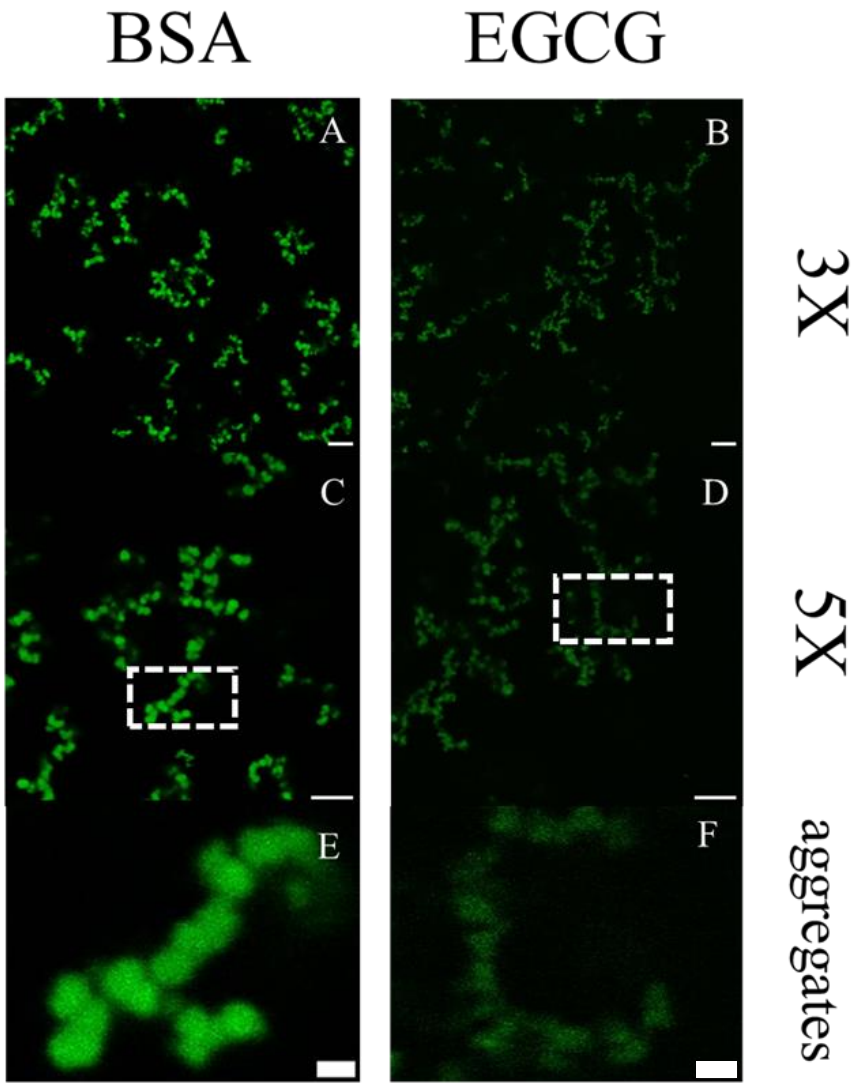

Figure 4.11. Confocal fluorescence microscopy of BSA aggregates. Representative 1024x1024 images from Confocal fluorescence microscopy of protein aggregates of BSA 7μM (A-C) and BSA with 8.8μM of EGCG (D-E) after kinetic at 60°C pH5, solved in a Potassium phosphate buffer 0.1M in presence of 40 μM of Nile Red. Bars are 5 μm for images with 3x and 5x of magnifications and 1 μm for single protein aggregate.

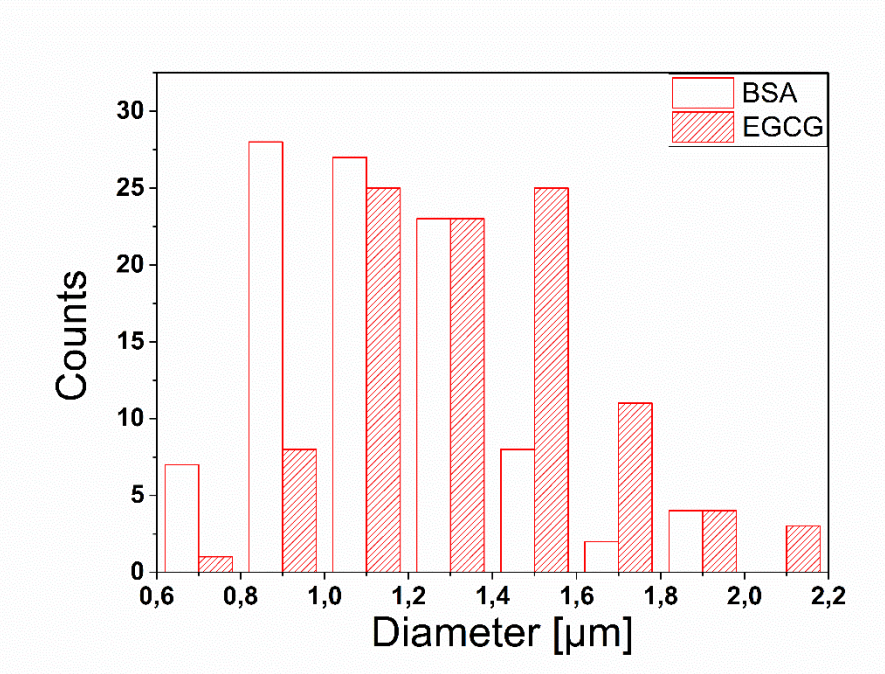

Figure 4. 12. Analysis of BSA particle dimensions. Aggregates size dependence of BSA 7 µM and BSA with EGCG 8.8 µM at pH5, solved in Potassium phosphate buffer in presence of 40 µM of Nile Red.

An innovative technique, fluorescence lifetime imaging (FLIM), was used for a comprehensive assessment of BSA aggregates by characterizing their lifetimes. The goal of FLIM is the creation of a colour-mapped image in which different colours represent the different fluorescence decay [116]. The fluorescence decay is directly transformed to a phasor plot by simple mathematics in which phasor points originating from different pixels in the image are represented by their location in the phasor plot. The phasor plot is a polar plot in which each decay is represented with two coordinates. In phasor plot similar fluorescence decay were easily detected [116]. Phasor plot convert the fluoresce lifetime information into a plot with different coloured area. Every colour of the map called "universal circle" corresponds to a typical value of fluoresce lifetime. When using phasor analysis, each pixel of the intensity images is mapped to a point in the phasor plot corresponding to the measured fluorescence lifetime. Single exponential lifetimes lie on the universal circle; long lifetimes are located near the origin (0 on the x axis), while short lifetimes are shifted on the circumference toward the bottom right intersection with the x axis (1 on the x axis)[71], [117]. In Figure 14.13 were reported the Phasor FLIM approach for the sample characterization in presence of 40 µM of Nile Red. Fig. 14.13A reports the universal circles related to the measurements of the aggregates of BSA reported in green and of BSA with EGCG reported in cyan. Figure 14.13A identifies two single different exponential decays. For BSA lifetime, the value was 2 ns, reported in 14.13B (green), while BSA in

presence of EGCG (cyan) shows a different lifetime value, 0.8 ns. From 14.13A it is noted that BSA in the universal circle is associated with a well-defined fluorescence lifetime decay, while BSA with EGCG was represented with a large fluoresce lifetime distribution, where more than one lifetime can be distinguished [71]. In Figure 14.13D it was reported the other universal circle for the phasor approach of the aggregates where it was possible to individuate two different exponentials for BSA with EGCG, associated to two different fluorescence lifetimes reported in 14.13F. Figure 14.13F reveals one inner part of aggregates coloured in yellow with lower value of lifetime and one external part coloured in cyan. Native BSA lifetime was reported as a value between 6 and 5ns[23], [21] BSA lifetime was strictly related to the two tryptophans located in the protein, Trp134 and Trp213[23], [118].

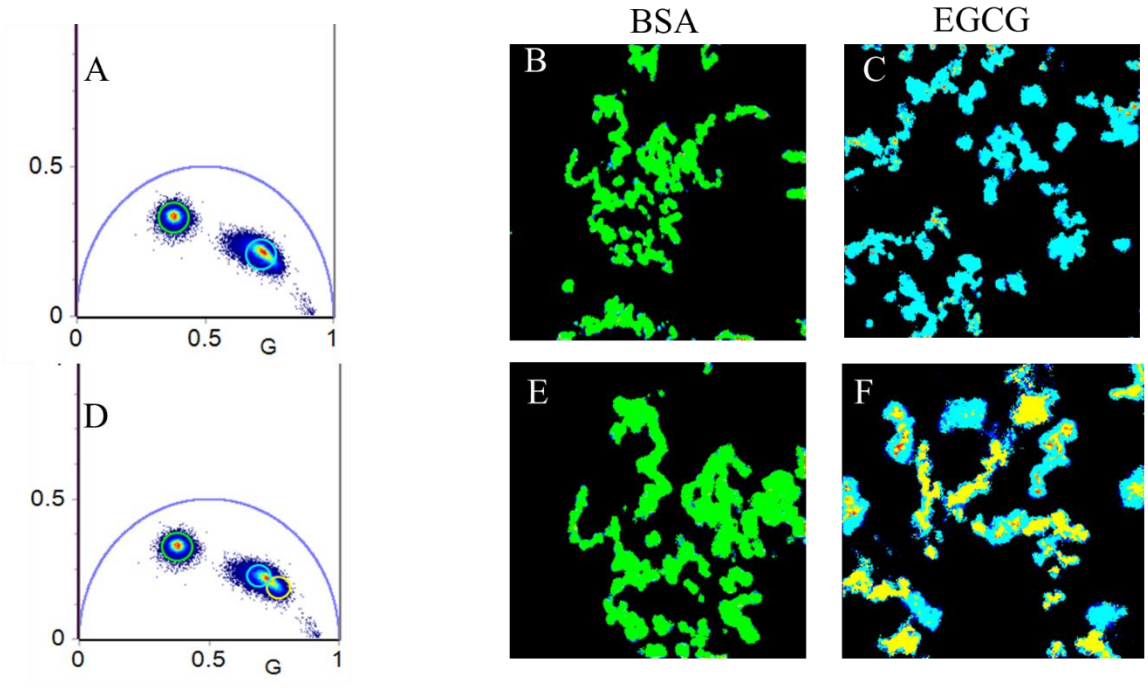

Figure 14.13 Phasor plot analysis on BSA aggregates. Phasor plot analysis of 256 x 256 pixels FLIM measurement maps of aggregates of BSA 7 μM (green) and BSA with EGCG 8.8 μM (cyan and cyan, yellow) after kinetic at 60°C pH5, solved in Potassium phosphate buffer in presence of 40 μM of Nile Red. In A is reported the universal circle related to aggregates of BSA and BSA with EGCG wild field (B and C). In D is reported the universal circle related to aggregates of BSA and BSA with EGCG magnification (E and F). Phasor colour map: each pixel is coloured according to the colour of the corresponding circle in the phasor plot. The choice of the size and the position of the circles is arbitrary, and it is used to highlight average properties of the lifetime distributions, which are located on the same line.

In Li et al.[23] works, they use Time resolved fluoresce lifetime, it was found a change in term of lifetime value of BSA in presence of EGCG at pH5. Values of Trp lifetime dropped about 50% in presence of EGCG. Reduction interested the Trp213 that have short lifetime range about 2-3 ns. The reduction in lifetime was maybe due to the different conformational change in the tertiary structure of the protein[21]. While change in the secondary structure with EGCG before and after the aggregation of the protein were not present. Probably the binding of EGCG near the Domain II of BSA near the Trp213, also changed the accessibility of Nile Red, as reported in Fig.12. A change also in the Trp environment exposure with different polarity were in accord with the previous results. All results confirm that modification due to the conformational change of the protein and the polar environment exposure were strictly correlated and confirmed from all data.

4.10.2 Characterization of BSA aggregates at pH 7

The BSA and BSA with EGCG aggregates produced at pH7 showed a different aggregation kinetics due to the electrostatic effect which makes the aggregation processes more orderly. The aggregate solutions clearly show the absence of visible particulates, which indicates that the present aggregates do not reach visible length. Therefore, Atomic force microscopy (AFM) was chosen to characterize these types of aggregates[81]. The characterization was made in dry samples, deposited on mica. Samples were dried with nitrogen flux and let dried overnight in order to have the security to have

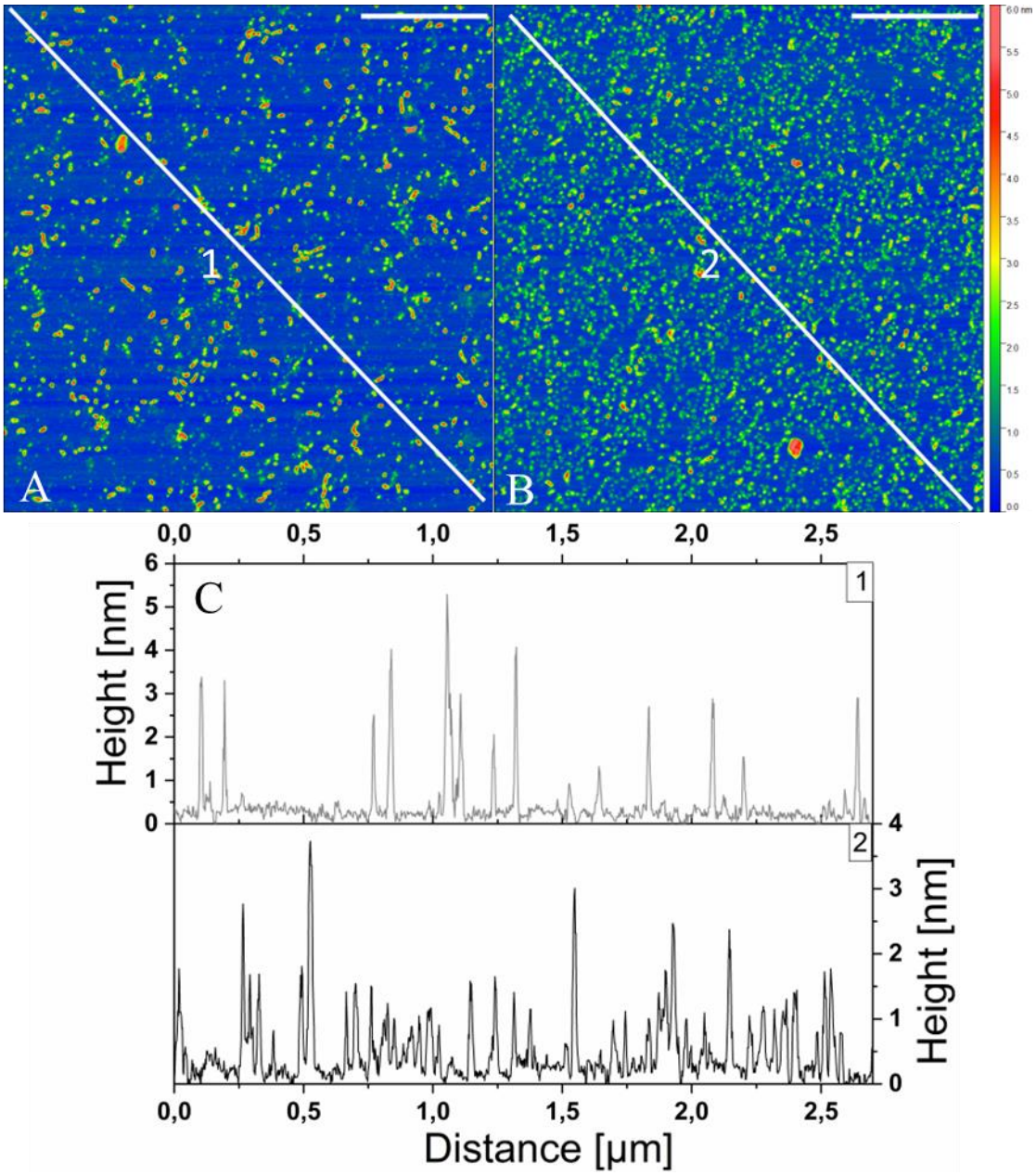

Figure 4.14. **AFM images of BSA aggregates**. A) 2 µm x 2 µm Image AFM, of BSA aggregates at pH 7. B) 2 µm x 2 µm Image AFM, of BSA in presence of EGCG aggregates at pH 7. Bars are 500 nm. C) AFM Profiles of BSA (1) and BSA in presence of EGCG (2) aggregates. Measured were performed in tapping in air mode.

dried samples. In Figure 4.14 were reported the two images of AFM for BSA in A and BSA with 8.8 μM of EGCG at pH7 in Potassium phosphate buffer after kinetic at 60 °C.

Figure 4.14A showed BSA aggregates at pH 7, the presence of a few particles can be noted, it shows a dimension of a few nanometres in length (2-3nm), sample shows a heterogeneity of morphology, there are globular aggregates and aggregates with an elongated shape, like protofibrils. Figure 4.14B shows that in the presence of EGCG, the aggregates exhibited the presence of smaller particles measuring approximately 1-2 nm in diameter. These aggregates were more heterogeneous, with only globular aggregates present, resembling a dimeric form of BSA. As regards the data, it seems that the presence of EGCG, did not allow the nucleation of the protofibrils present instead in the sample reported in 4.14A. Two BSA height profiles images were reported in 4.14C: profile 1 and profile 2 of BSA with EGCG. In profile1 they show only a few well-defined peaks, with an average height of 3nm. While in profile 2, they show the presence of many more peaks, small ones with an average height of 1.5 nm. Table 2 reported some statistics related to different linear profile for BSA and BSA with EGCG. Different images for single sample aggregates were selected, from images are extrapolated the profile, which are zeroed and analysed with Origin. From the data reported in Table 2, it can be noticed that the average height of BSA aggregates is about 0.6 higher in the absence of EGCG compared to when it is present. This result is consistent with the kinetics data presented in the preceding paragraphs and confirms that at this pH, EGCG has an anti-aggregating behaviour. Standard deviation in both case was low, a sign that the values show a small dispersion. Data confirm our first kinetics results which are reported above, particles with EGCG showed a small dimension in term of height and diameter. Interaction with EGCG appears to effectively inhibit the growth of fibrils within the BSA sample, so EGCG has an effect on the change of the protein's tertiary structure.

Table2. Height peak statistics on BSA and BSA with EGCG pH 7.

Samples	Mean [nm]	Sum	Standard Deviation	Median	Minimum	Maximum
BSA	2,7	252,93	1,21	2,81	0,68	4,91

BSA+EGCG	2,15	236,88	0,80	1,85	0,90	4,78

At pH7, EGCG and BSA interactions and the solution conditions, lead to the formation of globular aggregates smaller than the native BSA. Aggregates that were formed in the presence of EGCG are smaller in diameter than in height compared to those of the native protein at pH7. As a comparison and confirmation, our results were performed on aggregates solution with Dynamic Light Scattering measurement (DLS). The measurement made in bulk on the already formed solutions helps us to compare the dimensions of the protein aggregates in dry and wet conditions. Figure 4.15 reported the DLS measurements size and distribution of BSA and BSA with EGCG aggregates at pH7. DLS determines size and size distribution by measuring the rapid changes in laser light intensity being scattered by molecules or particles in solution.

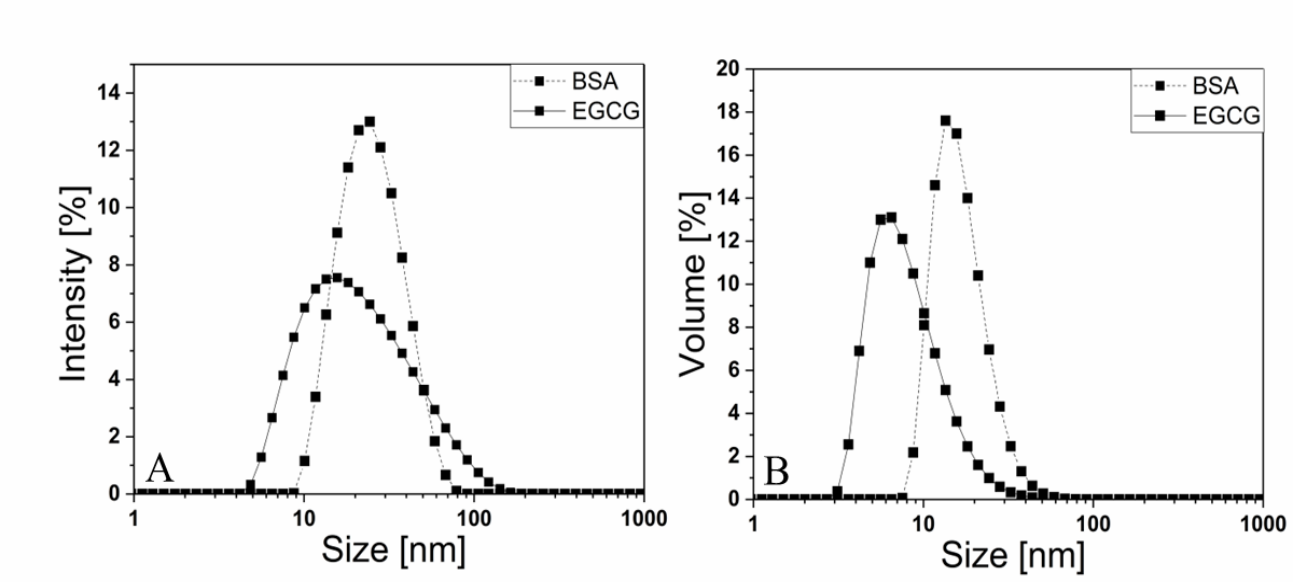

Figure 4.15. DLS on BSA aggregates. Dynamic light scattering (DLS) of particle size and distribution of aggregates formed at 60°C of BSA and BSA in presence of EGCG 8.8 μM at pH 7. A) Intensity DLS measurement as a function of aggregates particle size. B) Volume measurement as a function of aggregates particle size DLS measurement.

Figure 4.15A reported the DLS intensity measurements as a function of diameters of BSA and BSA with EGCG aggregates, native BSA showed a tight distribution of particles of protein with the

maximum peak 17,2 nm, while with EGCG the intensity value decreases, and the distribution becomes wide with maximum peak at 13nm. Results demonstrate that the BSA sample presents more homogeneous aggregates, with an average diameter around 17 nm. While the BSA sample with EGCG has a lower peak and a broader distribution (7 to 130 nm), therefore it has a more heterogeneous conformation with the presence of smaller particles in the middle than those of BSA. In Figure 4.15B was reported the DLS volume measurement as a function of particle size, results confirm the first distribution reported in A. A tight distribution of BSA particle was found with maximum at 13 nm. While in presence of EGCG, the volume value decreases and the maximum was peaked at 8nm. Both measurements confirm our previous AFM data. BSA aggregates present a diameter bigger, than aggregates in presence of EGCG. Differences in term of dimension value from AFM and DLS measurements are due to the presence of hydrodynamic radius of solvent in DLS, while in AFM only the single dry particle were measured[119], [120]. EGCG neutral pH, shows an antiaggregogenic behaviour which slows down the BSA aggregation process, it inhibits the conformational changes that lead to the formation of the prefibrillar structure. Thus, EGCG leads to the formation of globular aggregates smaller in size than the native aggregates.

4.11 Conclusions

This work was focused on the characterization of the interaction process between EGCG, a potential molecule reported by many studies as antiaggregogenic molecule[121]–[123], and BSA, a widely studied model protein[21], [22], [94]. The chosen solution conditions led to the obtaining a protein negatively charged at pH 7 and uncharged at pH 5. Various spectroscopic techniques and Isothermal Titration Calorimetry were used to investigate the possible interactions between the two molecules. The outcome of the study showed that EGCG is a potent quencher for BSA, which led to a change in the tryptophan environment of the protein. Additionally, fluorescence data revealed a significant red shift in the spectra, indicating a possible alteration in the tertiary structure of the protein. EGCG changes dramatically its behaviour as at change of solution conditions[124], the electrostatics and hydrophobic interactions involved in aggregation processes of the protein modulate EGCG comportment. Near p.I. EGCG behaviour has an aggregogenic behaviour and increases the process of protein aggregation. While away from the p,I, EGCG changes into antiaggregogenic molecule slowing down the protein aggregation and inhibit the protofibrils formation. Our study confirms that the solution conditions modulate the behaviour of the EGCG. Changing in solution condition increases or decreases dramatically the antiaggregogenic properties of the polyphenol. EGCG proves to be a promising molecule under many aspects, further studies will have to be carried out to better understand the mechanism of interaction between the polyphenol and the proteins.

The results show that even BSA undergoes fibril formation, if appropriately exposed to certain chemical and physical parameters (such as pH). Its stability, ease of availability and comparability certainly make it a model system for studying more complex aggregation and interaction phenomena, such as those involved in neurodegenerative diseases. This innovative approach to the work is given using an exemplary protein model, which allows the analysis of certain components and behaviours that can be extrapolated to more complex proteins, such as those involved in neurodegeneration. Furthermore, the interaction of EGCG with the protein is evaluated by using advanced spectroscopic and microscopic approaches. It provides an overall view of the problem. The use of EGCG as an anti-aggregating molecule is highly debated. The proposed study aims to provide clarity regarding the anti-aggregating behaviour of EGCG and EGCGox, which drastically changes depending on the surrounding conditions.

5 Protein membrane interactions: an innovative approach

5.1 Aim of the Chapter

This Chapter analyses the role of biological membrane surface as promoter of pathological aggregation of protein. The scientific community has identified protein-membrane interaction as a basic process of many neurodegenerative diseases[26], [39], [125]. To date, it is still unclear how this process evolves and what is the process involved into the evolution of the interaction between the cell membrane surface and the proteins involved in neurodegenerative processes. For example, it appears that the composition (including the presence of cholesterol within the phospholipid bilayer) and charge plays a role, as a higher occurrence of negative charges on the surface favours the binding process between proteins and the membrane. The process remains poorly understood, due to the complexity of observable systems. The development of a ”simplified system” that replicates only a part of the whole system allows for observation through modern fluorescence microscopy techniques. This can better define what occurs before and after the protein-membrane interaction process. The objective of this section is the creation of a platform that allows the generation of objects mimicking the surface of the cell membrane. These objects can be printed using a printing biology technique. The developed system, (which uses micro cantilever spotting) enables the construction of a platform composed of thousands of spots that can be modified in terms of size, geometry, ink content, electrostatic charge, etc. The technique utilizes minuscule amounts of ink, allowing the production of thousands of testable systems with low reagent consumption. Obtaining a compact and stable analytic platform, with a good signal-to-noise ratio, allows a thorough and intuitive study of protein-membrane interactions. Furthermore, it will enable the testing of molecules that potentially could slow down or hinder the interaction using fluorescence microscopy like Epigallocatechingallate (EGCG)[7], [15]. In an initial part of these study, the use of another interesting technique for compartment formation, called “drop casting”, had been evaluated, but the difficult stabilization of the drops and the low repeatability of the process led to the use of the microcantilever spotting. Compared to other techniques, for example drop casting, Microcantilever spotting allows the rapid generation of multiple testable systems on a solid substrate that can be easily observed using any fluorescence microscope. The obtained systems can be modified in terms of size, geometries, electrostatic charge, and more. Additionally, the ink used in the process is reusable for multiple prints, reducing the consumption of reagents. All these advantages contribute to the development of a customizable analytical platform.

5.2 Micro-Cantilever Spotting Approach

Microcantilever spotting (μCS) it is a powerful constructive patterning technique based on the atomic force microscope (AFM), μCS permits printing of patterns of an extraordinary variety of materials onto surfaces with lateral dimensions ranging from sub -100 nm to the micrometre regime. The idea was the development of a stable ink for the deposition of phospholipids onto a glass surface. Those printing phospholipids mimic the membrane surface, like a membrane models named Supported lipid Bilayers (SLBs)[126]. The incorporation of a fluorescent dye inside of the phospholipids, allows the vision of SLBs with fluorescence microscope. When a protein solution dropped on the spots, it was possible to follow the time evolution of the membrane-protein interactions. Development starts from the ink formation, were we chased two different phospholipids: 1,2-dioleoyl-sn-glycero-3-phosphoethanolamine (DOPE) a neutral saturated phospholipid, N-(Fluorescein-5-Thiocarbamoyl)-1,2-Dihexadecanoyl-sn-Glycero 3Phoshpoethanolammine (DHPE-FITC) a fluorescent unsaturated phospholipid, negatively charged. DOPE is an ordered, unsaturated helper lipid, with net charge near to zero, that can stabilize the final droplet formed[127], [128], while DHPE-FITC a saturated phospholipid with a FITC molecule on the head (1:1), was a fluorescent phospholipid very responsive probe, useful for the fluorescence confocal studies. In Figure 5.1 the development of the phospholipid compartments was reported. The fluorescent ink was charged (0.4 μl) in the reservoir of surface patterning tool (SpT) 5.1A, then printed onto microscope slice (treated or not treated) using 50% of relative humidity 5.1B. After the printing, the printed slice was dried overnight and characterized in the fluorescence microscope 5.1C. With these developed inks it was possible to print, without refill of inks, more than 1000 spots per session. In 5.1D were reported a possible scheme of phospholipid multilayer after the printing session. Two different inks were developed with resuspension of the phospholipids: ethanolic and aqueous solutions. The solutions show different advantages and disadvantages, these are summarized in Table3. The ethanolic ink shows greater ease of preparation, this because phospholipids were easily resuspended in ethanol, but it can only be used for one printing session. While, the aqueous ink was a reusable ink for more than one printing session and it allows to print more than 5 slides without needing an ink refill.

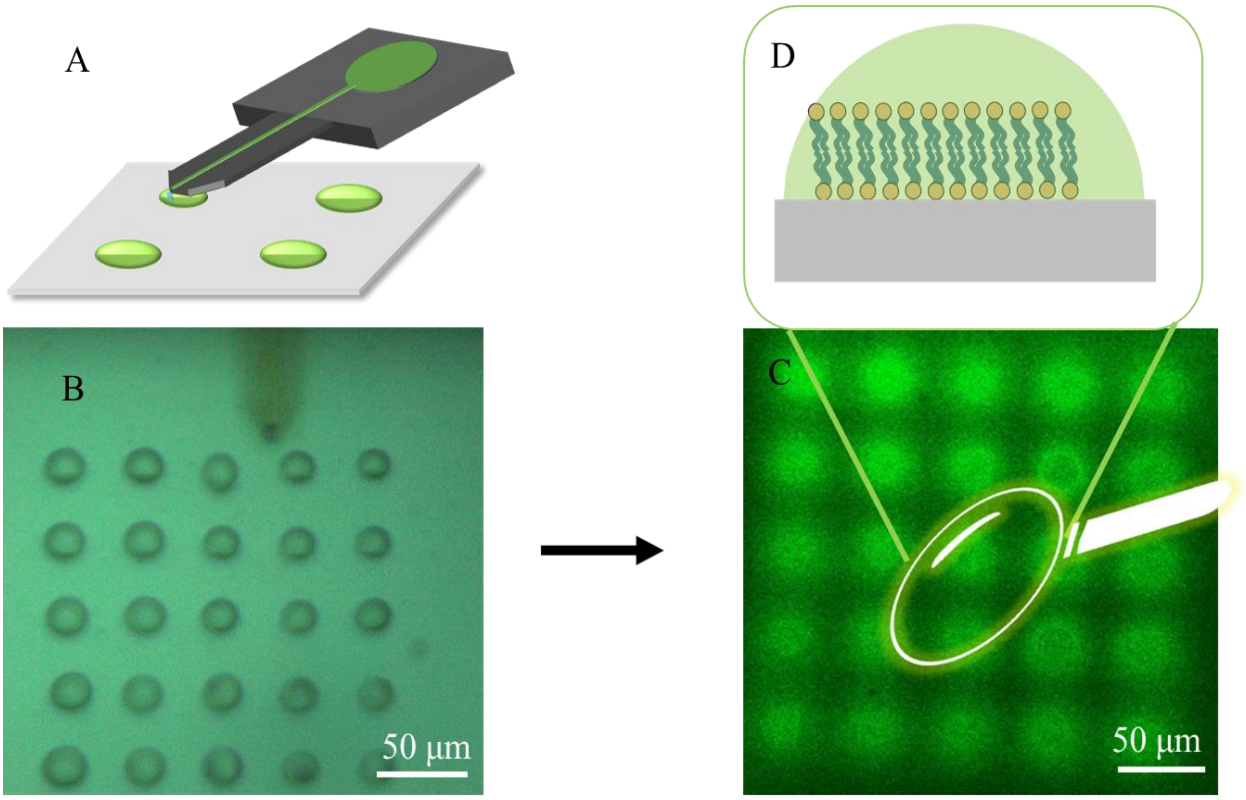

Figure 5.1. **Phospholipids droplet development**. Phospholipids droplet formation process. A) Scheme of µCS printing with patterning tools. B) image camera of the printed droplets. C) Confocal fluorescence microscopy image of droplets. D) Scheme of multilayers formed.

The aqueous ink formation was more time consuming, this because favourite the resuspension of phospholipids into water requires more than an hour and half of sonication.

Table 3. Advantages and disadvantages of the ethanolic and water inks.

INKS	ADVANTAGES	DISADVANTAGES
Ethanolic ink	easier ink preparation good spot reproducibility	not reusable ink solution more refills of ink solution

Aqueous ink	reusable ink solution good spot stability low refill of ink	time consuming ink preparation more ink residues present in micropatterning

Both of inks contain glycerol, that allows our ink to be printed and avoiding fast evaporation of the ink in reservoir. It also was a template for the phospholipids, allowing the formation of a multilayer in results. Differences in term of different glycerol concentration were studied during the development of the inks. These and other printing parameters, were better described in the following paragraph.

5.3 Modulation parameters of printed phospholipids

Modulation of various parameters of μCS can change and modulate the lateral dimension, diameter, and geometry of the printed phospholipids. In Figure5.2 an example of the influence of different

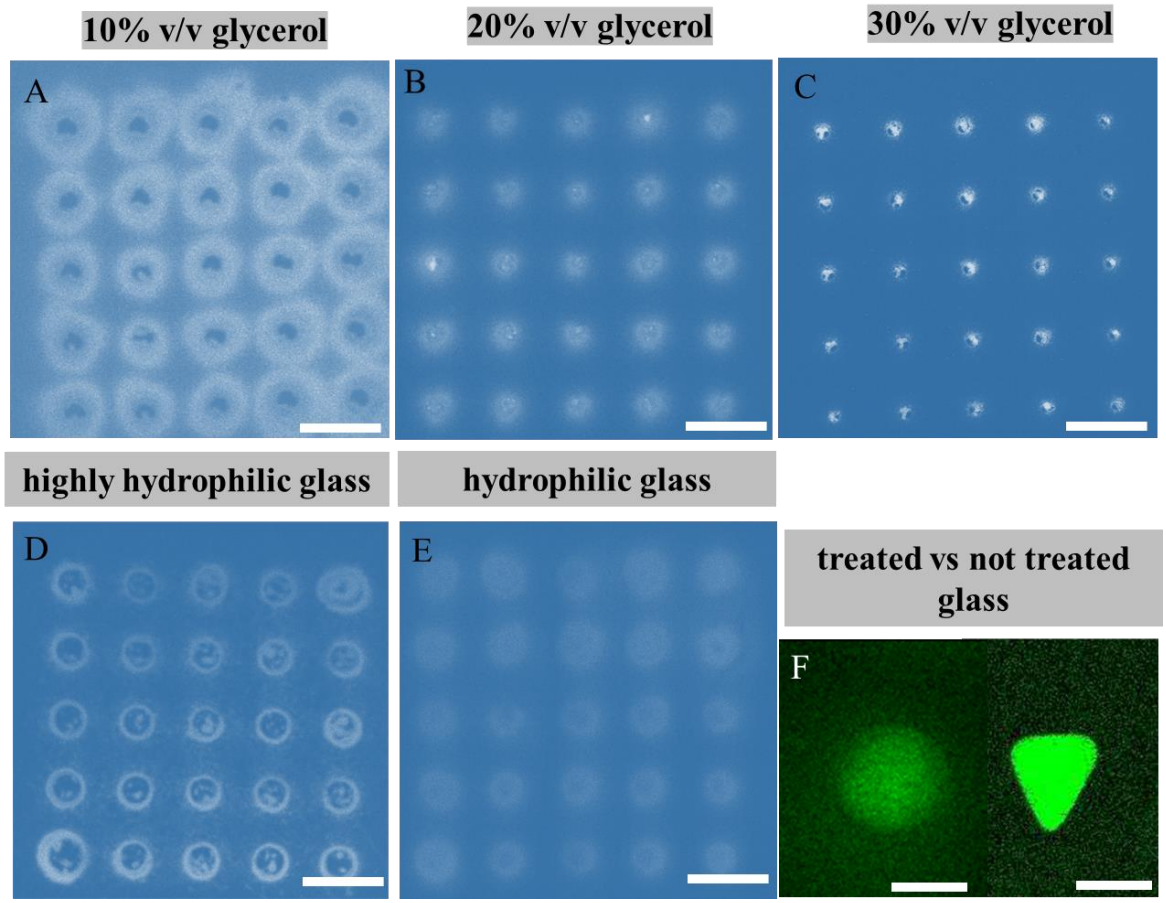

Figure 5.2. Glycerol concentration, hydrophilicity and treatments on slices modulate dimension and geometry of membrane models. A-C) Representative confocal fluorescence images of DHPE:DOPE-FITC (100:1) spots of ethanolic ink, after the deposition, with different glycerol v/v concentration with the other parameters being the same. D-E) Representative confocal fluorescence images of DHPE:DOPE-FITC (100:1) spots of aqueous ink, after the deposition, with different hydrophilic glasses, with the other parameters being the same. F) Representative confocal fluorescence images of DHPE:DOPE-FITC (100:1) spots with treated glass vs not treated glasses. Scale Bars is 50 μm for (A-E) and for F is 20 μm. Fluorescence confocal images have been acquired in the range 500-600 nm with λ_{exc}= 488nm.

parameters on the final spots were presented. Different parameters were involved during the μCS printing that can modify the geometric characteristics and the dimensions of the spots. In this paragraph, we will discuss how parameters such as hydrophilicity, contact time and glycerol percentage affect the final features of the spots. Differences in term of glycerol concentration have a big impact on dimension and geometry of the spots. Figure 5.3 A, B and C reported different confocal

images of different DOPE-DHPE-Fitc (1:100) spots with an increasing concentration of glycerol from 10% v/v in A to 30% v/v in C at the same contact time, after the printing deposition. Images demonstrates that is it possible to modulate the diameters and the lateral dimensions of the printed micropatches. The diameters change from 50 μm for the ink with 10% of glycerol to a reduction of 60% of the dimensions for a 30% printed micropatches. The increasing in glycerol content leads to a higher viscosity of the ink, which can lead to blockage of the microchannel. The best result for the final ink was the 20% glycerol v/v rating. This allows to print micropatches for a long time without stop. Figure 5.2D and E shows a confocal image of the aqueous ink with same contact time (1 second) after the μCS deposition. Different hydrophilicity of the glasses, correspond with an increase of lateral dimensions of the printed spots. The different hydrophilicity was given by the different cleaning treatments for the glasses, in particular:

- **Highly hydrophilic glasses** were obtained with a doble cleaning process with a solution with alkaline 2% v/v Hellmanex ™ III (10 min) and 20 min with Uv cleaner.

- **Hydrophilic glasses** were obtained with a single cleaning process with alkaline 2% v/v Hellmanex ™ III (10 min).

These treatments enhance the exposure of hydroxyl group on the surface of the glasses, modify the lateral dimensions of the printed spots, that vary from 32 μm for highly hydrophilic glasses to a 28 μm for hydrophilic glasses. Worked through untreated glasses it gives us the possibility to modify the geometry of the spots. Figure 5.2F reported a confocal image of aqueous ink with glasses treated (on the left) and not treated (on the right) with same external conditions and parameters. Differences of hydrophilicity from SpT (which has a triangular shape) and the glass surface with hydrophilic treatment or not are present. So, it is possible modulate the geometry as a function of the ratio between the hydrophilicity degree of the SpT and the hydrophilicity degree of the surface. During the printing process it was possible to change the contact time of the SpT, increasing in contact time of the SpT, enhanced the lateral dimension of the spots[43], [45]. After the deposition of the spots, the printed phospholipids were vacuum dried overnight. After drying, the printed phospholipids were visioned on confocal fluorescence microscope. The dimensions of phospholipid printed before and after deposition processes were assessed. In Figure 5.3 a graphical representation of the dimensions of the ethanolic spots before and after the deposition were reported.

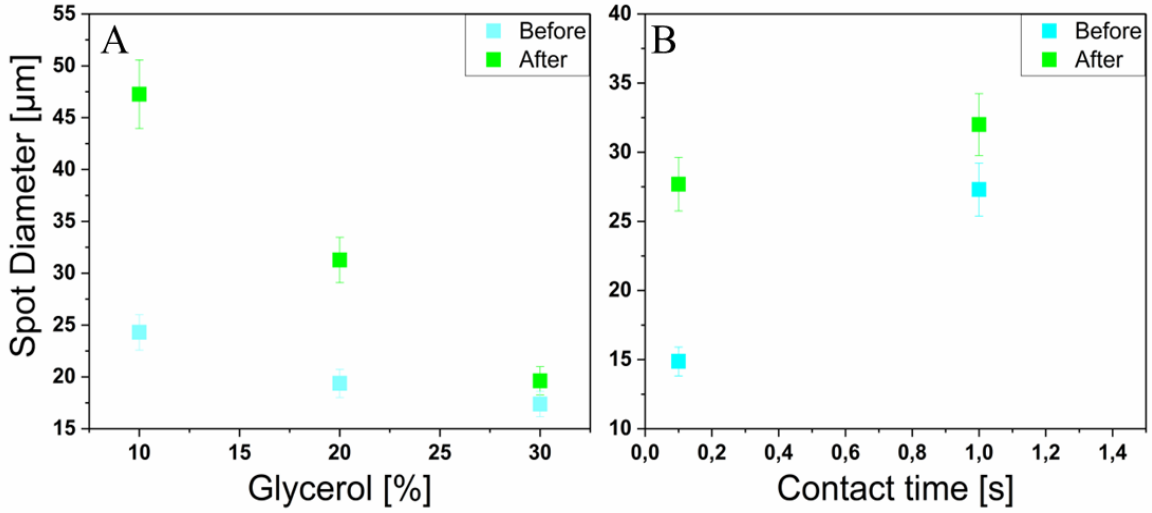

Figure 5.3. Evaluation of the size of the spots according to the concentration of glycerol and the contact time before and after the deposition. A) graphical representation of ethanolic ink spot dimensions before and after drying as a function of different glycerol concentration, with the other parameters being the same. B) graphical representation of aqueous ink spot dimensions, before and after drying, as a function of different contact time before and after printing processes, with the other parameters being the same. Error bars are 7% for both.

In Figure 5.3A, a graph depicting the lateral enlargement of the spots as a function of different percentages of glycerol content was presented. The sizes before and after drying, were very different. In particular, the lower the glycerol content, the greater the enlargement of the drop after drying. In presence of 10% v/v of glycerol there was an increase in term of dimensions of 90% after drying. While with 30% v/v of glycerol, the spots dimension increasing only of 10% after drying. The progressive dimensions of the spots as a function of the glycerol content before and after drying process result linear, and drastically decrease to a value of 30% v/v of glycerol. A graphic depicting changes in spot dimensions before and after the drying process was presented in Figure 5.3B. The dimensions were plotted as a function of two different contact times, 0.1 and 1 second, while keeping the other parameters constant. Graph shows a linear trend both before and after drying, also in this case. With 0,1s of contact time, spots show 80% of lateral enlargement. While with 1second of contact time, it was reduced up to 20% of lateral enlargement. These graphs were effective to understand how we can modify the printed phospholipid system and make it functional for our needs. So, through the changing of the parameters it is possible to modulate diameters, geometries and lateral enlargement of the spots. The preliminary study also allowed us to analyse the characteristics of the inks and evaluate the best one. Aqueous ink has been considered the optimal choice because it is possible to

reuse, this allows a more fluid phospholipid printing, minimizing ink refills. Aqueous ink has been chosen as the best to be ink to be used in our studio.

5.4 PH stability of the spots

After the characterization of the printing process, we choose two possible model proteins that could fit with the phospholipid spots. We choose two different model proteins: Concanavalin A (ConA)[87] a lectin (carbohydrate-binding protein) originally extracted from the jack-bean and Lysozyme (Lys) an enzyme known for its ability to degrade the polysaccharide architecture of many kinds of cell walls, normally for the purpose of protection against bacterial infection[129]. The two proteins present different isoelectric point (pI), ConA have a pI of 4.5-5[87] while Lys [130] was 10.7.

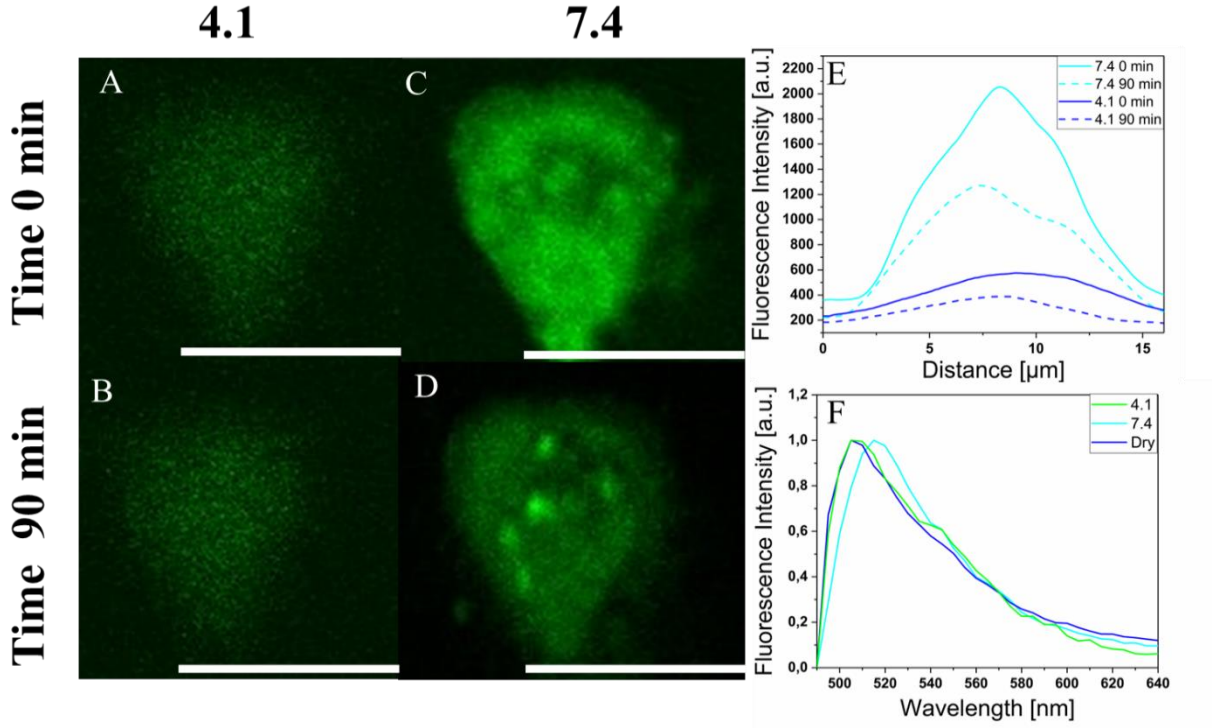

Figure 5.4. Confocal images of printed phospholipids at the two different pH. A-B) pH stability test for DOPE:DHPE-FITC (100:1) printed phospholipids at pH 4.1 Acetate buffer 0.1M from 0 to 90 min. C-D)pH stability test for DOPE:DHPE-FITC (100:1) printed phospholipids at pH 7.4 in Potassium phosphate buffer 0.1M from 0 to 90 min. E) Fluorescence intensity area of spots at time 0 and 90 minute. F) Normalized Fluorescence emission spectra of spots dry and in presence of buffer pH 4.1 and 7.4 at λ_{exc}= 488nm. Scale bars are 15 μm. Fluorescence confocal images have been acquired in the range 500-600 nm with λ_{exc}= 488nm. Experiments are carried out at room temperature.

Membrane-protein interaction was governed by electrostatic interaction[131], two pH values 4.1 and 7.4 which give the possibility of having all the possible combinations of charges between protein and membrane (membrane negative-protein negative, membrane negative-protein not charged and

membrane negative-protein positive). Before starting the membrane-protein interactions experiment of the pH stability tests were performed. Figure 5.4 shows the pH stability tests at pH 4.1(A-B) and 7.4 (C-D) from 0 to 90 minute. This time frame was considered suitable to follow the next experiments. In Figure 5.4A and 5.4B representative confocal images of the spot in Acetate buffer 0.1 M at pH 4.1 were showed. A homogeneous fluorescence signal of the spot at pH 4.1 was showed in Figure5.4. After 90 minutes, the spot is quietly the same. No change in term of intensity or geometry of the spot were found. While, Figure 5.4C and D show respectively the confocal images of DOPE:DHPE-FITC (100:1) in Potassium phosphate buffer 0.1M with pH 7.4 from 0 to 90 min. In C spot, it appears with a good fluorescence signal, and the intensity was homogeneous. After 90 minutes the fluorescence intensity of the spots quenches. No changing in spot geometry were found. Throughout the entire characterization process, the spot remained constant (data do not shown). Suggestions were confirmed from the graphic reported in Figure 5.4E, where it was reported the fluorescence intensity of the spots area in both pH before and after 90 min. From 5.4E a difference in fluoresce intensity from pH 4.1 and pH 7.4 was showed. A relative quenching of the printed phospholipids in both cases were showed, partially loss of intensity was due to the diffusion of phospholipids in the buffer[132]. At pH 7.4 fluorescence signal was reduced by 40% after 90 minutes. PH 4.1 shows a starting fluorescence intensity reduced by 80% compared to pH 7.4, but after 90 minutes spots lose only 10% of the fluorescence signal. No differences in term of geometry of the spots was found, while a non-symmetric fluorescence inside of spots were found. it was also evaluated the fluorescence emission of the spots (FITC) at the two different pH at λ_{exc}= 488nm in presence or not in presence of both buffers. Data showed in 5.4F reported the three different curves of fluorescence emission at 488 in presence or not in presence of buffers. Maximum emission peak for dry phospholipids and phospholipids at pH 4.1 coincide at 510nm. While at pH7.4 the fluorescence peak of FITC was red shifted. These probably happens, because FITC changes its ionic form as pH changing. At neutral pH, under excitation at 490 nm, the most fluorescent di-anionic form of FITC takes prominence over other forms. Below pH 6 mono-anionic fluorescein displays a blue-shifted absorption. At lower pH, neutral and further cationic forms of fluorescein become non-fluorescent [133]. Furthermore, during the measurements on the individual spot, the laser power can affect the measurement. All measurements were in fact carried out with laser powers at 0.2%. The fluorescent phospholipids showed a good stability with a higher fluorescence signal at pH 7.4. While fluoresce intensity of FITC resulted affected from the presence of acidic environment, because FITC is a very sensitive dye[134]. As FITC is a probe highly reactive to changes in pH and modification of its surrounding environment, it is a probe that is suitable for characterizing an interaction between protein and membrane.

5.5 Nile red and Leakage characterization

Nile Red (9-diethylamino-5H-benzo[α]phenoxazine-5-one) is an ideal probe for the detection of lipids as it exhibits high affinity, specificity and sensitivity to the degree of hydrophobicity of lipids[68]. With Nile Red, it was possible to discriminate from polar or not polar lipids as a function of the shift from red to yellow shift. Fluorescence lifetime distribution of Nile Red was used to infer the heterogeneity of membranes. The width of fluorescence lifetime was larger, and the lifetime was shorter in lipid supported membranes when compared to vesicle membranes[135]. Nile red is a sensitive probe for changing in surrounding environment. Nile Red discriminate the orientation and the organization of the Supported lipid bilayers (SLBs) using the blue shift of the fluorescence intensity, it can characterize the typical order of the membrane (I_0 liquid order phase and I_d liquid disorder phase)[136]. Printed lipids were hydrated with buffer solutions for both pH, then were inserted 0.5 µM of Nile Red inside of the solutions.

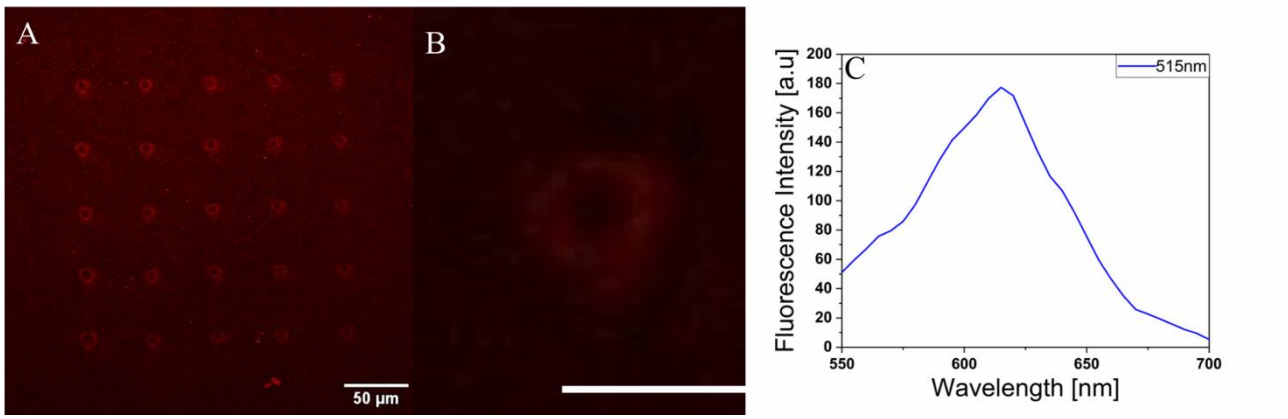

Figure 5.5. Confocal characterization of lipid order using Nile Red. A) Representative confocal fluoresce image of SLBs (DOPE:DHPE- FITC (100:1)) in presence of 0.5 µM of Nile Red at pH 7.4. B) Representative zoom of confocal fluoresce image of single SLBs (DOPE:DHPE- FITC (100:1) in presence of Nile Red. Scale bar is 15 µm. C) Fluorescence spectra of SLBs in presence of Nile Red. Fluorescence confocal images have been acquired in the range 550-650 nm with λ_{exc}= 515nm. Experiments are carried out at room temperature.

A confocal fluorescence characterization in presence of Nile Red was performed at λ_{exc}= 515nm and λ_{exc}= 559 nm. Figure 5.5A showed two confocal images of printed phospholipids in presence of Nile red at 515nm. The image shows the presence in all the sample of a big red signal at 515, no other variant of the colours was present. In the zoom image (Figure 5.6 B) only red fluoresce signal is visible; the sample presents a homogenous distribution of the Nile Red signal on the surface. The presence of the FITC in our sample, does not influence the fluorescence the signal of Nile Red. Same

characterization was performed for both pH, but no differences in term of Nile Red emission or changing in colour emission was found. An experimental fluorescence spectrum of the spots in presence of Nile Red, was showed in Figure 5.5C. The maximum of the peak was found at 615nm, while at 559 the maximum was found at 620 nm (Data do not shown). Results suggest that the printed SLBs were polar lipids, according with Diaz et al.[68], not blue shift of the fluoresce signal for both pH were found. These suggestions show that the lipid order of the phospholipid system was probably in the I_0 phase. This result was in agree with the ink composition: DOPE was a helper lipid[137], [138], a lipid that can stabilize the structure of the membrane that have an unsaturated chain. DHPE-FITC is a fluorescent phospholipid, with saturated chain and a different steric hindrance, mainly due to the presence of FITC linked to the nitrogen atom, in the phospholipid head. The presence of the big fluorophore on the phospholipid head leads to a structure I_d[139].

Last characterization of the SLBs was performed using a surfactant, to test the mechanical stability of the membrane. Membrane lysis, disruption and solubilization were studied in many biological function and technical application for example, the lysis of the membrane by antibiotics or antiseptic[140].The key to the interaction between the membrane phospholipids and surfactants was in the similar hydrophilic head and hydrophobic tail (Fig. 5.6A). The amphiphilic tail of surfactant inserts into the lipid bilayer and induces a local curve of the membrane as showed in Figure 5.6B. Usually, the surfactants are present in solution in two different forms: monomers, when the concentration of surfactants was under the Critical micelles concentration (CMC), or micelles, when the concentration was over the CMC concentration. In the last case surfactants were organized into a micelle to minimize the interaction between the hydrophobic tails and the water. This unnatural curvature of the phospholipid membranes due to the insertion of the detergent monomers, leads to the rupture of the membrane[141]. Generally, a fundamental parameter of the membrane surfactants interaction was the rate of the surfactant flip-flop across the phospholipid layers. Phospholipids general present low flip-flop rate. Usually, the flip-flop process is a typical function of detergent solution and experimental conditions. Different experiments of interaction were performed between the Supported lipid and Tween20, a non-ionic polysorbate with a typical critical micelles concentration (CMC) about 0.076%[142]. Experiments were performed with a concentration of Tween 20 about 0.01%, a value under the CMC. From Figure 5.6C to Figure 5.6F it was presented the interaction between Tween 20 and printed phospholipids followed by confocal fluoresce images taken every 10 min. When the Tween20 was inserted a big decrease in term of fluoresce intensity was

found and after 60 minutes. Figure 5.6F showed the partial destruction of the spot due to the Tween20 insertion.

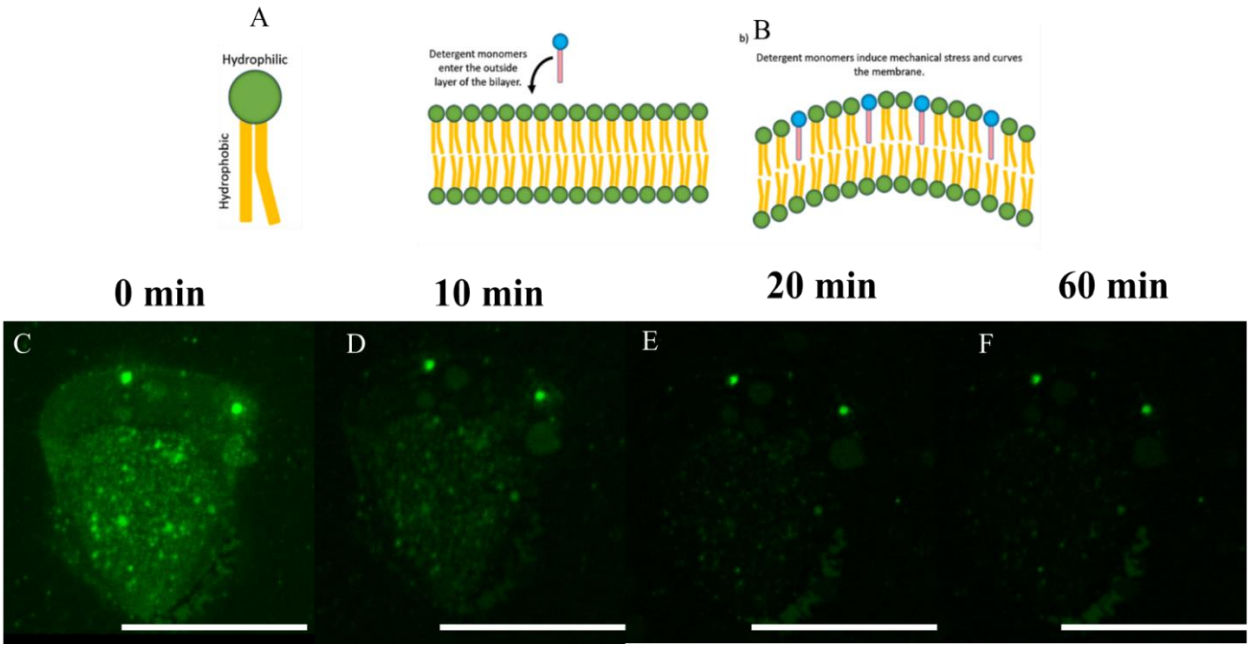

Figure 5.6. Phospholipids and Tween20 interactions. A) Description of the phospholipid structure B) Description of the interaction between the surfactants and phospholipid membranes was modified from: https://lifecanvastech.com/how-do-detergents-dissolve-lipid-membranes/ C-E) Representative Confocal fluorescence microscope images of a single SLBs of DOPE:DHPE-FITC(1:100) before and after the interaction with Tween20 0.01% v/v from 0 to 60 minutes at pH 7.4. Scale Bars are 15 µm. Fluorescence confocal images have been acquired in the range 500-600 nm with λ_{exc}= 488nm. Experiments are carried out at room temperature.

The internal part of the spot was broken from Tween20 monomers present in solution. The burst of the phospholipid membrane takes time and after 60 minutes only the external part of the phospholipid membrane remained attached to the glass. The spot appears at the end emptied internally. The geometry of the spots does not change during the interaction process. Same results were founded at the other pH (data do not shown). This is coherent with the fact that Tween20 being non-ionic has not been affected by pH. This result shows us that the developed SLBs was a reactive system that responds to external stimuli, and therefore it can be used in a process of interaction with a protein.

5.6 Concanavalin and Lysozyme interactions

The printed SLBs, were tested with two different proteins Concanavalin A (ConA) and Lysozyme (Lys) at pH 4.1 and 7.4. Con A a lectin (carbohydrate-binding protein) originally extracted from the jack-bean[143], [144] and Lysozyme, a globular protein of 14.4 kDa molecular weight is a bacteriolytic enzyme that is used as a natural food preservative[145], [146] were reported in many papers as proteins that interact strongly with membranes. Con A interact better whit glycolipids, biomolecules composed of a lipophilic chain and a monosaccharide as hydrophilic group[147].Lys is instead known for binding to negative charged phospholipids[148]. The lipid-protein interactions were mediated from the electrostatic interactions[146], [149]. Electrostatics interactions were also involved in membrane stability and curvature. Changing of electrostatic forces between the bilayer and the external of the membrane leads to a destabilization that can lead to breakdown of the lipid bilayer[150]. Membrane-protein interactions are also involved in ethology of many neurodegenerative diseases. The understanding these processes was fundamental in order to counteract to the disease[27], [35], [151]. At first, an evaluation of the interactions between ConA

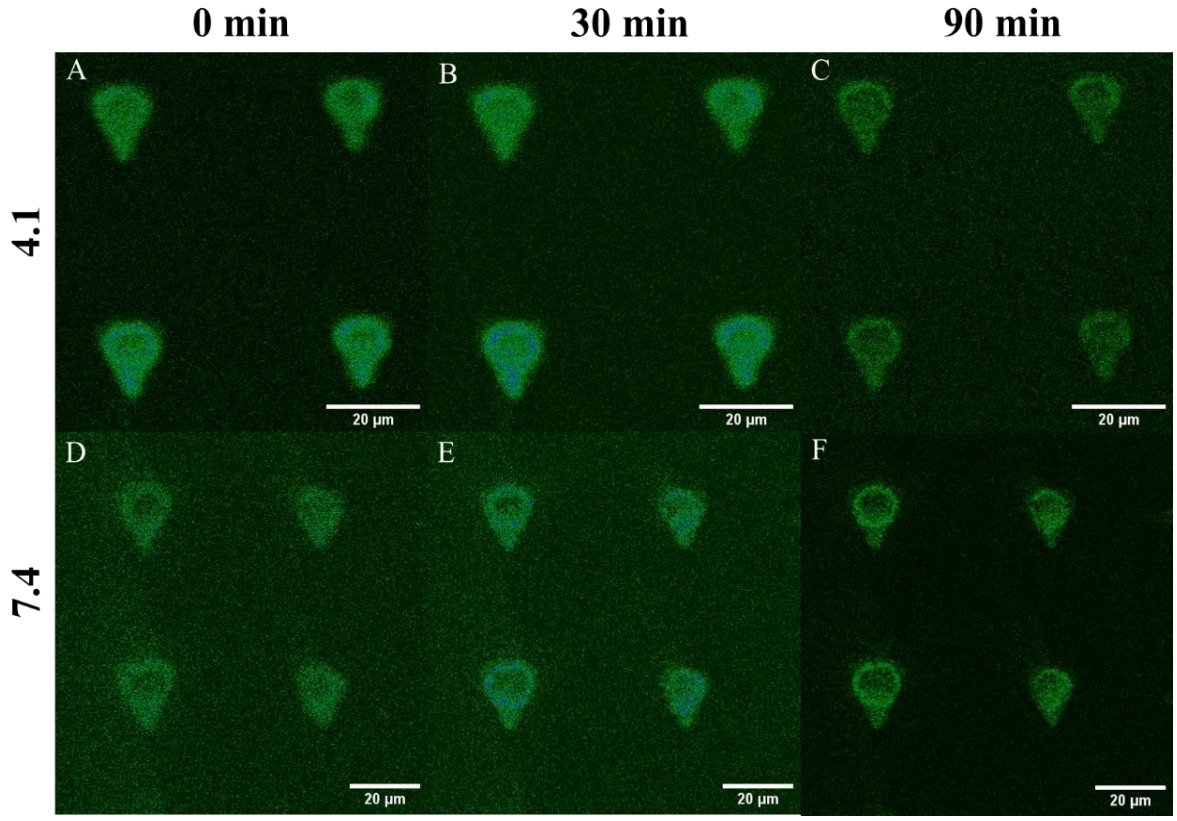

Figure 5.7. Concanavalin A vs printed phospholipids interactions. A-F) Representative Confocal Fluorescence images of SLBs of DOPE:DHPE- FITC (100:1) and ConA 0.1 mg/ml interaction at room temperature following FITC from 0 to 90 minutes, at pH 4.1 and 7.4 solutions. Fluorescence confocal images have been acquired in the range 500-600 nm with λ_{exc}= 488nm. Experiments are carried out at room temperature.

and

Lys were conducted at pH 7.4 and 4.1 at the same protein concentration 0.1 mg/ml. This initial protein concentration was sought as the minimum concentration, this enabled us to work with excess protein. The processes were followed for 90 minutes using Confocal fluorescence microscopy, monitoring changes in FITC fluorescence and in spot morphology. The first printed phospholipoids were hydrated with the relative buffer solution and then after some minutes it was inserted a protein solution with known concentration. During all the measurements the Z-axis remains constant throughout the process.

Figure 5.7. showed different representative confocal fluorescence images of SLBs DOPE: DHPE-FITC (1:100) before and after the exposure after 90 minutes to a solution 0.1 mg/ml of ConA at pH 4.1 and 7.4 from 0 to 90 minutes. Figure 5.7A showed the initial step of the interaction between DOPE:DHPE- FITC (1:100) and Con A at pH 4.1, the four spots selected for the following during the entire process show continuous spot fluorescence and a well-defined triangular geometry, no FITC signal in solution was detected. After 30 minutes (Fig.5.7 B) the fluorescence intensity of the two spots below increases a bit and the FITC present in solutions increases too, but no aggregates and no change in term of geometry was found. After 90 minutes (Figure 5.7 C) the FITC signal in solution reduced and it reduced the intensity signal of single spots. No aggregates and no change in term of geometry were found. On the other hands, Figure 5.7D showed the initial step of the interaction between DOPE:DHPE-FITC(1:100) and ConA at pH 7.4. Presence of FITC in solution were found at the starting point, the intensity signal of the spots and the spots geometry appears constant. After 90 minutes, Figure 5.7 F shows a decreasing in term of fluorescence intensity and no FITC signal was detected in solution. No changes in term of geometry of the spots or aggregates were found. ConA shows two different forms as a function of pH, a dimeric form at pH 4.1 while at pH 7.4, it changes in a tetramer form[152]. The isoelectric point of the protein was between 4.5 and 5.5 [152], so at pH 4.1 the protein net charge near to zero, while at 7.4 the protein presents a net negative charge. The SBLs maintain probably in both case a negative charge, FITC present in the spots, exposed to the solvent solution presents a anionic charge at pH4.1 and dianionic charge at pH7.4[88]. During the process no changes in term of geometry or aggregates present, and no changes in term of fluoresce spectra before and after the interaction was found (data do not shown). The data do not show a change in size or fluorescence intensity that would suggest an interaction under these experimental conditions.

Same experiments were conducted with Lys at 0.1 mg/ml with same protocol. Lys present a I.p. of 10.7 [153], so with our experimental conditions the protein maintains a net positive charge for both

pH conditions. Lys was reported as globular protein that interacts with negatively charged phospholipids, Lys presents two or three positive charges at pH 7.4 while at pH 4.1 it presents twelve positive charges[148]. As a function of the different pH, an increase in term of positive charge was reported as the interaction to negative phospholipids increases [148]. Figure 5.8 reported representative confocal fluorescence image of SLBs DOPE: DHPE- FITC (100:1) before and after the exposure to a solution 0.1 mg/ml of Lys at pH 4.1 and 7.4 from 0 to 90 minutes.

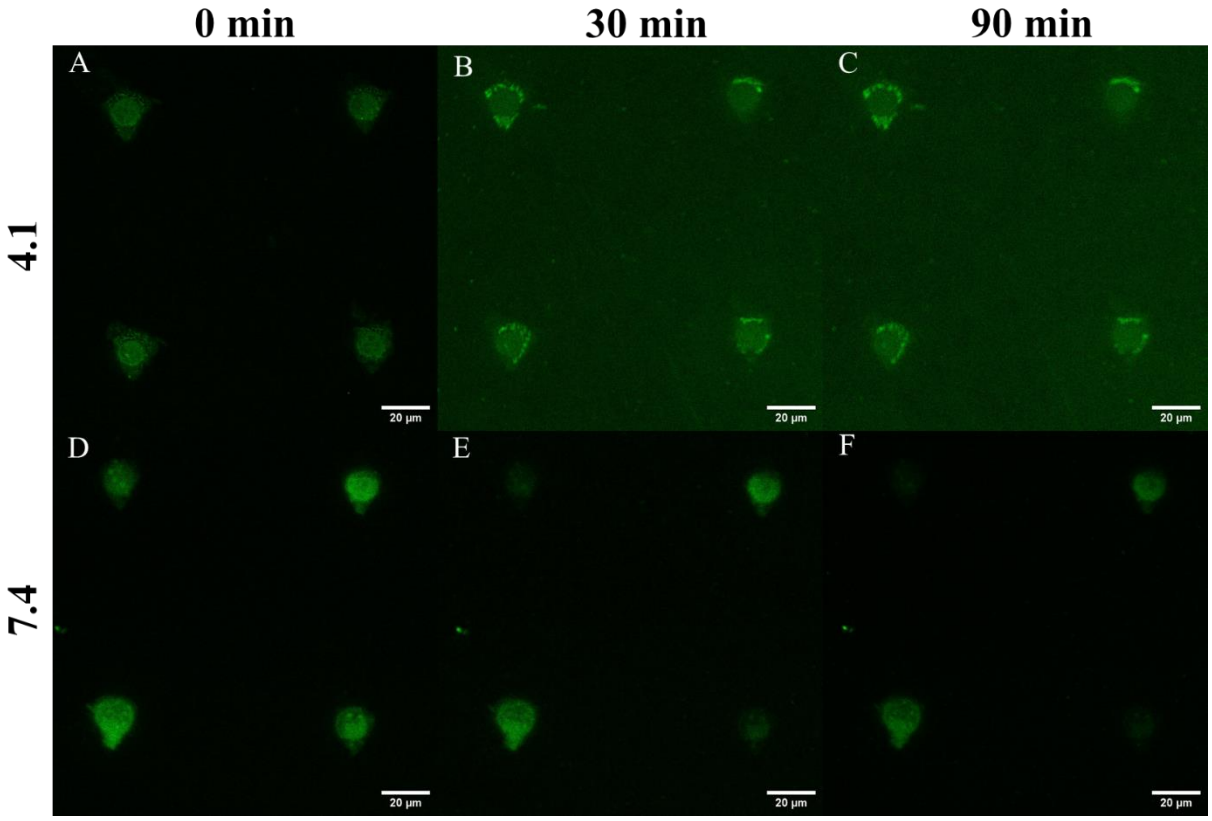

Figure 5.8. Lysozyme vs printed phospholipids interactions. A-F) Representative Confocal Fluorescence images of SLBs of DOPE:DHPE- FITC (100:1) and Lys 0.1 mg/ml interaction at room temperature following FITC from 0 to 90 minutes, at pH 4.1 and 7.4 solutions. Fluorescence confocal images have been acquired in the range 500-600 nm with λ_{exc}= 488nm. Experiments are carried out at room temperature.

In Figure 5.8A the starting point of the interaction process at pH 4.1 between Lys and DOPE:DHPE-FITC spots was presented. The images show the triangular spots with a globular fluorescence intensity on the centre of the spots, no FITC signal on the ground was found. After 30 minutes (Figure 5.8B) a big fluoresce intensity of FITC on the ground was found and the intensity of the spots changeed a lot, in particular the external part on the spots turned out to be much more fluorescent of the inner part. After 90 minutes, same results were showed, no differences from B and C in term of

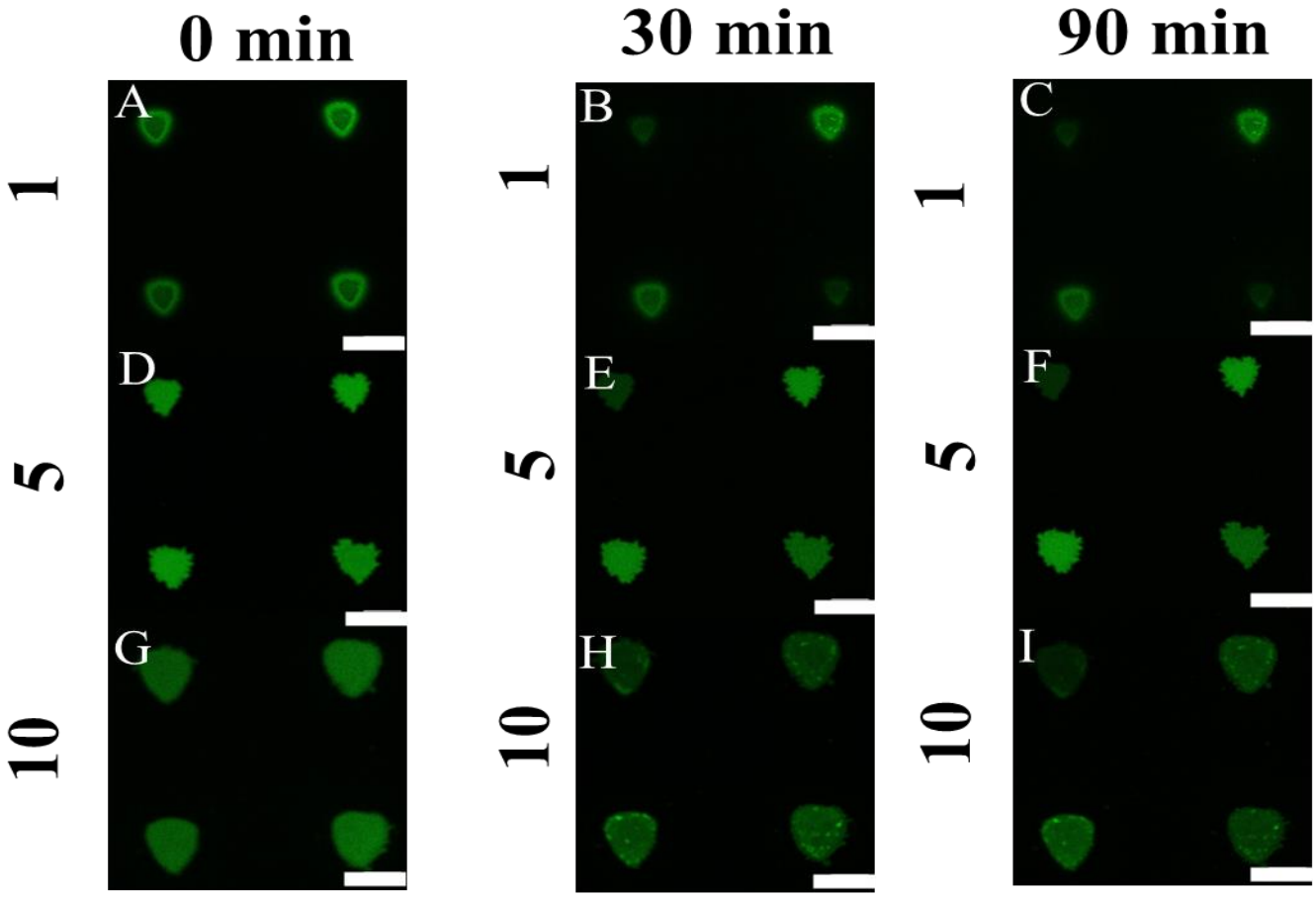

Figure 5.9. Protein membrane concentration as a function of increasing protein concentration. A-I) Representative Confocal fluoresce images of DOPE:DHPE- FITC (100:1) with an increasing concentration of Lys 1-5-10 mg/ml at pH7.4. Confocal fluorescence images have been acquired in the range 500-600 nm with λ_{exc}= 488nm. Scale Bars are 20 µm. Experiments are carried out at room temperature.

geometric or intensity of fluorescence were found. In Figure 5.8D the starting point of the interaction at pH7.4 process between Lys and DOPE:DHPE- FITC spots were showed. From the first images 5.8D to 5.8F no differences in term of geometry or ground fluoresce intensity was found. A quenching of the spot form D to F was showed. A large difference in terms of FITC in solution was found at pH 4.1 in the presence of lysozyme, while similar modification was found in the interaction with ConA at pH 7.4. No changes in term of the triangular geometry of the spots were found. It has also been evaluated whether the concentration of the protein could affect the interaction with membrane models. This study was conducted using Lysozyme. Some experiment with Lysozyme at pH7.4 were performed, we changed the concentration of the protein form 1 to 10mg/ml. Figure 5.10 showed the different experiment by varying the concentration of the protein from 1 (Fig.5.10A-5.10C) to 10 (Fig.5.10 G-5.10I). Form 5.10A to 5.10F no differences in term of intensity of the ground or geometrical modification of the spots were found. While in 5.10H after the interaction with the

protein, inside the spots, an interesting change in term of fluorescence intensity of the spots was found. From 5.10G to 5.10H it has been showed a big increase in fluorescence intensity only in in well-defined areas of the spots, FITC is affected by a local change in its environment. This could be related to the interaction between the membrane and the protein. These interaction from Lysozyme and membranes, can take place, but at a very high concentration of protein. This happens even if the forces involved of the electrostatic type are in opposite directions. At the starting stage of the process (0-30 minute) no differences in term of fluoresce intensity, geometry or fluoresce spectra was found (data do not shown). So, at starting point of the process no interaction between the membrane models and protein appears. Only with increasing concentration of protein were founded the surface modifications (Figure 5.10H). at lower concentration of protein, no changes occur. All experiments were performed with an excess of protein concentration, to increase the possibility of binding and therefore of interaction of the system. Protein in solution goes from $1,02*10^{15}$ to $1,05*10^{16}$ molecules as compared to $5*10^{11}$ phospholipids molecules. Lysozyme was reported as high lysis activity in the pH range from 6.2 to 9.2[154], and was function of ionic strength of the aqueous solution. Lysozyme activity decrease as a function of increasing in salt concentration, while in the experiment were used 100 mM, that was in the range to maximum activity of the protein[86]. Different studies were performed with phospholipid membranes, membranes models and vesicles[155]–[157]. All the papers about the lysozyme-membrane interactions talk about a non-destructive interaction with the membrane, such as an adsorption of the protein itself on the charged residues. Electrostatics interactions were reported as the specific interactions involved in the process. Our data support this thesis, the modifications of the spots visioned in the experiments do not present destruction or the presence of membrane aggregates in solution.

A schematic representation of the Lysozyme interactions with phospholipid membrane was showed in Figure 5.10. In the initial state of the process the protein does not interact with the phospholipid bilayer, after a typical time of twenty or thirty minutes, the protein interacts with the negative charge of the phospholipid membrane and was adsorbed upon the membrane at the final stage. Among these process destabilization and protein-protein aggregation can occur[157]. The negative residues charges drive the process of the interaction, and electrostatics mediate the interactions. The concentration of the protein was fundamental too. No big changes in phospholipids spots were found under the 10mg/ml condition in our work. Different concentrations of phospholipids, at the final stage change the molar ratio between DOPE and DHPE- FITC phospholipids, but this has led to a modification of the membrane model printing protocol, and it has made printing of phospholipid spots very difficult.

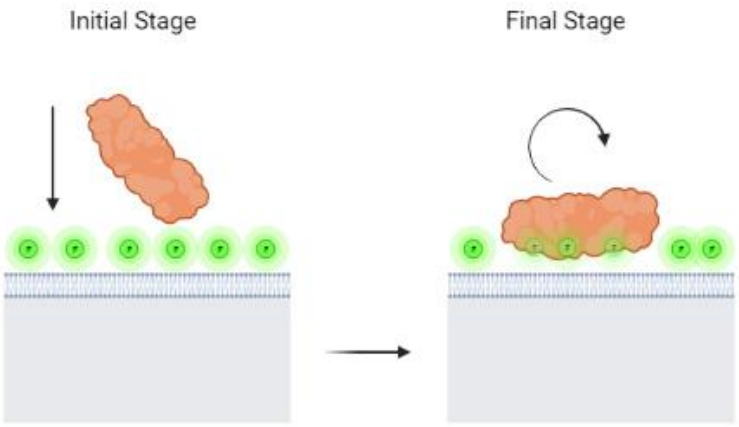

Figure 5.10. Possible Lysozyme-membrane models interactions. Scheme of possible lysozyme (reported in orange) and printed membrane phospholipids interactions during time at pH7.4.

Different studies have investigated the interaction between lysozyme and membrane models. Some support the hypothesis of a membrane disruption[41] caused by protein aggregates, while others have found that lysozyme does not induce significant changes on phospholipids, but at most modifies their intensity or fluorescence shift[96], [148]. Our data support this hypothesis because no structural modifications, no aggregated solution was found. It is likely that lysozyme inserts into the phospholipid layer, modifying its hydration.

5.7 Conclusions

This Chapter has proposed an innovative approach in order to follow the protein-membrane interaction, this was possible by using a useful printing biology technique named Micro-contact spotting (μCS). The scientific interest in protein membrane interactions is given by the fact that the process affects many biological processes and one of them underlies many neurodegenerative diseases[26], [27], [149].

μCS was chosen to make a model membrane system named Solid supported Lipid bilayers (SLBs) or multilayer composed from two phospholipids DOPE, a helper lipid that can stabilize our membrane spots and DHPE-FITC a fluorescent phospholipid, with the presence of Fluorescein attached to the head of phospholipid; this is helpful for monitoring some modification in the surrounding environment. The model developed it had shown to be geometrically and dimensionally modifiable, chemically stable, and highly reactive when subjected to surfactants.

Membrane models were subjected to interactions with two model proteins: Lysozyme and Concanavalin A which are scientifically recognized as proteins that interact with membranes[41], [144]. The findings confirm the basic role of electrostatic interactions as the main interactions involved in membrane-protein interactions. Concanavalin A show smaller important interaction with membrane models at the two pH, this was probably due to the net charge of the protein, which at pH 4.1 has nearly zero net charge, and at neutral pH it shows a net negative charge[87]. Also, in presence of 0.1mg/ml Lysozyme smaller modification were found at neutral pH. Smaller modification of the spots appears at high concentration of protein (10 mg/ml). Charged spots do not show geometrical or structural changes under this protein concentration. The low changes of spot intensity, was in accordance with literature[155]–[157], a weak type modification of the spots is shown, probably due to an adsorption of the protein over the membrane. Further studies about protein aggregates must be carried out in order to get a global overview of the interactions.

6 Conclusions and future perspectives

Neurodegenerative processes have affected almost 40% of the world's population for over 100 years, yet the mechanisms underlying neurodegeneration are still poorly understood. Among the mechanisms that have long been recognized as contributing to the formation of neurodegenerative diseases, we must consider the protein aggregation and the interaction between proteins and the cell membrane. The understanding of these basic processes can help science counteract the progression of these class of disease. A more model-based approach can simplify the understanding of phenomena that would otherwise be impossible to decipher.

Bovine Serum Albumin has been used as a model protein to characterize the interaction between the protein and a promising non-aggregating substance, EGCG. The interaction was evaluated by varying the electrostatic interactions involved. A first spectroscopic approach was conducted to characterize the potential interaction between EGCG and BSA under varying charge conditions. The interaction was assessed by varying the pH. At pH 5, BSA is nearly neutrally charged, while at pH 7, the protein carries a net negative charge. As confirmed by fluorescence studies, a quenching effect on the intrinsic fluorescence of BSA confirms a possible interaction between BSA and EGCG. The red shift observed only at pH 7 suggests that electrostatics influence the process and that a change in the protein's tertiary structure occurs at pH 7. This result aligns with Li's findings[23], which yielded similar results at the same pH values. Circular Dichroism studies confirm that there are minimal effects on the protein's secondary structure. The interaction or binding of EGCG and BSA is evaluated by using a technique that allows the determination of thermodynamic variables and the potential binding of the small molecule. The result of the ITC (Isothermal Titration Calorimetry), consistent with spectroscopic analyses, indicates a potential binding in a single binding site involving electrostatic and hydrophobic forces. The presence of hydrophobic forces is confirmed by the ANS study. Spectroscopic studies confirm an electrostatic binding, likely involving hydrophobic forces and hydrogen bonds that stabilize the interaction. The results suggest a binding in proximity to one of the protein's hydrophobic pockets, particularly the one near Trp213. This finding aligns with the works of Li[23] and Skrt [24]. Following the spectroscopic analysis, the second part of the study aims to characterize the nature of EGCG as an anti-aggregating molecule. The evaluation was performed by using fluorescence, specifically by monitoring the evolution of Rayleigh scattering. The results showed that EGCG drastically changes its anti-aggregating characteristic depending on the pH change. At pH7, EGCG behaved as an anti-aggregating molecule. Whereas at lower pH, close to the protein's isoelectric point, the molecule helped protein aggregation. The same result occurred in the presence of EGCGOx. The

process of interaction between BSA and EGCGC through spectroscopy up to micro/macroscopic characterizations has allowed for a global view of the interaction. All results are consistent with each other and find broad support by the literature.

The second part of the thesis related the interaction between the protein and the surface membrane, an approach through models of cellular membrane allowed the testing of the interaction. The interaction between the cell membrane surface and proteins is of utmost relevance in the pathological processes leading to neurodegeneration. Currently, certain aspects regarding the composition and charge of the membranes are being elucidated, which appears to enhance the likelihood of interaction between membranes and proteins. The dynamics of interaction and the binding mode of the protein to the membrane are still debated topics to date. The approach to the problem is often very complex, given the challenging observability of events. The aim of this work is to create an analytical platform that utilizes fluorescent molecules, which is simple and capable of mimicking the phospholipid surface of the membrane. This platform can be modified in various aspects, including geometry, electrostatics, and more. By printing it on standard microscope slides, we obtain a system that can be easily observed using any fluorescence microscope. Once the stability and high signal-to-noise ratio of the system were characterized, the platform was tested in the presence of two model proteins, Concanavalin A and Lysozyme. The two proteins were tested under varying electrostatic forces. Concanavalin A (ConA) did not show any potential interaction with the membrane models during the studies. Also, Lysozyme at lower concentration of the protein, do not show an interaction. The increasing in Lysozyme concentration (conducted many times), showed a small modification of the printed phospholipid state. The limited or no-interaction of ConA was attributed probably to the electrostatic charge present in the system. While in the case of lysozyme, the two charges present are opposite in nature.

BSA and membrane systems have demonstrated characteristics that make them good model systems. BSA, a highly studied and economical protein, can form fibrils under certain conditions. This characteristic can be used to conduct basic science studies. While the developed analytical platform allows for hundreds of testable systems, achievable with 0.4 microliters of ink. The aqueous ink has proven to be stable and reusable for an extended period. The membrane models prove to be stable and highly responsive.

In the future, interactions between cellular membranes and protein aggregates, will be evaluated to assess their different interactions compared to native protein. Finally, EGCG will be used as an anti-

aggregating agent in protein-membrane interaction processes, to determine its behaviour in that context. This process can be monitored by advanced microscopy techniques.

Bibliography

[1] A. N. Shrivastava, A. Aperia, R. Melki, and A. Triller, 'Review Physico-Pathologic Mechanisms Involved in Neurodegeneration: Misfolded Protein-Plasma Membrane Interactions', 2017, doi: 10.1016/j.neuron.2017.05.026.

[2] C. M. Dobson, 'Principles of protein folding, misfolding and aggregation', *Semin Cell Dev Biol*, vol. 15, no. 1, pp. 3–16, 2004, doi: 10.1016/J.SEMCDB.2003.12.008.

[3] R. L. Baldwin, 'Energetics of Protein Folding', *J Mol Biol*, vol. 371, no. 2, pp. 283–301, Aug. 2007, doi: 10.1016/J.JMB.2007.05.078.

[4] T. R. Jahn and S. E. Radford, 'Folding versus aggregation: polypeptide conformations on competing pathways', *Arch Biochem Biophys*, vol. 469, no. 1, pp. 100–117, Jan. 2008, doi: 10.1016/J.ABB.2007.05.015.

[5] K. Beyreuther, G. Multhaup, and C. L. Masters, 'Alzheimer's Disease: Genesis of Amyloid', *CIBA Foundation Symposia*, no. 199, pp. 119–131, 1996, doi: 10.1002/9780470514924.CH8.

[6] C. A. Ross and M. A. Poirier, 'Protein aggregation and neurodegenerative disease', *Nature Medicine 2004 10:7*, vol. 10, no. 7, pp. S10–S17, Jul. 2004, doi: 10.1038/nm1066.

[7] J. E. Yang *et al.*, 'EGCG-mediated Protection of the Membrane Disruption and Cytotoxicity Caused by the "Active Oligomer" of α-Synuclein', 2017, doi: 10.1038/s41598-017-18349-z.

[8] L. Nielsen *et al.*, 'Effect of Environmental Factors on the Kinetics of Insulin Fibril Formation: Elucidation of the Molecular Mechanism †', *Biochemistry*, 2001, doi: 10.1021/bi002555c.

[9] S. Giorgetti, C. Greco, P. Tortora, and F. A. Aprile, 'Molecular Sciences Targeting Amyloid Aggregation: An Overview of Strategies and Mechanisms', *MDPI*, 2018, doi: 10.3390/ijms19092677.

[10] L. A. Munishkina and A. L. Fink, 'Fluorescence as a method to reveal structures and membrane-interactions of amyloidogenic proteins', *Biochimica et Biophysica Acta (BBA) - Biomembranes*, vol. 1768, no. 8, pp. 1862–1885, Aug. 2007, doi: 10.1016/J.BBAMEM.2007.03.015.

[11] H. S. Kim, M. J. Quon, and J. a. Kim, 'New insights into the mechanisms of polyphenols beyond antioxidant properties; lessons from the green tea polyphenol, epigallocatechin 3-gallate', *Redox Biol*, vol. 2, no. 1, pp. 187–195, Jan. 2014, doi: 10.1016/J.REDOX.2013.12.022.

[12] C. Ramassamy, 'Emerging role of polyphenolic compounds in the treatment of neurodegenerative diseases: A review of their intracellular targets', *Eur J Pharmacol*, vol. 545, no. 1, pp. 51–64, Sep. 2006, doi: 10.1016/J.EJPHAR.2006.06.025.

[13] M. F. M. Engel, C. C. Vandenakker, M. Schleeger, K. P. Velikov, G. H. Koenderink, and M. Bonn, 'The Polyphenol EGCG Inhibits Amyloid Formation Less Efficiently at Phospholipid Interfaces than in Bulk Solution', *JACS*, 2012, doi: 10.1021/ja3031664.

[14] B.-B. Wei, M.-Y. Liu, X. Zhong, W.-F. Yao, and M.-J. Wei, 'Increased BBB permeability contributes to EGCG-caused cognitive function improvement in natural aging rats: pharmacokinetic and distribution analyses', 2019, doi: 10.1038/s41401-019-0243-7.

[15] S. K. Sonawane *et al.*, 'EGCG impedes human tau aggregation and interacts with tau', vol. 10, p. 12579, 2020, doi: 10.1038/s41598-020-69429-6.

[16] L. Fernandes *et al.*, 'Green Tea Polyphenol Microparticles Based on the Oxidative Coupling of EGCG Inhibit Amyloid Aggregation/Cytotoxicity and Serve as a Platform for Drug Delivery', *ACS Biomaterials Science e Engineering*, 2020, doi: 10.1021/acsbiomaterials.0c00188.

[17] J. Bieschke *et al.*, 'EGCG remodels mature α-synuclein and amyloid-β fibrils and reduces cellular toxicity', *PNAS*, vol. 107, 2010, doi: 10.1073/pnas.0910723107.

[18] T. T. An, S. Feng, and C. M. Zeng, 'Oxidized epigallocatechin gallate inhibited lysozyme fibrillation more strongly than the native form', *Redox Biol*, vol. 11, pp. 315–321, Apr. 2017, doi: 10.1016/j.redox.2016.12.016.

[19] V. Vetri, F. Librizzi, M. Leone, and V. Militello, 'Thermal aggregation of bovine serum albumin at different pH: Comparison with human serum albumin', in *European Biophysics Journal*, Sep. 2007, pp. 717–725. doi: 10.1007/s00249-007-0196-5.

[20] G. Sancataldo, V. Vetri, V. Foderà, G. di Cara, V. Militello, and M. Leone, 'Oxidation enhances human serum albumin thermal stability and changes the routes of amyloid fibril formation', *PLoS One*, vol. 9, no. 1, Jan. 2014, doi: 10.1371/journal.pone.0084552.

[21] V. Vetri *et al.*, 'Bovine Serum Albumin protofibril-like aggregates formation: Solo but not simple mechanism', *Arch Biochem Biophys*, vol. 508, no. 1, pp. 13–24, Apr. 2011, doi: 10.1016/j.abb.2011.01.024.

[22] V. Militello, V. Vetri, and M. Leone, 'Conformational changes involved in thermal aggregation processes of bovine serum albumin', *Biophys Chem*, vol. 105, no. 1, pp. 133–141, Aug. 2003, doi: 10.1016/S0301-4622(03)00153-4.

[23] M. Li and A. E. Hagerman, 'Role of the flavan-3-ol and galloyl moieties in the interaction of (-)-epigallocatechin gallate with serum albumin', *J Agric Food Chem*, vol. 62, no. 17, pp. 3768–3775, Apr. 2014, doi: 10.1021/jf500246m.

[24] M. Skrt, E. Benedik, Č. Podlipnik, and N. P. Ulrih, 'Interactions of different polyphenols with bovine serum albumin using fluorescence quenching and molecular docking', *Food Chem*, vol. 135, no. 4, pp. 2418–2424, Dec. 2012, doi: 10.1016/J.FOODCHEM.2012.06.114.

[25] S. Soares, N. Mateus, and V. De Freitas, 'Interaction of Different Polyphenols with Bovine Serum Albumin (BSA) and Human Salivary r-Amylase (HSA) by Fluorescence Quenching', 2007, doi: 10.1021/jf070905x.

[26] T. Inoshita, C. Cui, N. Hattori, and Y. Imai, 'Regulation of membrane dynamics by Parkinson's disease-associated genes', *Journal of Genetics 2018 97:3*, vol. 97, no. 3, pp. 715–727, Jul. 2018, doi: 10.1007/S12041-018-0959-Z.

[27] A. Iyer and M. M. A. E. Claessens, 'Disruptive membrane interactions of alpha-synuclein aggregates', *Biochimica et Biophysica Acta - Proteins and Proteomics*, vol. 1867, no. 5. Elsevier B.V., pp. 468–482, May 01, 2019. doi: 10.1016/j.bbapap.2018.10.006.

[28] V. Shukla, S. K. Mishra, and H. C. Pant, 'Oxidative Stress in Neurodegeneration', *Adv Pharmacol Sci*, vol. 2011, p. 13, 2011, doi: 10.1155/2011/572634.

[29] J. E. Straub and D. Thirumalai, ‘Membrane-protein interactions are key to understanding amyloid formation’, *Journal of Physical Chemistry Letters*, vol. 5, no. 3, pp. 633–635, Feb. 2014, doi: 10.1021/JZ500054D/ASSET/IMAGES/LARGE/JZ-2014-00054D_0001.JPEG.

[30] R. Ventura, I. Martínez-Ruiz, and M. I. Hernández-Alvarez, ‘Phospholipid Membrane Transport and Associated Diseases’, *Biomedicines 2022, Vol. 10, Page 1201*, vol. 10, no. 5, p. 1201, May 2022, doi: 10.3390/BIOMEDICINES10051201.

[31] J. Roel-Touris, B. Jiménez-García, and A. M. J J Bonvin, ‘Integrative modeling of membrane-associated protein assemblies’, doi: 10.1038/s41467-020-20076-5.

[32] B. H. Honig, W. L. Hubbell, R. F. Flewelling, and J. Stein, ‘ELECTROST ATIC INTERACTIONS IN MEMBRANES AND PROTEINS’, *Ann. Rev. Biophys. Biophys. Chem*, vol. 15, pp. 163–93, 1986, Accessed: Apr. 24, 2023. [Online]. Available: www.annualreviews.org

[33] A. K. Mahakud, J. Shaikh, V. V Rifa Iqbal, A. Gupta, A. Tiwari, and · Mohammed Saleem, ‘Amyloids on Membrane Interfaces: Implications for Neurodegeneration’, *J Membr Biol*, vol. 255, no. 3, pp. 705–722, 2022, doi: 10.1007/s00232-022-00245-x.

[34] T. Skamris, C. Marasini, K. L. Madsen, V. Foderà, and B. Vestergaard, ‘Early Stage Alpha-Synuclein Amyloid Fibrils are Reservoirs of Membrane-Binding Species’, *Scientific Reports 2019 9:1*, vol. 9, no. 1, pp. 1–11, Feb. 2019, doi: 10.1038/s41598-018-38271-2.

[35] T. Das and D. Eliezer, ‘Membrane interactions of intrinsically disordered proteins: The example of alpha-synuclein’, *Biochimica et Biophysica Acta - Proteins and Proteomics*, vol. 1867, no. 10. Elsevier B.V., pp. 879–889, Oct. 01, 2019. doi: 10.1016/j.bbapap.2019.05.001.

[36] J. B. Schulz, L. Hausmann, and J. Hardy, ‘199 years of Parkinson disease – what have we learned and what is the path to the future?’, *Journal of Neurochemistry*. Blackwell Publishing Ltd, pp. 3–7, Oct. 01, 2016. doi: 10.1111/jnc.13733.

[37] Y. Zarbiv, D. Simhi-Haham, E. Israeli, S. A. Elhadi, J. Grigoletto, and R. Sharon, ‘Lysine residues at the first and second KTKEGV repeats mediate α-Synuclein binding to membrane phospholipids’, *Neurobiol Dis*, vol. 70, pp. 90–98, 2014, doi: 10.1016/j.nbd.2014.05.031.

[38] J. Burré, ‘The Synaptic Function of-Synuclein’, *J Parkinsons Dis*, vol. 5, pp. 699–713, 2015, doi: 10.3233/JPD-150642.

[39] A. Mori, Y. Imai, and N. Hattori, ‘Lipids: Key Players That Modulate α-Synuclein Toxicity and Neurodegeneration in Parkinson’s Disease’, *International Journal of Molecular Sciences 2020, Vol. 21, Page 3301*, vol. 21, no. 9, p. 3301, May 2020, doi: 10.3390/IJMS21093301.

[40] C. Galvagnion *et al.*, ‘Lipid vesicles trigger a-synuclein aggregation by stimulating primary nucleation’, *nature CHeMICaL BIOLOGY |*, vol. 11, 2015, doi: 10.1038/nCHeMBIO.1750.

[41] V. M. Trusova and G. P. Gorbenko, ‘Membrane interactions of fibrillar lysozyme: Effect of lipid bilayer composition’, *J Mol Liq*, vol. 274, pp. 338–344, Jan. 2019, doi: 10.1016/j.molliq.2018.10.103.

[42] V. Vetri, R. Carrotta, P. Picone, M. Di Carlo, and V. Militello, ‘Concanavalin A aggregation and toxicity on cell cultures’, *Biochimica et Biophysica Acta (BBA) - Proteins and Proteomics*, vol. 1804, no. 1, pp. 173–183, Jan. 2010, doi: 10.1016/J.BBAPAP.2009.09.013.

[43] G. Arrabito, D. Gulli, C. Alfano, and B. Pignataro, '"Writing biochips": high-resolution droplet-to-droplet manufacturing of analytical platforms', *Analyst*, vol. 147, no. 7, pp. 1294–1312, Mar. 2022, doi: 10.1039/D1AN02295D.

[44] G. Arrabito, V. Ferrara, A. Bonasera, and B. Pignataro, 'Artificial Biosystems by Printing Biology', *Small*, vol. 16, no. 27, p. 1907691, Jul. 2020, doi: 10.1002/SMLL.201907691.

[45] G. Arrabito and B. Pignataro, 'Inkjet printing methodologies for drug screening', *Anal Chem*, vol. 82, no. 8, pp. 3104–3107, Apr. 2010, doi: 10.1021/AC100169W/SUPPL_FILE/AC100169W_SI_001.PDF.

[46] R. Bumgarner, 'Overview of DNA microarrays: types, applications, and their future', *Curr Protoc Mol Biol*, vol. Chapter 22, no. SUPPL.101, 2013, doi: 10.1002/0471142727.MB2201S101.

[47] B. Schweitzer, P. Predki, and M. Snyder, 'Microarrays to characterize protein interactions on a whole-proteome scale', *Proteomics*, vol. 3, no. 11, pp. 2190–2199, Nov. 2003, doi: 10.1002/PMIC.200300610.

[48] T. Elad and S. Belkin, 'Whole-cell biochips for online water monitoring', *Bioeng Bugs*, vol. 3, no. 2, p. 122, Mar. 2012, doi: 10.4161/BBUG.18879.

[49] M. A. J. Roberts, R. M. Cranenburgh, M. P. Stevens, and P. C. F. Oyston, 'Synthetic biology: biology by design', *Microbiology (Reading)*, vol. 159, no. Pt 7, pp. 1219–1220, Jul. 2013, doi: 10.1099/MIC.0.069724-0.

[50] M. Weiss *et al.*, 'Sequential bottom-up assembly of mechanically stabilized synthetic cells by microfluidics', 2018, doi: 10.1038/NMAT5005.

[51] B. M. Discher *et al.*, 'Polymersomes: Tough Vesicles Made from Diblock Copolymers', *Science (1979)*, 1999, Accessed: Apr. 14, 2023. [Online]. Available: https://www.science.org

[52] I. Platzman, J.-W. Janiesch, and J. Pius Spatz, 'Synthesis of Nanostructured and Biofunctionalized Water-in-Oil Droplets as Tools for Homing T Cells', 2013, doi: 10.1021/ja311588c.

[53] T. W. Lowry *et al.*, 'Quantification of Protein-Induced Membrane Remodeling Kinetics In Vitro with Lipid Multilayer Gratings', *Small*, vol. 12, no. 4, pp. 506–515, Jan. 2016, doi: 10.1002/SMLL.201502398.

[54] A. Vikulina, A. Wulf, G. Guday, R. Fakhrullin, and D. Volodkin, 'A lipid membrane supported on an artificial extracellular matrix made of polyelectrolyte multilayers: towards nanoarchitectonics at the cellular interface', *Nanoscale*, vol. 15, p. 2197, 2023, doi: 10.1039/d2nr05186a.

[55] P. E. Milhiet, M. C. Giocondi, O. Baghdadi, F. Ronzon, B. Roux, and C. Le Grimellec, 'Spontaneous insertion and partitioning of alkaline phosphatase into model lipid rafts', *EMBO Rep*, vol. 3, no. 5, pp. 485–490, Jan. 2002, doi: 10.1093/EMBO-REPORTS/KVF096.

[56] K. J. Seu, A. P. Pandey, F. Haque, E. A. Proctor, A. E. Ribbe, and J. S. Hovis, 'Effect of surface treatment on diffusion and domain formation in supported lipid bilayers', *Biophys J*, vol. 92, no. 7, pp. 2445–2450, 2007, doi: 10.1529/BIOPHYSJ.106.099721.

[57] P. P. Cheney, A. W. Weisgerber, A. M. Feuerbach, and M. K. Knowles, ‘Single Lipid Molecule Dynamics on Supported Lipid Bilayers with Membrane Curvature’, *Membranes 2017, Vol. 7, Page 15*, vol. 7, no. 1, p. 15, Mar. 2017, doi: 10.3390/MEMBRANES7010015.

[58] S. Sekula-Neuner *et al.*, ‘Phospholipid arrays on porous polymer coatings generated by micro-contact spotting’, *Beilstein Journal of Nanotechnology*, vol. 8, no. 1, pp. 715–722, Mar. 2017, doi: 10.3762/bjnano.8.75.

[59] G. Arrabito *et al.*, ‘Imbibition of Femtoliter-Scale DNA-Rich Aqueous Droplets into Porous Nylon Substrates by Molecular Printing’, 2019, doi: 10.1021/acs.langmuir.9b02893.

[60] R. L. Maynard, ‘The Merck Index: 12th edition 1996’, *Occup Environ Med*, vol. 54, no. 4, p. 288, 1997, Accessed: Mar. 14, 2023. [Online]. Available: https://www.ncbi.nlm.nih.gov/pmc/articles/PMC1128712/

[61] N. J. Greenfield, ‘Using circular dichroism spectra to estimate protein secondary structure’, *Nature protocol*, 2007, doi: 10.1038/nprot.2006.202.

[62] V. I. Dodero, Z. B. Quirolo, and M. A. Sequeira, ‘Biomolecular studies by circular dichroism’, *Front Biosci (Landmark Ed)*, vol. 16, no. 1, pp. 61–73, Jan. 2011, doi: 10.2741/3676.

[63] H. Moosmüller and W. P. Arnott, ‘Particle optics in the rayleigh regime’, *J Air Waste Manage Assoc*, vol. 59, no. 9, pp. 1028–1031, 2009, doi: 10.3155/1047-3289.59.9.1028.

[64] J. R. Lakowicz, *Principles of fluorescence spectroscopy*. Springer, 2006.

[65] R. Datta, T. M. Heaster, J. T. Sharick, A. A. Gillette, and M. C. Skala, ‘Fluorescence lifetime imaging microscopy: fundamentals and advances in instrumentation, analysis, and applications’, *J Biomed Opt*, vol. 25, no. 7, p. 1, May 2020, doi: 10.1117/1.JBO.25.7.071203.

[66] H. Yang, X. Xiao, X. Zhao, and Y. Wu, ‘Intrinsic fluorescence spectra of tryptophan, tyrosine and phenyloalanine’, *https://doi.org/10.1117/12.2268397*, vol. 10255, pp. 1199–1206, Mar. 2017, doi: 10.1117/12.2268397.

[67] O. K. Gasymov and B. J. Glasgow, ‘ANS Fluorescence: Potential to Augment the Identification of the External Binding Sites of Proteins’, *Biochim Biophys Acta*, 2007.

[68] G. Diaz, M. Melis, B. Batetta, F. Angius, and A. M. Falchi, ‘Hydrophobic characterization of intracellular lipids in situ by Nile Red red/yellow emission ratio’, *Micron*, vol. 39, no. 7, pp. 819–824, Oct. 2008, doi: 10.1016/J.MICRON.2008.01.001.

[69] B. Demeule, R. Gurny, and T. Arvinte, ‘Detection and characterization of protein aggregates by fluorescence microscopy’, *Int J Pharm*, vol. 329, no. 1–2, pp. 37–45, Feb. 2007, doi: 10.1016/j.ijpharm.2006.08.024.

[70] Michiel. Muller and Society of Photo-optical Instrumentation Engineers., ‘Introduction to confocal fluorescence microscopy’, *Spie*, p. 119, 2006.

[71] M. A. Digman, V. R. Caiolfa, M. Zamai, and E. Gratton, ‘The phasor approach to fluorescence lifetime imaging analysis’, *Biophys J*, vol. 94, no. 2, Jan. 2008, doi: 10.1529/BIOPHYSJ.107.120154.

[72] Y. Sun and S.-C. Liao, ‘The Ultimate Phasor Plot and beyond’, Accessed: Apr. 11, 2023. [Online]. Available: www.iss.com/resources/research/technical_notes.

[73] S. W. Huang and E. N. Frankel, 'Antioxiciant Activity of Tea Catechins in Different Lipid Systems', *J Agric Food Chem*, vol. 45, no. 8, pp. 3033–3038, 1997, doi: 10.1021/JF9609744/ASSET/IMAGES/LARGE/JF9609744F00008.JPEG.

[74] J. Hu, D. Zhou, and Y. Chen, 'Preparation and antioxidant activity of green tea extract enriched in epigallocatechin (EGC) and epigallocatechin gallate (EGCG)', *J Agric Food Chem*, vol. 57, no. 4, pp. 1349–1353, Feb. 2009, doi: 10.1021/JF803143N/ASSET/IMAGES/LARGE/JF-2008-03143N_0001.JPEG.

[75] Y. C. Wang and U. Bachrach, 'The specific anti-cancer activity of green tea (-)-epigallocatechin-3-gallate (EGCG)', *Amino Acids*, vol. 22, no. 2, pp. 131–143, 2002, doi: 10.1007/S007260200002/METRICS.

[76] X.-L. Bu, P. P. N. Rao, and Y.-J. Wang, 'Anti-amyloid Aggregation Activity of Natural Compounds: Implications for Alzheimer's Drug Discovery', *Mol Neurobiol*, 2016, doi: 10.1007/s12035-015-9301-4.

[77] M. Ziaunys and V. Smirnovas, 'Exploring Epigallocatechin-3-Gallate Autoxidation Products: Specific Incubation Times Required for Emergence of Anti-Amyloid Properties', *Antioxidants*, vol. 11, no. 10, Oct. 2022, doi: 10.3390/antiox11101887.

[78] M. Hirohata *et al.*, 'The anti-amyloidogenic effect is exerted against Alzheimer's β-amyloid fibrils in vitro by preferential and reversible binding of flavonoids to the amyloid fibril structure', *Biochemistry*, vol. 46, no. 7, pp. 1888–1899, Feb. 2007, doi: 10.1021/bi061540x.

[79] V. Snitsarev, M. N. Young, R. M. S. Miller, and D. P. Rotella, 'The spectral properties of (-)-epigallocatechin 3-O-gallate (EGCG) fluorescence in different solvents: Dependence on solvent polarity', *PLoS One*, vol. 8, no. 11, Nov. 2013, doi: 10.1371/journal.pone.0079834.

[80] N. Li, L. S. Taylor, M. G. Ferruzzi, and L. J. Mauer, 'Kinetic study of catechin stability: Effects of ph, concentration, and temperature', *J Agric Food Chem*, vol. 60, no. 51, pp. 12531–12539, Dec. 2012, doi: 10.1021/jf304116s.

[81] I. Rousso and A. Deshpande, 'Applications of Atomic Force Microscopy in HIV-1 Research', *Viruses*, vol. 14, no. 3. MDPI, Mar. 01, 2022. doi: 10.3390/v14030648.

[82] R. P. Richter, R. Bérat, and A. R. Brisson, 'Formation of Solid-Supported Lipid Bilayers: An Integrated View', 2006, doi: 10.1021/la052687c.

[83] G. Liu, S. H. Petrosko, Z. Zheng, and C. A. Mirkin, 'Evolution of Dip-Pen Nanolithography (DPN): From Molecular Patterning to Materials Discovery', *Chem Rev*, vol. 120, no. 13, pp. 6009–6047, Jul. 2020, doi: 10.1021/ACS.CHEMREV.9B00725/ASSET/IMAGES/LARGE/CR9B00725_0011.JPEG.

[84] A. Annular *et al.*, 'Inkjet printing-the physics of manipulating liquid jets and drops You may also like Inkjet printing-the physics of manipulating liquid jets and drops', *Journal of Physics: Conference Series OPEN ACCESS*, doi: 10.1088/1742-6596/105/1/012001.

[85] E. Berganza and M. Hirtz, 'Direct-Write Patterning of Biomimetic Lipid Membranes in Situ with FluidFM', *ACS Appl Mater Interfaces*, vol. 13, no. 43, pp. 50774–50784, Nov. 2021, doi: 10.1021/ACSAMI.1C15166/SUPPL_FILE/AM1C15166_SI_001.PDF.

[86] K. Y. Chang and C. W. Carr, 'Studies on the structure and function of lysozyme: I. The effect of pH and cation concentration on lysozyme activity', *Biochimica et Biophysica Acta (BBA)* -

Protein Structure, vol. 229, no. 2, pp. 496–503, Feb. 1971, doi: 10.1016/0005-2795(71)90210-8.

[87] V. Vetri, M. Leone, L. A. Morozova-Roche, B. Vestergaard, and V. Foderà, 'Unlocked Concanavalin A Forms Amyloid-like Fibrils from Coagulation of Long-lived "'Crinkled'" Intermediates', 2013, doi: 10.1371/journal.pone.0068912.

[88] R. Sjöback, J. Nygren, and M. Kubista, 'Absorption and fluorescence properties of fluorescein', *Spectrochim Acta A Mol Biomol Spectrosc*, vol. 51, no. 6, pp. L7–L21, Jun. 1995, doi: 10.1016/0584-8539(95)01421-P.

[89] G. Prasanna and P. Jing, 'Polyphenol binding disassembles glycation-modified bovine serum albumin amyloid fibrils', *Spectrochim Acta A Mol Biomol Spectrosc*, vol. 246, Feb. 2021, doi: 10.1016/j.saa.2020.119001.

[90] H. Tang, L. Huang, D. Zhao, C. Sun, and P. Song, 'Interaction mechanism of flavonoids on bovine serum albumin: Insights from molecular property-binding affinity relationship', *Spectrochim Acta A Mol Biomol Spectrosc*, vol. 239, Oct. 2020, doi: 10.1016/J.SAA.2020.118519.

[91] R. Li, Z. Wu, Y. Wangb, L. Ding, and Y. Wang, 'Role of pH-induced structural change in protein aggregation in foam fractionation of bovine serum albumin', *Biotechnology Reports*, vol. 9, pp. 46–52, Mar. 2016, doi: 10.1016/j.btre.2016.01.002.

[92] S. Boyko, X. Qi1, T. H. Chen, K. Surewicz, and W. K. Surewicz, 'Liquid-liquid phase separation of tau protein: The crucial role of electrostatic interactions', *Journal of Biological Chemistry*, vol. 294, no. 29, pp. 11054–11059, Jul. 2019, doi: 10.1074/jbc.AC119.009198.

[93] J. L. Zhu *et al.*, 'Study on the interaction between ketoprofen and bovine serum albumin by molecular simulation and spectroscopic methods', *Spectroscopy*, vol. 26, pp. 337–348, 2011, doi: 10.3233/SPE-2012-0549.

[94] Y. li Wei, J. qing Li, C. Dong, S. min Shuang, D. sheng Liu, and C. W. Huie, 'Investigation of the association behaviors between biliverdin and bovine serum albumin by fluorescence spectroscopy', *Talanta*, vol. 70, no. 2, pp. 377–382, Sep. 2006, doi: 10.1016/J.TALANTA.2006.02.052.

[95] A. Papadopoulou, R. J. Green, and R. A. Frazier, 'Interaction of Flavonoids with Bovine Serum Albumin: A Fluorescence Quenching Study', *J Agric Food Chem*, 2005, doi: 10.1021/jf048693g.

[96] B. Yuan *et al.*, 'Penetration and saturation of lysozyme in phospholipid bilayers', *Journal of Physical Chemistry B*, vol. 111, no. 22, pp. 6151–6155, Jun. 2007, doi: 10.1021/jp071050u.

[97] S. Pal, C. Saha, M. Hossain, S. K. Dey, and G. S. Kumar, 'Influence of galloyl moiety in interaction of epicatechin with bovine serum albumin: A spectroscopic and thermodynamic characterization', *PLoS One*, vol. 7, no. 8, Aug. 2012, doi: 10.1371/journal.pone.0043321.

[98] R. Li, Z. Wu, Y. Wangb, L. Ding, and Y. Wang, 'Role of pH-induced structural change in protein aggregation in foam fractionation of bovine serum albumin', *Biotechnology Reports*, vol. 9, pp. 46–52, Mar. 2016, doi: 10.1016/j.btre.2016.01.002.

[99] L. Zhang, Y. Liu, and Y. Wang, 'Interaction between an (−)-epigallocatechin-3-gallate-copper complex and bovine serum albumin: Fluorescence, circular dichroism, HPLC, and docking studies', *Food Chem*, vol. 301, Dec. 2019, doi: 10.1016/J.FOODCHEM.2019.125294.

[100] K. P. M. Frin and V. M. Nascimento, 'Rhenium(I) polypyridine complexes as luminescence-based sensors for the BSA protein', *J Braz Chem Soc*, vol. 27, no. 1, pp. 179–185, Jan. 2016, doi: 10.5935/0103-5053.20150268.

[101] A. J. Guliyeva and O. K. Gasymov, 'ANS fluorescence: Potential to discriminate hydrophobic sites of proteins in solid states', *Biochem Biophys Rep*, vol. 24, Dec. 2020, doi: 10.1016/j.bbrep.2020.100843.

[102] H. Tang, L. Huang, D. Zhao, C. Sun, and P. Song, 'Interaction mechanism of flavonoids on bovine serum albumin: Insights from molecular property-binding affinity relationship', *Spectrochim Acta A Mol Biomol Spectrosc*, vol. 239, Oct. 2020, doi: 10.1016/j.saa.2020.118519.

[103] H. Tang, F. Ma, and D. Zhao, 'Integrated multi-spectroscopic and molecular modelling techniques to probe the interaction mechanism between salvianolic acid A and α-glucosidase', 2019, doi: 10.1016/j.saa.2019.03.109.

[104] D. M. Togashi and A. G. Ryder, 'A fluorescence analysis of ANS bound to bovine serum albumin: Binding properties revisited by using energy transfer', *J Fluoresc*, vol. 18, no. 2, pp. 519–526, 2008, doi: 10.1007/s10895-007-0294-x.

[105] W.M.Haynes, *CRC Handbook of Chemistry and Physics*. 2014.

[106] B. Z. Chowdhry and S. E. (Stephen E.) Harding, *Protein-ligand interactions : hydrodynamics and calorimetry : a practical approach*. Oxford University Press, 2001.

[107] R. A. Frazier, A. Papadopoulou, and R. J. Green, 'Isothermal titration calorimetry study of epicatechin binding to serum albumin', *J Pharm Biomed Anal*, vol. 41, no. 5, pp. 1602–1605, Aug. 2006, doi: 10.1016/j.jpba.2006.02.004.

[108] J. D. Eaton and M. P. Williamson, 'Multi-site binding of epigallocatechin gallate to human serum albumin measured by NMR and isothermal titration calorimetry', *Biosci Rep*, 2017, doi: 10.1042/BSR20170209.

[109] M. M. Ramos-Tejada, J. D. G. Durán, A. Ontiveros-Ortega, M. Espinosa-Jimenez, R. Perea-Carpio, and E. Chibowski, 'Investigation of alumina/(+)-catechin system properties. Part II: z-potential and surface free energy changes of alumina', 2002. [Online]. Available: www.elsevier.com/locate/colsurfb

[110] K. Baler, O. A. Martin, M. A. Carignano, G. A. Ameer, J. A. Vila, and I. Szleifer, 'Electrostatic Unfolding and Interactions of Albumin Driven by pH Changes: A Molecular Dynamics Study', *J Phys Chem B*, vol. 118, no. 4, p. 921, Jan. 2014, doi: 10.1021/JP409936V.

[111] M. Zhu, S. Han, and A. L. Fink, 'Oxidized quercetin inhibits α-synuclein fibrillization', *Biochim Biophys Acta Gen Subj*, vol. 1830, no. 4, pp. 2872–2881, Apr. 2013, doi: 10.1016/j.bbagen.2012.12.027.

[112] Y. Wei *et al.*, 'Certain (-)-epigallocatechin-3-gallate (EGCG) auto-oxidation products (EAOPs) retain the cytotoxic activities of EGCG', *Food Chem*, vol. 204, pp. 218–226, Aug. 2016, doi: 10.1016/j.foodchem.2016.02.134.

[113] M. Shi *et al.*, 'Food-grade Encapsulation Systems for (-)-Epigallocatechin Gallate', *Molecules*, vol. 23, no. 2. MDPI AG, 2018. doi: 10.3390/molecules23020445.

[114] M. Shi *et al.*, 'Food-grade Encapsulation Systems for (-)-Epigallocatechin Gallate', *Molecules*, vol. 23, no. 2. MDPI AG, 2018. doi: 10.3390/molecules23020445.

[115] S. A. Ghadami, Z. Ahmadi, and Z. Moosavi-Nejad, 'The albumin-based nanoparticle formation in relation to protein aggregation', *Spectrochim Acta A Mol Biomol Spectrosc*, vol. 252, May 2021, doi: 10.1016/J.SAA.2021.119489.

[116] S. Ranjit, L. Malacrida, D. M. Jameson, and E. Gratton, 'Fit-free analysis of fluorescence lifetime imaging data using the phasor approach', *Nat Protoc*, vol. 13, no. 9, pp. 1979–2004, Sep. 2018, doi: 10.1038/s41596-018-0026-5.

[117] G. de Luca, D. Fennema Galparsoro, G. Sancataldo, M. Leone, V. Foderà, and V. Vetri, 'Probing ensemble polymorphism and single aggregate structural heterogeneity in insulin amyloid self-assembly', *J Colloid Interface Sci*, vol. 574, pp. 229–240, Aug. 2020, doi: 10.1016/j.jcis.2020.03.107.

[118] X. Nai *et al.*, 'Temperature, pH and additives effects on the binding of Caffeic acid phenethyl ester to the native state of bovine serum albumin', *Journal of Chemical Thermodynamics*, vol. 168, May 2022, doi: 10.1016/j.jct.2022.106724.

[119] K. S. Schmitz, 'An introduction to dynamic light scattering by macromolecules', p. 449, 1990, Accessed: Mar. 07, 2023. [Online]. Available: https://books.google.com/books/about/Introduction_to_Dynamic_Light_Scattering.html?hl=it&id=UA5kAlG0jkgC

[120] U. Nobbmann and A. Morfesis, 'Light scattering and nanoparticles', *Materials Today*, vol. 12, no. 5, pp. 52–54, May 2009, doi: 10.1016/S1369-7021(09)70164-6.

[121] S. Pm *et al.*, 'CryoEM reveals how the small molecule EGCG binds to Alzheimer's brain-derived tau fibrils and initiates fibril disaggregation', 2020, doi: 10.1101/2020.05.29.124537.

[122] J. Zhao *et al.*, '(À)-Epigallocatechin-3-gallate (EGCG) inhibits fibrillation, disaggregates amyloid fibrils of a-synuclein, and protects PC12 cells against a-synuclein-induced toxicity', 2017, doi: 10.1039/c7ra03752j.

[123] A. Franko *et al.*, 'Epigallocatechin gallate (EGCG) reduces the intensity of pancreatic amyloid fibrils in human islet amyloid polypeptide (hIAPP) transgenic mice OPEN', *Sci Rep*, 2018, doi: 10.1038/s41598-017-18807-8.

[124] R. Sternke-Hoffmann, A. Peduzzo, N. Bolakhrif, R. Haas, and A. K. Buell, 'The Aggregation Conditions Define Whether EGCG is an Inhibitor or Enhancer of α-Synuclein Amyloid Fibril Formation', *Int J Mol Sci*, vol. 21, no. 6, Mar. 2020, doi: 10.3390/IJMS21061995.

[125] K. Wong *et al.*, 'Neuropathology provides clues to the pathophysiology of Gaucher disease', *Mol Genet Metab*, vol. 82, no. 3, pp. 192–207, Jul. 2004, doi: 10.1016/J.YMGME.2004.04.011.

[126] R. P. Richter, R. Bérat, and A. R. Brisson, 'Formation of solid-supported lipid bilayers: An integrated view', *Langmuir*, vol. 22, no. 8, pp. 3497–3505, Apr. 2006, doi: 10.1021/LA052687C/SUPPL_FILE/LA052687CSI20051122_072621.PDF.

[127] D. Hirsch-Lerner, M. Zhang, H. Eliyahu, M. E. Ferrari, C. J. Wheeler, and Y. Barenholz, 'Effect of "helper lipid" on lipoplex electrostatics', *Biochim Biophys Acta Biomembr*, vol. 1714, no. 2, pp. 71–84, Aug. 2005, doi: 10.1016/j.bbamem.2005.04.008.

[128] X. Cheng and R. J. Lee, 'The role of helper lipids in lipid nanoparticles (LNPs) designed for oligonucleotide delivery', *Adv Drug Deliv Rev*, vol. 99, no. Pt A, pp. 129–137, Apr. 2016, doi: 10.1016/J.ADDR.2016.01.022.

[129] S. A. Ragland and A. K. Criss, 'From bacterial killing to immune modulation: Recent insights into the functions of lysozyme', 2017, doi: 10.1371/journal.ppat.1006512.

[130] E. D. N. S. Abeyrathne, H. Y. Lee, and D. U. Ahn, 'Sequential separation of lysozyme, ovomucin, ovotransferrin, and ovalbumin from egg white', *Poult Sci*, vol. 93, no. 4, pp. 1001–1009, Apr. 2014, doi: 10.3382/PS.2013-03403.

[131] A. Mori, Y. Imai, and N. Hattori, 'Molecular Sciences Lipids: Key Players That Modulate α-Synuclein Toxicity and Neurodegeneration in Parkinson's Disease', doi: 10.3390/ijms21093301.

[132] M. Rose, N. Hirmiz, J. M. Moran-Mirabal, and C. Fradin, 'Lipid Diffusion in Supported Lipid Bilayers: A Comparison between Line-Scanning Fluorescence Correlation Spectroscopy and Single-Particle Tracking', *Membranes (Basel)*, vol. 5, pp. 702–721, 2015, doi: 10.3390/membranes5040702.

[133] F. Le Guern, V. Mussard, A. Gaucher, M. Rottman, and D. Prim, 'Molecular Sciences Fluorescein Derivatives as Fluorescent Probes for pH Monitoring along Recent Biological Applications', *MDPI*, 2020, doi: 10.3390/ijms21239217.

[134] E. Lanz, M. Gregor, J. Slavik, and A. Kotyk1, 'Use of FITC as a Fluorescent Probe for Intracellular pH Measurement', *J Fluoresc*, vol. 7, no. 4, 1997.

[135] I. G. Krishnamoorthy, 'Probing the dynamics of planar supported membranes by Nile red fluorescence lifetime distribution', *Biochimica et Biophysica Acta (BBA) - Biomembranes*, vol. 1414, no. 1–2, pp. 255–259, Nov. 1998, doi: 10.1016/S0005-2736(98)00157-6.

[136] A. Halder, B. Saha, P. Maity, G. S. Kumar, D. K. Sinha, and S. Karmakar, 'Lipid chain saturation and the cholesterol in the phospholipid membrane affect the spectroscopic properties of lipophilic dye nile red', *Spectrochim Acta A Mol Biomol Spectrosc*, vol. 191, pp. 104–110, Feb. 2018, doi: 10.1016/J.SAA.2017.10.002.

[137] S. Mochizuki *et al.*, 'The role of the helper lipid dioleoylphosphatidylethanolamine (DOPE) for DNA transfection cooperating with a cationic lipid bearing ethylenediamine', *Biochim Biophys Acta Biomembr*, vol. 1828, no. 2, pp. 412–418, Feb. 2013, doi: 10.1016/J.BBAMEM.2012.10.017.

[138] H. Farhood, N. Serbina, and L. Huang, 'The role of dioleoyl phosphatidylethanolamine in cationic liposome mediated gene transfer', *BBA - Biomembranes*, vol. 1235, no. 2, pp. 289–295, May 1995, doi: 10.1016/0005-2736(95)80016-9.

[139] S. Bordovsky, C. S. Wong, G. D. Bachand, J. C. Stachowiak, and D. Y. Sasaki, 'Engineering Lipid Structure for Recognition of the Liquid Ordered Membrane Phase', *Langmuir*, 2016.

[140] M. Ongena and P. Jacques, ‘Bacillus lipopeptides: versatile weapons for plant disease biocontrol’, *Trends Microbiol*, vol. 16, no. 3, pp. 115–125, 2008, doi: 10.1016/J.TIM.2007.12.009.

[141] T. P. Sudbrack, N. L. Archilha, R. Itri, and K. A. Riske, ‘Observing the solubilization of lipid bilayers by detergents with optical microscopy of GUVs’, *Journal of Physical Chemistry B*, vol. 115, no. 2, pp. 269–277, Jan. 2011, doi: 10.1021/JP108653E/SUPPL_FILE/JP108653E_SI_001.PDF.

[142] A. Patist, S. S. Bhagwat, K. W. Penfield, P. Aikens, and D. O. Shah, ‘On the measurement of critical micelle concentrations of pure and technical-grade nonionic surfactants’, *J Surfactants Deterg*, vol. 3, no. 1, pp. 53–58, 2000, doi: 10.1007/S11743-000-0113-4/METRICS.

[143] U. Bakowsky *et al.*, ‘Characterization of the interactions between various hexadecylmannoside–phospholipid model membranes with the lectin Concanavalin A’, *Physical Chemistry Chemical Physics*, vol. 2, no. 20, pp. 4609–4614, Jan. 2000, doi: 10.1039/B003727N.

[144] C. A. Chicken and F. J. Sharom, ‘Lipid-protein interactions of the human erythrocyte concanavalin a receptor in phospholipid bilayers’, *Biochimica et Biophysica Acta (BBA) - Biomembranes*, vol. 774, no. 1, pp. 110–118, Jul. 1984, doi: 10.1016/0005-2736(84)90281-5.

[145] E. Posse, B. F. De Arcuri, and R. D. Morero, ‘Lysozyme interactions with phospholipid vesicles: relationships with fusion and release of aqueous content’, *Biochimica et Biophysica Acta (BBA) - Biomembranes*, vol. 1193, no. 1, pp. 101–106, Jul. 1994, doi: 10.1016/0005-2736(94)90338-7.

[146] O. Zschörnig, G. Paasche, C. Thieme, N. Korb, and K. Arnold, ‘Modulation of lysozyme charge influences interaction with phospholipid vesicles’, *Colloids Surf B Biointerfaces*, vol. 42, no. 1, pp. 69–78, Apr. 2005, doi: 10.1016/J.COLSURFB.2005.01.008.

[147] C. Sandoval-Altamirano, S. A. Sanchez, N. F. Ferreyra, and G. Gunther, ‘Understanding the interaction of concanavalin a with mannosyl glycoliposomes: A surface plasmon resonance and fluorescence study’, *Colloids Surf B Biointerfaces*, vol. 158, pp. 539–546, Oct. 2017, doi: 10.1016/j.colsurfb.2017.07.026.

[148] O. Zschörnig, G. Paasche, C. Thieme, N. Korb, and K. Arnold, ‘Modulation of lysozyme charge influences interaction with phospholipid vesicles’, *Colloids Surf B Biointerfaces*, vol. 42, no. 1, pp. 69–78, Apr. 2005, doi: 10.1016/j.colsurfb.2005.01.008.

[149] A. G. Lee, ‘Lipid–protein interactions in biological membranes: a structural perspective’, *Biochimica et Biophysica Acta (BBA) - Biomembranes*, vol. 1612, no. 1, pp. 1–40, May 2003, doi: 10.1016/S0005-2736(03)00056-7.

[150] J. Bigay and B. Antonny, ‘Curvature, Lipid Packing, and Electrostatics of Membrane Organelles: Defining Cellular Territories in Determining Specificity’, *Dev Cell*, vol. 23, no. 5, pp. 886–895, Nov. 2012, doi: 10.1016/J.DEVCEL.2012.10.009.

[151] A. N. Shrivastava, A. Aperia, R. Melki, and A. Triller, ‘Review Physico-Pathologic Mechanisms Involved in Neurodegeneration: Misfolded Protein-Plasma Membrane Interactions’, 2017, doi: 10.1016/j.neuron.2017.05.026.

[152] G. H. McKenzie, W. H. Sawyer, and L. W. Nichol, ‘The molecular weight and stability of concanavalin A’, *Biochimica et Biophysica Acta (BBA) - Protein Structure*, vol. 263, no. 2, pp. 283–293, Apr. 1972, doi: 10.1016/0005-2795(72)90081-5.

[153] E. D. N. S. Abeyrathne, H. Y. Lee, and D. U. Ahn, ‘Sequential separation of lysozyme, ovomucin, ovotransferrin, and ovalbumin from egg white’, *Poult Sci*, vol. 93, no. 4, pp. 1001–1009, Apr. 2014, doi: 10.3382/PS.2013-03403.

[154] R. C. Davies, A. Neuberger, and B. M. Wilson, ‘The dependence of lysozyme activity on pH and ionic strength’, *Biochimica et Biophysica Acta (BBA) - Enzymology*, vol. 178, no. 2, pp. 294–305, Apr. 1969, doi: 10.1016/0005-2744(69)90397-0.

[155] B. Yuan *et al.*, ‘Penetration and saturation of lysozyme in phospholipid bilayers’, *Journal of Physical Chemistry B*, vol. 111, no. 22, pp. 6151–6155, Jun. 2007, doi: 10.1021/jp071050u.

[156] G. P. Gorbenko, V. M. Ioffe, and P. K. J. Kinnunen, ‘Binding of lysozyme to phospholipid bilayers: Evidence for protein aggregation upon membrane association’, *Biophys J*, vol. 93, no. 1, pp. 140–153, 2007, doi: 10.1529/biophysj.106.102749.

[157] S. Islam and C. Mukhopadhyay, ‘Aggregation of Lysozyme in the Presence of a Mixed Bilayer of POPC and POPG’, *ACS Omega*, vol. 6, no. 28, pp. 17861–17869, Jul. 2021, doi: 10.1021/acsomega.1c01145.